Genetically Engineered Human Stem Cell-Derived Cardiomyocytes to Study the Novel Titin Isoform Cronos in Development and Disease

Rebecca J. Zaunbrecher

A dissertation

submitted in partial fulfillment of the

requirements for the degree of

Doctor of Philosophy

University of Washington

2018

Reading Committee:

Charles E. Murry, Co-Chair

Michael Regnier, Co-Chair

Jennifer Davis

Program Authorized to Offer Degree:

Department of Bioengineering

University of Washington

Abstract

Genetically Engineered Human Stem Cell-Derived Cardiomyocytes to Study the Novel Titin Isoform Cronos in Development and Disease

Rebecca J. Zaunbrecher

Co-Chairs of the Supervisory Committee:

Charles E. Murry, MD, PhD
Departments of Bioengineering and Pathology

Michael Regnier, PhD
Department of Bioengineering

The giant sarcomere protein titin plays a number of important roles in the cardiomyocyte, and truncating mutations to the gene that encodes this protein (*TTN*) are the leading known cause of dilated cardiomyopathy. Despite the frequency with which these mutations occur, significant questions remain about how they act to cause disease. Of particular interest is the clustering of truncating mutations to the A-band of *TTN* in DCM cohorts. To investigate this phenomenon, we genetically engineered human induced pluripotent stem cell (hiPSC) lines carrying homozygous mutations in the Z-disk (TTN-$Z^{-/-}$) and A-band (TTN-$A^{-/-}$) region of the gene. Surprisingly, TTN-$Z^{-/-}$ cardiomyocytes (CMs)

visibly contracted and were found to express a C-terminal portion of titin, which we determined to be the isoform Cronos titin. TTN-A$^{-/-}$ CMs produce truncation products of both full-length and Cronos titin and are not able to produce sarcomeres. Using a custom antibody, we demonstrate that TTN-Z$^{-/-}$ CMs only express Cronos titin and are able to form sarcomeres with this isoform in the absence of full-length titin. However, these cells produce drastically reduced contractile force as both single cells and in engineered heart tissues (EHTs). Using live cell imaging, we determine this is due to an inability of TTN-Z$^{-/-}$ CMs to properly bundle myofibrils, resulting in sarcomeric instability. We further investigate the biological relevance of Cronos titin by investigating its expression in human cardiac tissue. Genomic methylation, transcript levels, and immunostaining indicate that Cronos titin is most highly expressed in fetal cardiac tissue and is present at lower but detectable levels in adult left ventricular tissue. This indicates that Cronos titin is predominantly a developmental isoform. Finally, we investigate the role of Cronos titin by generating two Cronos knock-out (KO) hiPSC lines. When differentiated into cardiomyocytes, these cells do not express Cronos but do express full-length titin at comparable levels to wildtype controls. EHTs generated with Cronos KO CMs produce drastically lower force than control cells and exhibit significant myofibrillar disarray, indicating that Cronos titin is necessary for proper cardiomyocyte function. As a whole, this work demonstrates for the first time that Cronos titin is expressed in human cardiomyocytes, is necessary for proper sarcomere function, and is an important isoform of titin that may play a role in dilated cardiomyopathy.

TABLE OF CONTENTS

LIST OF FIGURES

LIST OF TABLES

ACKNOWLEDGEMENTS

First and foremost, I would like to thank my advisors Drs. Chuck Murry and Mike Regnier for their support, scientific guidance, and mentorship during graduate school. I am amazed by both of your perseverance and unending enthusiasm for science, and grateful to have trained under two world-class scientists and wonderful people. I would also like to thank the members of my supervisory committee, Drs. Jennifer Davis and Jay Shendure for their guidance and advice throughout the years on my project. I am deeply grateful to all current and past members of the Murry and Regnier labs for their technical support, unending helpfulness, thoughtful discussions, supportive words, and fun happy hours: Lil Pabon, Hans Reinecke, Xiulan Yang, Galina Flint, An-Yue Tu, Maria Razumova, Kaytlyn Gerbin, Meredith Redd, Nicole Zeinstra, Christine Yoo, Shiv Bhandari, Jason Murray, Joe Powers, Yuanhua Cheng, Jordan Klaiman, Farid Moussavi-Harami, Martha Mathiason, Kristen Meredith, Soley Olafsson, Alice Racca, Mary Beth O'Kelly, Lauren Neidig, Amy Martinson, Alessandro Bertero, Vicky Yuan, Paul Fields, Peter Hofsteen, Andrea Leonard, Katie Mitzlefelt, Shin Kadota, Ping Ong, Ben Cashdollar, Billy Chen, Daniel Yang, and Xuan Guan. I would particularly like to thank Dr. Nathan Palpant, who patiently mentored me during my first two years as a graduate student and has been integral to my successful completion of my PhD, and Ashley Abel, the hardest working and most enthusiastic student I have ever met and who has contributed innumerable hours to support the research outlined in this thesis.

I would also like to thank my boyfriend Graham Welch for his unending support of my academic and extracurricular pursuits, and my amazing friends Tory Stolper, Avi DeSharone, Alli Penfield, Avery Newton, and Jenny Shafer for their love and laughter through the years. Finally, I would like to thank my parents Richard and Judy Zaunbrecher, for their unending support and for instilling in me a love of science my entire life, and my sister Ginny Zaunbrecher, her husband Joey McInnis, and their son Bailey for always lending an ear or providing comic relief when I needed it most.

Chapter 1. Introduction

1.1 Titin

1.1.1 *Titin in the sarcomere*

Titin is the largest known protein and resides in the sarcomeres of striated muscle. In adult cardiac and skeletal muscle, the majority of titin molecules extend an entire half-sarcomere length from Z-disc to M-line and interact with both the thick and thin filaments (Figure 1.1)[1]. The N-terminal of titin is anchored to the Z-disk of the sarcomere through interactions with the proteins T-cap and α-actinin[2,3], as well as the cytoskeleton[4,5]. The I-band of titin contains immunoglobulin-like (Ig) domains and a region rich in proline, glutamate, valine, and lysine residues called the PEVK segment which act as extensible, molecular spring-like structures. Cardiac isoforms of titin also contain a unique sequence called N2B-Us, and together with the Ig and PEVK domains provides the majority of passive tension in cardiomyocytes and the heart as a whole in physiologic ranges of stretch[6,7]. This passive tension can be modulated in the short-term by post-translational modifications to titin, including phosphorylation[8–10] and covalent bond formation[11,12], or on a more long-term basis by changes in isoform expression[13–16]. The rigid A-band region of titin interacts with the thick filament, and has been proposed to act as a molecular ruler that establishes the patterning of myosin[17–19], although this remains a contentious role of the protein[20,21]. The C-terminal of titin is anchored in the M-line of the sarcomere by myomesin and contains a kinase domain, which is activated by stretch to promote sarcomere protein expression through the serum response factor pathway[22,23].

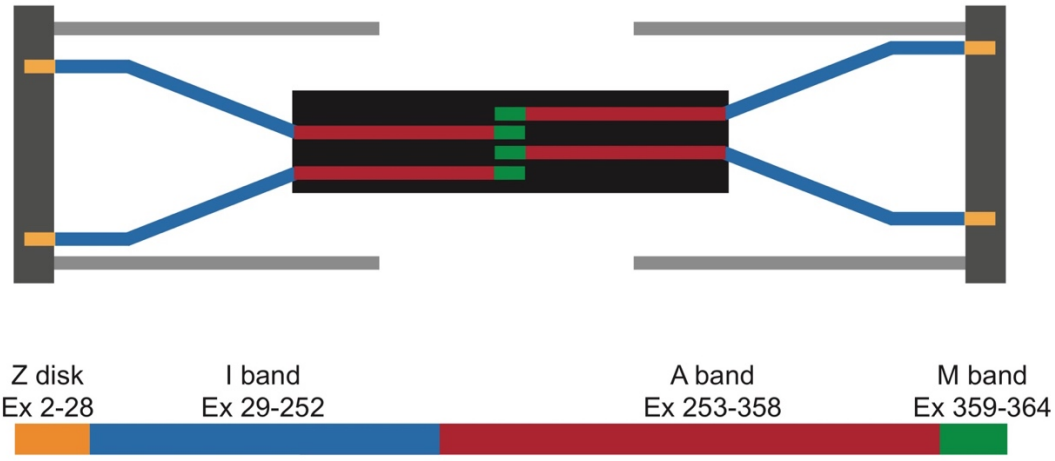

Figure 1.1. Overview of titin domains. Titin extends an entire half-sarcomere and interacts with the Z-disk (dark gray), think filament (light gray) and thick filament (black).

1.1.2 *Titin's role in sarcomerogenesis*

Because titin extends an entire half-sarcomere length from Z-disc to M-line, it has been proposed to act as a scaffold during sarcomerogenesis[24]. However, studies to determine how necessary titin is during sarcomere formation have been technically difficult due to titin's large size and genetic complexity. *In vitro* studies have largely depended upon overexpression of titin fragments and binding partners to prevent integration into the sarcomere and have provided conflicting evidence for the necessity of titin for sarcomere formation[2,25]. *In vivo* studies have been similarly conflicting: while a morpholino-based knockdown of titin indicated it was necessary for early sarcomere formation[26], genetic mutations in zebrafish causing a premature truncation indicate that titin becomes necessary after formation for myofibril stability and function[27,28]. However, zebrafish express titin from two genes in the heart, making it difficult to relate these findings to

human biology. Homozygous truncating mutations in constitutively expressed exons of titin are embryonic lethal in both rats[29] and mice[30], suggesting titin is crucial for viability but making it challenging to study early stages of sarcomere formation. Although titin is known to be important for proper sarcomere function, it's role in sarcomere formation in human cardiomyocytes remains unclear.

1.1.3 *Titin in the nucleus*

Titin has also been identified in non-muscle cells and has a putative, less well-studied role in the nucleus. Titin has been found to play important roles as a structural protein in the nucleus, contributing to the elasticity and organization of chromosomes during mitosis, and interacting with lamin in the nuclear envelope[31,32]. Additionally, a nuclear localization signal has been identified in the Z-disk region of titin, and a fragment of titin expressing this signal has been shown to affect cell proliferation through interaction with Wnt/β-catenin signaling[33]. However, much of this work has been performed using invertebrate animal models, which generally express versions of titin that are significantly shorter and lacking in several domains found in the human homologues. Thus, further studies are necessary to determine the relevance of nuclear titin to human biology.

1.1.4 *Titin isoforms*

The predominant isoforms of titin found in adult mammalian hearts are N2B and N2BA, both of which are encoded from the gene *TTN* but differ in the exons included in the spring-like I-band region. N2B is the shorter, stiffer isoform with a molecular mass of

approximately 3 MDa while N2BA is the longer, more compliant isoform with a molecular mass of 3.2-3.7 MDa[34]. N2B and N2BA can be co-expressed within the same sarcomere, and the ratio of their expression has been shown to alter passive tension of individual cardiomyocytes[35]. Additionally, these isoforms are consistently expressed at different ratios between species, with smaller rodents expressing almost exclusively N2B, medium-size mammals (i.e. dogs, humans, and pigs) expressing slightly more N2BA than N2B, and cows expressing predominantly N2BA[16].

1.2 Titin in Disease

1.2.1 *Titin truncations are the most common cause of genetic dilated cardiomyopathy*

Dilated cardiomyopathy (DCM) is a serious but common disease: it is one of the leading causes of heart failure and estimated to affect 1 in 250 people[36]. DCM is characterized by increased ventricular volume and attenuated contractile (systolic) function of the heart and is the leading indicator for heart transplant. Few treatments exist for this disease, and the health and economic burden it causes are significant: DCM is the most frequent cause of heart transplantation and is estimated to cost $4-10 billion to manage each year in the United States[37,38]. Although the causes of DCM are heterogeneous, a landmark study in 2012 by Herman et al found that heterozygous truncating mutations in the gene that encode for the large protein titin (*TTN*) account for 25% of familial DCM[39,40]. Follow-up studies have confirmed the high prevalence of titin truncating mutations in DCM[41–45], as well as implicated them in peripartum cardiomyopathy[46], making truncating mutations in *TTN* the most common known cause of both familial and idiopathic DCM.

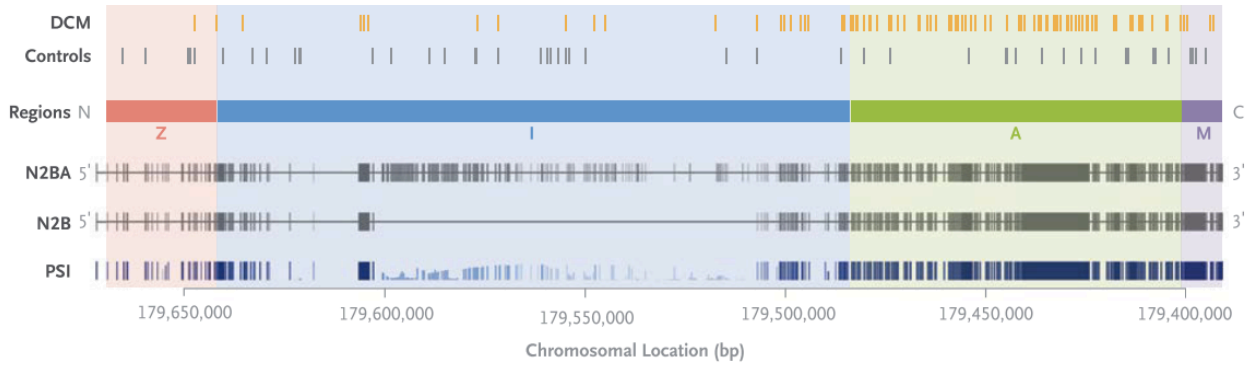

Figure 1.2. Distribution of titin mutations found in DCM and control patients. Mutations found in DCM patients cluster in the A-band of the *TTN* gene, while those found in control patients are more evenly distributed throughout the gene. The N2BA isoform of titin includes more exons in the I-band region of the protein compared to N2B. Adapted from [46].

1.2.2 *Titin truncating mutation distribution and pathogenicity*

Despite the high prevalence of titin truncating mutations in DCM patients, the pathogenicity of these mutations in the general population is not straightforward: approximately 1.5-2% of healthy, control populations carry truncating mutations in *TTN*, a rate of nearly five times that of nonischemic DCM[39,46,47]. Because of the high occurrence of apparently non-deleterious titin truncating mutations, there has been significant interest in determining if the pathogenicity of variants can be predicted based on their location within *TTN*. Titin truncating mutations identified in DCM patients are found predominantly in the A-band region of *TTN*, while those identified in control populations are distributed more evenly throughout the gene (Figure 1.2)[39,47]. One hypothesis to explain this distribution and predict the disease-causing potential of variants is that mutations occurring in highly expressed exons are more pathogenic than those in exons that are usually spliced out of the transcript. In fact, the average percent spliced in (PSI, a measure

of exon usage) of titin truncating variants in DCM patients was found to be significantly higher than in control populations[47], and the odds ratio (OR, indicating the likelihood that a mutation causes disease) was increased when mutations occurred in highly expressed exons (PSI>0.75)[48]. Although the majority of mutations in the A-band region of titin are constitutively spliced in, this hypothesis does not explain the lower OR of mutations in other constitutively expressed regions of *TTN*, such as the Z-disk and some portions of the I-band[29].

1.2.3 *Animal models of truncated titin DCM*

Since titin truncating mutations were first identified as a cause of DCM nearly 15 years ago[49], several experimental models have been developed to study the mechanism of these mutations. A mouse model harboring a clinical heterozygous truncating mutation in the A-band of titin was found to develop DCM only after stressing with angiotensin, and unstressed mice exhibited normal cardiac physiology and expressed only a small amount of truncated titin protein[30]. Two knock-in rat models have also been established with heterozygous truncating mutations in the Z-disk and A-band domains of titin[29]. These rat models exhibited slight systolic dysfunction when aged more than a year, and the hearts failed more dramatically when stressed *ex vivo*, although the position-dependent effects of each truncation were not fully defined. It is notable that titin isoform expression varies greatly between rodents and humans, which may confound results from these studies[16]. Thus, it is desirable to study titin truncations in systems that more closely mimic that observed in the clinic.

1.3 Human Induced Pluripotent Stem Cells for Cardiac Disease Modeling

The following section was adapted from [50]

It has now been over thirty-five years since the first report of a genetic linkage between a sarcomere protein mutation (or variant) with a disease phenotype[51]. Since then well over one thousand genetic variants of sarcomere proteins have been reported as associated with diseases such as hypertrophic, dilated or restrictive cardiomyopathy, though many fewer have been confirmed as having causative roles[45,52]. The vast majority of research to understand the phenotypic consequences of these genetic variants has been done using post-natal animals, cell culture and recombinant protein models. Thus, much has been learned about later stages of the disease process, likely after multiple compensatory processes have been invoked and often when hearts are in failure. However, there is growing consensus that to find effective treatments for these familial diseases it is important to understand the role of these mutations in earlier stages in disease progression, before clinical signs manifest and perhaps at the earliest stages of human development.

1.3.1 *Approaches to using hiPSC-CMs for disease modeling*

The development of technologies to derive human pluripotent stem cells and differentiate them into cardiomyocytes has provided a model system in which to study these crucial early stages of development. Beginning with the derivation of the first human embryonic stem cell line in 1998[53] and continuing with the derivation of human induced pluripotent

stem cells (hiPSCs) in 2007[54], it has been theoretically possible to generate any tissue in the lab. However, early differentiation protocols for cardiomyocytes depended upon the spontaneous formation of embryoid bodies and resulted in low yields of cardiomyocytes (~1-5%)[55]. Better understanding of pathways involved in heart development in vivo has since been leveraged to develop more efficient differentiation protocols and it is now possible to achieve >90% pure cardiomyocyte populations using multiple methods[56]. Additionally, these technologies in reprogramming and directed differentiation have made it possible to generate cell lines and large numbers of cardiomyocytes from patient samples and have laid the foundation for hiPSC-based cardiac disease modeling.

A series of technological advances in genomic engineering have also advanced the ability to model cardiomyopathies with hiPSC-derived cardiomyocytes (hiPSC-CMs). Until recently, cell lines have largely been generated using samples from patients who both 1) carry a known or suspected pathogenic mutation and 2) clinically present with cardiomyopathy. A major benefit of this approach is that the resulting cell line will carry both the mutation of interest as well as any undefined or unknown genetic modifiers that may be necessary for presentation of the disease phenotype. This enhances the likelihood that a phenotype will emerge in vitro. However, it can often be difficult to establish appropriate controls for patient-derived cell lines. Even control cell lines established from healthy close relatives can have significant genetic variation compared to the cardiomyopathy line, and when relatives' samples are unavailable often completely unrelated wildtype cell lines are used[57,58]. Nevertheless, this has been used

to successfully study both hypertrophic[59] and dilated[60,61] cardiomyopathy and gain mechanistic insights into the pathogenesis of these mutations.

Breakthroughs in genome engineering technologies, notably the development of the CRISPR/Cas9 system for use in mammalian systems, currently allow for the generation of isogenic control lines in hiPSC-CM modeling. Using a 20-base pair single guide RNA, the CRISPR/Cas9 system can create double-stranded breaks at nearly any location in the genome. This allows for the straightforward generation of random mutations using non-homologous end joining (NHEJ), as well as specific base pair changes at lower efficiencies by supplying a template for homology-directed repair (HDR)[62]. More recent advances have focused on improving the efficiency of HDR[63,64] and increasing the target range of CRISPR systems by mutating the commonly used Cas9 nuclease[65] and deriving nucleases from different species of bacteria[66].

Two general approaches are available for using genome engineering in hiPSC-CM modeling. In the first, mutations can be specifically engineered into a healthy, wildtype hiPSC line. A significant benefit to this approach is that many different mutations can be tested on the same genetic background, allowing for a rigorous comparison. Particularly for nonsense mutations, this can be done in a relatively high-throughput manner through the use of NHEJ. Alternatively, mutations in a patient-derived line can be corrected using HDR. However, this is often technically more problematic. Although these genome engineering technologies are still relatively new, it is clear that controls generated using these techniques are more accurate than cell lines created from unaffected relatives or

unrelated individuals. In the future, isogenic controls should be considered a standard in hiPSC-CM disease modeling.

1.3.2 *Phenotyping hiPSC-CM disease models*

There are numerous technologies for phenotyping hiPSC-CMs. Of particular interest in many cardiomyopathies are mechanical function measurements of hiPSC-CMs, which can be acquired on single cells or in the context of a multicellular tissue engineered system. Current assays allow for highly sensitive measurements of both force production and kinetics of hiPSC- CM contraction and relaxation, and these measurements have been successfully used to characterize the phenotype of several hiPSC-CM cardiomyopathy models[60,67]. Recent reviews provide comprehensive coverage of both single cell measurement systems[68] and multicellular tissue engineering approaches[69]. Of note, a method has recently been developed to mature hiPSC-CMs sufficiently to harvest isolated myofibrils for mechanics measurements to determine how sarcomeric mutations directly affect the organelle in which they are located[70].

With the addition of this assay, it is now possible to characterize the functional properties of hiPSC-CMs on subcellular, cellular, and multicellular levels, a crucial set of tools for cardiomyopathy disease modeling. Studying the effects of disease-associated mutations at each level of organization provides insight into distinct aspects of cardiomyocyte function and how they are affected by the mutation of interest. Myofibril mechanics measurements assess the contractile ability of the hiPSC-CMs

independent of the influences of the cell's Ca2+ handling properties or intracellular signaling pathways. Single cell measurements assess the function of myofibrils in the context of whole-cell function, but without the influence of cell-cell communication. Finally, multicellular tissue constructs provide insight into the effects of cellular junctions and environmental cues from extracellular matrix and is currently the most physiological setting in which to study hiPSC-CMs *in vitro*. By performing these multiscale analyses in an *in vitro* setting, where the internal and external environments can be manipulated, it is now possible to study how molecular level changes in myofilament protein structure and function (with mutations) affect contractile fibrils and how this may influence coupled systems such as the calcium handling, energetic production and protein expression systems in cells and tissue. In turn this should provide new insight into which levels of structural organization are most affected during the initiation and propagation of disease phenotype, and whether the disease phenotype requires neuro-hormonal input.

1.3.3 *The issue of hiPSC-CM maturity*

A blessing and a curse central to the use of hiPSC-CMs as models for familial cardiomyopathies is the maturity of the cells. By most electrophysiological, morphological, metabolic, and mechanical measures, these cells are far from an adult phenotype[71]. Although it can be difficult to match hiPSC-CMs to an exact gestational age in vivo, a recent study suggests when cells are matured on nanopatterned surfaces for out to 80-100 days in culture they have drastically matured cell size and morphological characteristics compared to younger cells. These cells express the adult

form of cardiac myosin (β-myosin from MYH7), although isoform studies of troponin I suggest a fetal stage of expression[72]. Additionally, their myofibril mechanical properties and sarcomere ultrastructure match those of myofibrils from 75 day fetal heart tissue[70]. Thus, caution should be used in judging the developmental state of these hiPSC-CMs, based on appearance at the light microscope level.

Table 1.1. Summary of the benefits and drawbacks of using hiPSC-CMs to study familial cardiomyopathies

Pros	**Cons**
Moderate throughput for studying different mutations using CRISPR/Cas9	Lack of neuro-hormonal, endocrine, and paracrine responses
Able to study mutations that would be lethal *in vivo*	Immaturity of protein expression, ultrastructure, morphology, mechanical properties
Provides insight during development of disease to understand mechanisms	
Using isogenic controls allows for rigorous tests of causality and comparisons of mutations	

Phenotyping cells at such an immature state is also a double-edged sword for studying genetic cardiomyopathies (summarized in Table 1.1). Many genetic cardiomyopathies clinically present in adulthood, and there are concerns about whether in vitro modeling will demonstrate an appropriate disease phenotype that recapitulates what occurs in vivo. However, in these familial-based diseases there are likely changes occurring in the myocardium well before many cardiomyopathies are detected clinically that can be identified using in vitro assays. For example, a recent study using hiPSC-CMs to study

titin truncating mutations as a basis for dilated cardiomyopathy noted a disease phenotype in several assay systems, despite the fact that DCM associated with these mutations is usually detected well into adulthood[67].

In fact, the immaturity of hiPSC-CMs can be beneficial for studying genetic cardiomyopathies. Studies that utilize animal models of cardiomyopathy often focus on characterizing end-stage phenotypes, contributing data mostly to enhance understanding of the final presentation of the disease. Alternatively, the fetal-like properties of hiPSC-CMs can provide mechanistic insight into early differences in function and structure present in cardiomyopathy that may be difficult or impossible to tease out in an in vivo system. For mutations in proteins that are not expressed initially in cardiomyocyte differentiation, but later in the timeline of development, it should be possible to determine the seminal event that leads to disease development and associated compensatory mechanisms. This developmental view of disease progression is particularly important as genetic testing grows in prevalence and robustness, and the possibility of pre-emptively treating genetic diseases before they present clinically becomes more likely. Using hiPSC-CMs as a model of genetic cardiomyopathies can allow for these crucial studies to understand how they develop, so that the progression or development of them can be prevented.

Looking forward, additional new tools are being developed that, combined with current technology, will allow for more and better models of disease in a dish. One example of this is the development of hiPSC lines that express proteins from the endogenous loci

with a linked fluoro-tag that allow for studies of structural development with repeated live cell imaging[73,74]. Another tool is optogenetics, which has been used primarily by neuroscientists to date[75]. The ability to express channels that can provide temporal and spatial control of stimulation or inhibition of depolarization could be quite useful for developing culture-based models of arrhythmia-genesis and long Q-T syndrome but may also provide insight to how sarcomere protein mutations disrupt the balance between the contractile apparatus and Ca2+ cycling dynamics.

There still remain many limitations of in vitro models and some aspects of disease will be challenging or impossible to study using hiPSC-CMs. Examples include the complex temporal and spatial influence of neuro-hormonal, paracrine and endocrine factors and how these are influenced by the structural and functional changes resulting from mutant protein expression. On the other hand, these new and emerging approaches will allow for studies that are impossible to perform with other platforms (e.g. early development, studying mutations that would be lethal) and inform on design of animal models that can probe those aspects. Ultimately these tools will be most useful when used in conjunction with in vivo models.

In summary, a new generation of biophysical, gene editing and bioengineering approaches that are emerging holds great promise and potential as tools to improve our understanding of cardiac muscle development and the initiation and early-stage progression of disease development. These, in turn, will allow for better models used

for drug and small molecule screening and the next generation of targeted therapies for heart failure.

1.3.4 *HiPSC models of titin truncation DCM*

Several models of titin truncation DCM using hiPSC-CMs have been generated, both from reprogramming samples from DCM patients harboring titin truncating mutations and by engineering truncating mutations into a wild type cell line. A study by Hinson *et al* compared hiPSC-CMs carrying mutations in the I-band and A-band regions of *TTN* and demonstrated that these cells exhibited reduced systolic function, myofibril disorganization, and perturbed TGFβ signaling[67]. Additionally, they generated homozygous versions of these mutations and demonstrated that the I-band mutants formed sarcomeres, whereas the A-band mutants did not. They explain this observation by demonstrating that the mutation-containing I-band exon is only expressed in some versions of the transcript, while the A-band exon is constitutively expressed. They conclude that systolic dysfunction observed in titin truncation hiPSC-CMs are caused by a sarcomere insufficiency, although they do not elucidate the mechanism of this insufficiency.

Gramlich *et al* characterized hiPSC-CMs derived from DCM patients carrying A-band titin truncating mutations and demonstrated that these cells exhibited disorganized sarcomeres and blunted serum response factor signaling[76]. By blunting the serum response factor pathway, muscle protein transcription is disrupted, which they theorize is causing the disrupted myofibril morphology. They further showed that an antisense-

mediated exon skipping therapy rescued this phenotype in hiPSC-CM and a mouse model. Although their analysis of the sarcomeric disruption by blunted serum response factor signaling was not extensive, they successfully demonstrate a therapy to rescue the titin truncated DCM phenotype.

Most recently, Schick *et al* used patient-derived titin truncation hiPSC-CMs to investigate the effects of these mutations on excitation-contraction coupling and responses to positive inotropes[77]. The titin truncation cells did not respond to positive inotropes, which they attribute to perturbed calcium handling properties, particularly a reduction of proteins involved in calcium efflux. Proteomic analyses indicate that this may be due to a reduction in SERCA2 expression caused by a reduction in titin tyrosine kinase signaling caused by the truncating mutation. They also attribute a reduction in signaling from the titin tyrosine kinase domain to causing sarcomeric disarray by reduction of sarcomere protein turnover and resulting sarcomere instability. However, they never demonstrate that there is a reduction in titin expression or tyrosine kinase domains expressed in the DCM cells, leaving a major mechanistic question unanswered.

Of the model systems that have been used to study titin truncations in DCM, hiPSC-CMs display the largest functional difference and are the most easily manipulated, making them an attractive choice for future studies. In particular, they could be used to determine if there is a phenotypic difference between mutations in the A-band (where DCM mutations are commonly observed) and the Z-disk (where they are infrequently observed) on the level of the cardiomyocyte. A prominent hypothesis in the field is that the

pathogenicity of titin truncation mutations depends upon the frequency with which the exon it is in is expressed[29,47,67]. A study using genetically engineered hiPSC-CM would directly investigate this hypothesis and provide important data on the contributions of titin truncations to DCM and the structure of *TTN*.

1.4 Thesis Motivation & Overview

The goal of this thesis is to better understand the basic biology of titin in human cardiomyocytes relating to mutations carried in the Z-disk compared to the A-band of titin. To address this, we have chosen to primarily use genetically engineered hiPSC-CM as our system due to the benefits outlined above. This goal is broken down into three aims, each of which is detailed in a chapter of this thesis:

AIM 1. Define the necessity of titin expression for sarcomere formation and function in hiPSC-CMs (Chapter 2)

AIM 2. Establish Cronos titin expression in human cardiac tissue (Chapter 3)

AIM 3. Evaluate role of Cronos titin in sarcomere formation & function of hiPSC-CMs (Chapter 4)

Through experiments while completing the first aim of this thesis a novel isoform, Cronos titin, was discovered to be present in hiPSC-CMs. Using genetic engineering, we demonstrate that Cronos titin is sufficient for sarcomere formation in hiPSC-CMs, but these cells produced drastically reduced contractile force and had marked reduction in myofibril bundling. It has been proposed that the presence of the internal start site in *TTN*

encoding for Cronos accounts for differences in outcomes from Z-disk compared to A-band truncations, and thus it is important to understand the role of Cronos titin in hiPSC-CMs and human cardiac tissue. Having made the striking observation that sarcomere formation was present using only Cronos titin in hiPSC-CM, the following two aims were used to further explore the role of this novel isoform.

In the second aim of this thesis we investigate the expression of Cronos titin in developing and adult human cardiac tissue. Fetal and adult cardiac samples were studied on the genomic, transcriptional, and protein level to investigate the expression of Cronos and full-length titin. The data suggest that Cronos titin is differentially expressed depending on developmental stage and region within the heart, with highest expression occurring early in fetal development. Cronos titin is present in adult heart, but at significantly lower levels. Given the regulation of Cronos titin expression during development in the human heart, we hypothesized that this isoform played an important and crucial role in the cardiomyocyte.

In the third aim of this thesis we investigate the role of Cronos titin in human cardiomyocytes by generating and characterizing Cronos knock-out hiPSC-CMs. These cells express full-length titin normally, but do not have Cronos titin integrated in the sarcomere. Cardiomyocytes without Cronos titin produced reduced contractile force and formed disarrayed myofibrils compared to wild type controls. We conclude that Cronos titin is necessary for normal sarcomere formation and function in human cardiomyocytes.

To our knowledge, this is the first time that Cronos titin has been identified in human tissue. We further demonstrate that Cronos titin is necessary for proper sarcomere formation and function. The work presented in this thesis provide crucial new evidence and understanding of the role of Cronos titin.

Chapter 2. Cronos Titin is Sufficient for Sarcomere Formation in hiPSC-CMs

2.1 Abstract

To investigate the necessity of titin in sarcomere formation and function in human cardiomyocytes, we used the CRISPR/Cas9 system to generate homozygous truncating mutations in the Z-disc (TTN-$Z^{-/-}$) and A-band (TTN-$A^{-/-}$) regions of *TTN* in hiPSCs. We were surprised to find that although both cell lines differentiated into highly pure populations of cardiomyocytes as measured by cardiac troponin T expression, the TTN-$Z^{-/-}$-CMs visibly contracted while the TTN-$A^{-/-}$-CMs did not. We hypothesized that this was due to the presence of a recently discovered isoform of titin, Cronos, which is expressed from a start site downstream of the truncating mutation in the TTN-$Z^{-/-}$ cell line. Immunohistochemistry of samples from each cell line using antibodies that recognize epitopes along the length of titin supported this hypothesis. When characterized for force production, we found TTN-$Z^{-/-}$-CMs produced significantly lower forces in the context of both multicellular, engineered heart tissues and as single cells. Calcium transient magnitudes were not different in single TTN-$Z^{-/-}$-CMs compared to wild type, indicating that this was not the source of reduced force. Morphologically, TTN-$Z^{-/-}$-CMs had drastically smaller Z-discs and the myofibrils were noticeably sparser, although sarcomere length was found to be the same as wild type. From this study we conclude that some sarcomere formation is possible when only Cronos titin is expressed, but that full-length titin is necessary for proper sarcomere formation and function.

2.2 Rationale

The first aim of this thesis investigates the necessity of full-length titin for sarcomere formation in human cardiomyocytes. The hypothesis we tested was that full-length titin was necessary for the formation and function of sarcomeres in hiPSC-CMs.

Studies performed *in vivo* and *in vitro* have provided conflicting evidence regarding the necessity of titin for sarcomere formation. In cell culture studies, titin is difficult to specifically and completely knockdown due to its genetic complexity and large size[78]. Transgenic approaches in rodent models allow for more consistent control over titin expression, but the embryonic lethality of homozygous truncating mutations makes *in vivo* studies of early sarcomerogenesis challenging[29,30]. Because of these roadblocks, it is unclear whether titin is crucial for sarcomere formation or only necessary for the proper function of sarcomeres once they are fully formed. To elucidate the role of titin during sarcomere development, we have taken the approach of genetically engineering homozygous truncating mutations into human induced pluripotent stem cells (hiPSCs) and studying their function following differentiation into cardiomyocytes (hiPSC-CMs). The use of genetic engineering in an *in vitro* setting allows for studies of the effects of titin-specific knockouts at early developmental stages that would not be possible using animal models. Additionally, the use of hiPSCs provides maximal relevance to human biology. Because heterozygous truncating mutations in the A-band of titin are more pathogenic than those in the Z-disc region, we introduced homozygous truncating mutations in each of these locations to determine if they caused different phenotypes. Due to the embryonic lethality of homozygous titin truncations in both of these locations

in animal models[29,30], and the inability of hiPSC-CMs with homozygous A-band truncations to forms sarcomeres[67], we hypothesized that both would prevent sarcomere formation in hiPSC-CMs. We were interested to find that hiPSC-CMs harboring homozygous mutations in the Z-disc region of *TTN* visibly contracted and hypothesized that some sarcomere formation was possible due to the expression of a C-terminal isoform of titin called Cronos.

2.3 Methods

2.3.1 *Human Induced Pluripotent Stem Cell Culture*

The WTC hiPSC line[79] was generously provided by Dr. Bruce Conklin (Gladstone Institute, UCSF) and maintained on plates coated with Matrigel (Corning) in mTeSR1 media (STEMCELL Technologies). When cells reached 70-80% confluency, they were dissociated using 0.48mM EDTA in PBS warmed to 37°C and replated in media containing 10μM Y-27632 ROCK Inhibitor (Tocris).

2.3.2 *Genetic Engineering of hiPSC*

Single guide RNAs (sgRNAs) targeting *TTN* Exon 2 and Exon 326 were designed using the online CRISPR design tool (crispr.mit.edu) and ligated into vector PX459v2 (Cas9-2A-Puro)[62] (sgRNA sequences are listed in Table 2.2) based on the hg19 assembly *TTN* sequence on the UCSC Genome Browser[80]. 300,000 WTC hiPSC were transfected with 1μg plasmid using GeneJuice (EMD Millipore) during replating and selected with 0.5μg/mL puromycin (ThermoFisher) for 2 days beginning the day after transfection. After

selection, cells were replated at low density in a 10cm plate to grow as single-cell colonies. Colonies were genotyped by amplifying the region around the targeted sgRNA site from 100-300ng genomic DNA using GoTaq Flexi DNA polymerase (Promega) following manufacturer's guidelines and primers listed in Table A.1. Following visualization by electrophoresis on a 0.8% agarose gel stained with ethidium bromide, PCR products were sequenced using the forward primer (Eurofins genetics). Colonies with homozygous mutations causing premature stop codons were also screened for mutations in the top 5 genes predicted to be most susceptible to off-target effects. Primers were designed using Primer-BLAST[81] and used to amplify the area surrounding the predicted off-target cut site using GoTaq Flexi DNA polymerase (Promega) and sequenced using the forward primer (see Table A.2. for accession numbers and primers). Mutant cell lines were cryopreserved and karyotyped (Diagnostic Cytogenetics Inc, Seattle, WA).

Table 2.2. sgRNA sequence for hiPSC gene editing

sgRNA name	**Sequence (5' to 3')**	**Cell lines used for**
TTN_Ex2_gRNA1	GCAGCCGTTACAAAGCGTTG	TTN-Z$^{-/-}$-1
TTN_Ex2_gRNA2	GGGTAGTACCGCAACCTTTG	TTN-Z$^{-/-}$-2
TTN_Ex326_gRNA1	GATCCGCCCAAAAACCCTGA	TTN-A$^{-/-}$-1
TTN_Ex326_gRNA2	GTGATAAAGCTGGCCAACGC	TTN-A$^{-/-}$-2

2.3.3 *Cardiac Differentiation of hiPSC*

Wild type and mutated WTC hiPSCs were differentiated into cardiomyocytes as previously described[82]. Briefly, cells were plated into a Matrigel-coated plate in mTeSR

media containing 10μM Y-27632 ROCK Inhibitor and 1μM Chiron 99021 (Tocris) at a density of $1.3x10^5$ cells/cm^2. The following day (Day 0 of differentiation), the media was changed to RPMI media (Gibco) supplemented with 2% B-27 without insulin (Life Technologies), 1X Matrigel, and 100ng/mL Activin A (R&D Systems). 17 hours later, the media was changed to RPMI supplemented with 2% B-27 without insulin, 5ng/mL BMP4 (R&D Systems), and 1μM Chiron 99021. 2 days later, media was changed to RPMI supplemented with 2% B-27 without insulin and 1μM XAV939 (Tocris). Media was changed to RPMI supplemented with 2% B-27 without insulin two days later. Beginning 7 days after the start of differentiation, cells were maintained in RPMI supplemented with 2% B-27 with insulin and 1% penicillin/streptomycin (Invitrogen), and media was changed every 2-3 days. For RNA isolation and single cell force mechanics, cardiomyocytes were purified using lactate selection by replating cells 14-18 days after the start of differentiation and feeding with DMEM without glucose (Gibco) supplemented with 4μM sodium lactate (Sigma-Aldrich) on days 18-22 after differentiation[83]. This workflow is outlined in Figure 2.1.

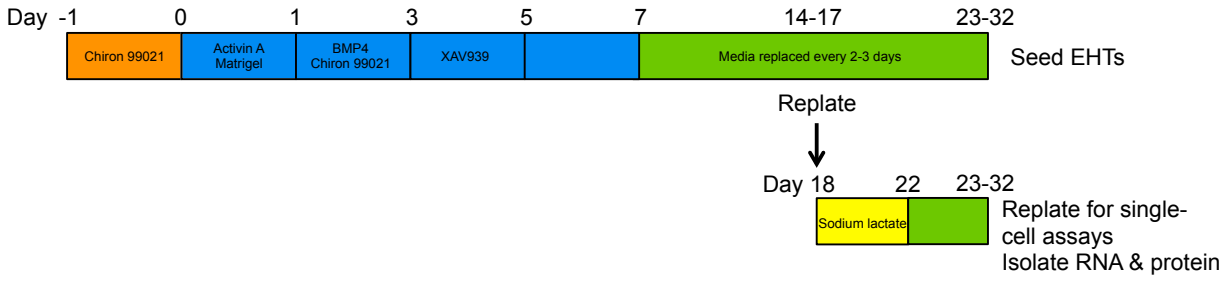

Figure 2.1. Cardiac differentiation protocol. Colors denote different medias used with the addition of compounds noted in the timeline. Orange: mTeSR1 supplemented with 10μM Y-27632 ROCK Inhibitor; blue: RPMI supplemented with 2% B-27 without insulin; green: RPMI supplemented with 2% B-27 with insulin and 1% penicillin/streptomycin; yellow: DMEM without glucose.

2.3.4 *Cardiac Troponin T Flow Cytometry*

Cells were fixed in 4% paraformaldehyde for 10 minutes at room temperature, pelleted, and resuspended in 5% fetal bovine serum (FBS, Gibco) in phosphate buffered saline (PBS, Gibco) and stored at 4°C for up to 1 week. For each sample being analyzed, half of sample was stained with a cardiac troponin T primary monoclonal mouse antibody (diluted 1:100, Invitrogen) and half was stained with a mouse IgG1 antibody (diluted 1:100, Affymetrix). After incubation for 30 minutes at room temperature, samples were incubated in goat-anti-mouse R-Phycoerythrin (1:200, Jackson Laboratories) for 30 minutes at room temperature. Cells were stored in 5% FBS in PBS plus 4% paraformaldehyde until analyzing by flow cytometry using a FACS CantoII machine, up to 1 week. Data was analyzed using FlowJo software and a 5% false positive rate to set the bounds using the isotype-stained sample.

2.3.5 *Engineered Heart Tissues*

Engineered heart tissues (EHTs) were seeded 23-32 days after the start of differentiation using a previously described fibrin scaffold system[84]. Each EHT was seeded with $4x10^5$ hiPSC-CMs and $4x10^4$ HS27a bone marrow stromal cells (ATCC) resuspended in 100µL of fibrin solution and cast between one rigid and one flexible PDMS post. EHTs were maintained in RPMI media supplemented with 2% B-27 with insulin, 1% penicillin/streptomycin, and 5mg/mL aminocaproic acid (Sigma-Aldrich), which was changed every 2-3 days. After 3 weeks in culture, EHTs were paced at 1Hz using 5V

pulses and the flexible post deflection was tracked by light microscopy and used to calculate force production and twitch kinetics.

2.3.6 *Single-cell Force Measurements*

Single-cell forces were measured using PDMS micropost arrays as previously described[85]. Wild type and TTN-Z$^{-/-}$ hiPSC-CMs were replated 29-33 after initiation of differentiation onto micropost arrays stamped with laminin. Videos were collected 6-7 days later while cells were kept at 37°C in Tyrode's buffer containing 1.8mM Ca^{2+} and analyzed to determine force magnitude and kinetics as previously described[85]. These assays were performed in collaboration with Kevin Beussman from the Sniadecki laboratory at the University of Washington.

2.3.7 *Calcium Transient Measurements*

Glass coverslips were coated by incubating in a 5μg/mL human fibronectin (Life Technologies) solution at 4°C overnight. Cells were replated as 23-32 days after the start of differentiation at a density of $1.1x10^4$ cells/cm^2 and imaged 21-28 days later. Cells were stained by incubating in 0.2μM Fura-2 AM (Thermo Scientific) at 37°C for 30 min, washed by incubating in Tyrode's buffer for 15 minutes at 37°C, and then imaged during gravity perfusion with Tyrode's buffer containing 1.8mM Ca^{2+} kept at 37°C using an in-line heater and heated FHD chamber (IonOptix). Cells were imaged with the MyoCamera (IonOptix) while paced at 1Hz using 10V pulses using a MyoPacer Field Stimulator (IonOptix). Transients were analyzed using IonWizard (IonOptix) by filtering the ratio of the signal,

averaging the peaks, and using the “Monotonic Transient Analysis” function with the change of measuring the “Time to % Baseline” from “t to bl 10%” to “t to bl 50%” and “t to bl 90%” and changing “Time Relative” to “t Peak”.

2.3.8 *Cronos titin custom antibody generation*

A custom rabbit polyclonal antibody was generated by Pierce Custom Antibodies (ThermoFisher). The antigen used for antibody production consisted of the entire N-terminal, Cronos titin-specific sequence (i.e. encoded by the intronic sequence upstream of *TTN* exon 241 as determined by the previously reported 5’ RACE data on human cardiac samples[86]) excluding the start methionine: SNAKLFLPSRLA. Plasma obtained from the rabbits 70-72 days following inoculation was affinity purified using the same antigen and then tested on hiPSC-CMs as a positive control and undifferentiated hiPSCs as a negative control. Staining with the Cronos titin antibody generated a striated pattern in the hiPSC-CMs that correlated with α-actinin co-staining and was absent in both undifferentiated hiPSC negative controls and a secondary-only group.

2.3.9 *Cell culture on nanopattern substrates*

Nanopatterned coverslips were generated as previously described [87] and kindly provided by Dr. Jesse Macadangdang in Dr. Deok-Ho Kim’s laboratory at the University of Washington. Nanopatterned coverslips were coated by incubating in a 5μg/mL human fibronectin (Life Technologies) solution at 4°C overnight. Cells were replated as 23-32 days after the start of differentiation at a density of 1.1×10^4 cells/cm^2 and fixed and stained

27-31 days (for the day 30 group) or 53-63 days (for the day 60 group) later. Cells were fixed and stained as described below.

2.3.10 *Immunostaining of single cells and EHTs*

Single cells were relaxed in 150mM KCl and fixed in 4% paraformaldehyde for 10 minutes at room temperature, and staining was started immediately. EHTs were relaxed in 150mM KCl, fixed in 4% paraformaldehyde for 15 minutes at room temperature, and kept in a 30% sucrose solution at 4°C overnight. The following day, EHTs were embedded in Tissue-Tek O.C.T. compound (VWR) using an ethanol-dry ice bath, and cryoblocks were sectioned at a 5µm thickness, at which point the staining protocol was started.

Following three PBS washes, samples were blocked in 1.5% normal goat serum for 1 hour at room temperature. Primary antibodies were diluted in blocking buffer (see Table 2.3 for details) and added to samples for overnight incubation at 4°C. The following day, samples were incubated in AlexaFluor-conjugated goat anti-mouse and anti-rabbit antibodies (Life Technologies, diluted 1:100) for 1 hour at room temperature and coverslipped using Vectashield with DAPI (Vector Laboratories).

Table 2.3. Primary antibodies used for immunostaining

Antibody name	**Species**	**Dilution**	**Company**	**Product #**
Sarcomeric α-actinin	Mouse	1:800	Abcam	ab68167
Titin Z-disk (Z1Z2)	Rabbit	1:300	Myomedix	TTN-Z
Titin I-band (MIR)	Rabbit	1:300	Myomedix	TTN-MIR
Titin M-line (M8M10)	Rabbit	1:300	Myomedix	TTN-M
β-myosin heavy chain	Mouse	1:10	DSHB	BA-D5
Cronos titin	Rabbit	1:15000	ThermoFisher	custom

2.3.11 *Live Cell Imaging & Analysis*

hiPSC-CMs were transduced with ELF1a-mCherry-a-actinin lentivirus ranging from day 23-35 post-differentiation. Viral media was changed 24 hours post-transduction. Cells recovered for 6 days with regular maintenance. On the 6th day, which was one day before imaging, cells were replated onto a Matrigel-coated chambered coverglass at a density of 500,000 cells/mL. Media was changed to regular RPMI + B27 with insulin + 1% pen/strep 24 hours after replating before imaging. 10-15 cells were tagged for imaging (NIS Elements) based on visible beating or appearance of sarcomere-like structures. Cells were imaged using a Yogokawa spinning-disk confocal (Institute for Stem Cells and Regenerative Medicine Garvey Imaging Core, University of Washington) using a 60x oil lens on a single focal plane every 30 minutes for 12 hours while maintained at 37°C and 5% CO_2. Images were analyzed by hand to measure number of myofibrils in the 1st, 13th, and 25th frames, using the basis of the most sarcomere-like structures observed in the cells. The maximal myofibril bundle width was measured for 3 consecutive Z-disks in 3

regions of the cell and averaged for the value for a single cell in the 1st and 25th frame for each cell. Both measurements were performed in Fiji[88].

2.3.12 *Statistical Analysis*

For assays with two groups, student's t-tests were performed in Excel. For assays with more than two groups, one-way ANOVAs were performed in MATLAB using the "anova1" function, and if the returned p-value was less than 0.01 Tukey's post-hoc analysis was performed using the "multcompare" function. These nominal p-values were then used to calculate adjusted p-values using the Benjamini & Hochberg method[89].

2.4 Results

2.4.1 *HiPSC line generation, differentiation, & titin expression*

The CRISPR/Cas9 system was used to introduce mutations in Exon 2 (in the Z-disk domain) and Exon 326 (in the A-band region) of *TTN* into the WTC hiPSC line (Figure 2.2). Single-cell colonies were expanded and screened for homozygous mutations expected to cause truncating mutations and the positive clones were then karyotyped. Both mutant cell lines were karyotypically normal and differentiated into high purity populations of cardiomyocytes as measured by flow cytometry after staining for cardiac troponin T (cTnT). Given that we had hypothesized that neither of the mutant cell lines would visibly contract, we were surprised to find that the TTN-$Z^{-/-}$ line formed monolayers of beating cardiomyocytes. The TTN-$A^{-/-}$ line did not visibly contract, even in populations that had a high percentage of cTnT+ cells.

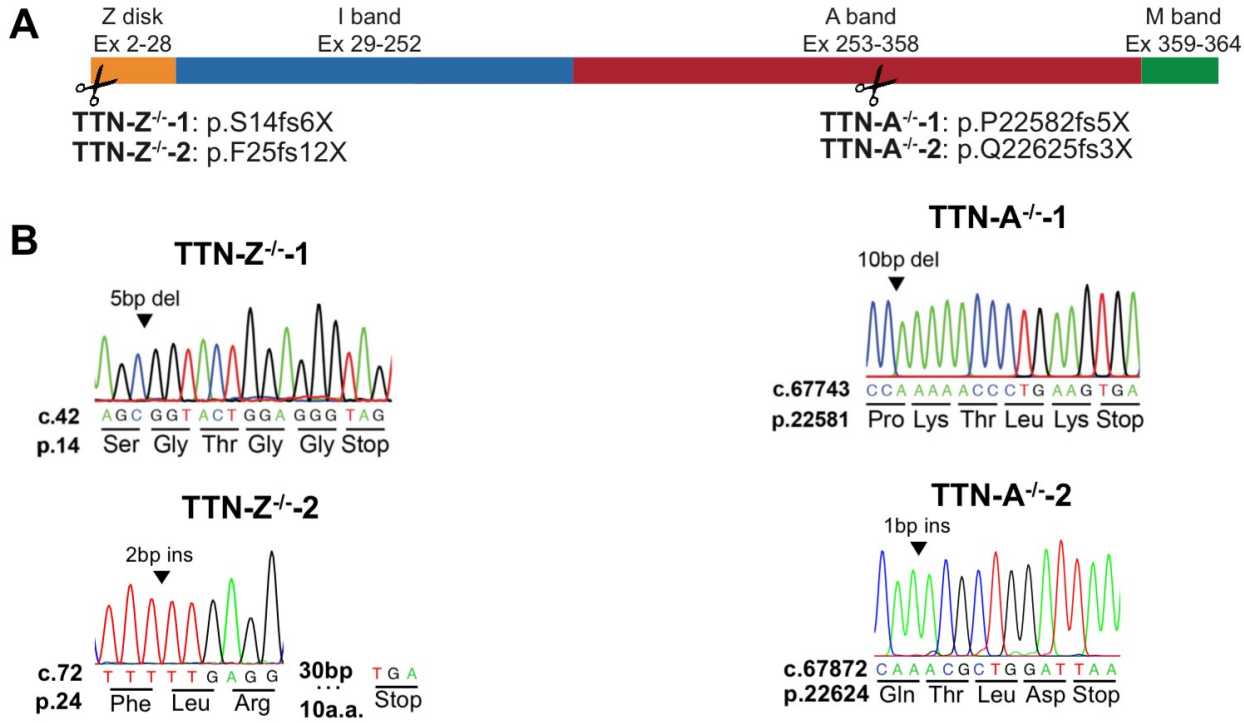

Figure 2.2. Genotype overview of homozygous Z-disk and A-band truncation hiPSC lines. (A) Exons of the *TTN* gene that encode for each domain of titin, and the locations along the titin meta-protein of homozygous mutations specifically engineered into hiPSC lines. (B) Chromatograms of the targeted region of *TTN* in the generated mutant hiPSC lines indicate homozygous mutations.

Because TTN-$Z^{-/-}$-CMs visibly contracted we hypothesized that these cells were expressing some form of titin that allowed them to form functioning sarcomeres. To investigate titin expression, we performed immunocytochemistry on hiPSC-CMs with antibodies to probe for the Z-disk, distal I-band, and M-line domains of titin (Figure 2.3). Wild type samples stained positively for all three titin epitopes, and the antibodies localized within the sarcomere in the expected patterns. TTN-$Z^{-/-}$-CMs demonstrated striated staining with α-actinin, and interestingly these sarcomeres only stained positively

for distal I-band and M-line titin, both of which are downstream of the mutation introduced into this cell line. Finally, the staining of TTN-A$^{-/-}$-CMs did not indicate formation of sarcomeres, and diffuse α-actinin, Z-disk, and I-band titin signals were observed. The M-line domain of titin, which is downstream of the mutation in these cells, was not detected. These data indicate that despite inducing a truncating mutation in a constitutively expressed N-terminal exon, the TTN Z$^{-/-}$ cells expressed distal elements of *TTN* that supported myofibrillogenesis and contractility.

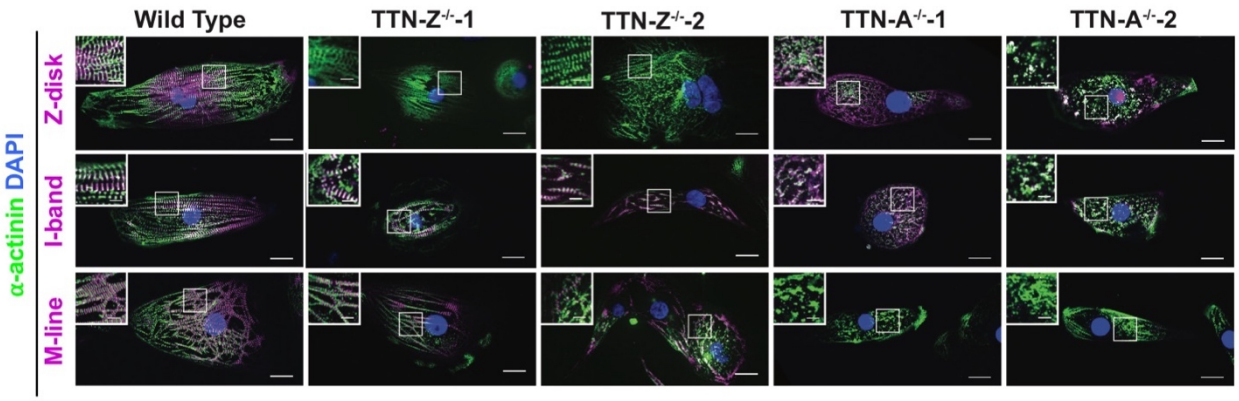

Figure 2.3. Immunostaining of hiPSC-CMs from each cell line using titin antibodies that recognize the Z-disk, distal I-band, and M-line. WT-CMs stain positively for all titin epitopes and show sarcomere formation. TTN-Z$^{-/-}$ CMs have sarcomere formation but only stain positively for C-terminal titin domains. TTN-A$^{-/-}$ CMs stain positively for N-terminal antibodies and do not form sarcomeres. In each panel, large image: scale bar = 20μm, inset image: scale bar = 5μm. White boxes indicate regions magnified in inset image. In each panel, large image: scale bar = 20μm, inset image: scale bar = 5μm. White boxes indicate regions magnified in inset image.

2.4.2 *Titin Z-Disk truncations are partially rescued by Cronos titin*

The expression of distal titin epitopes with Z-disk truncation mutations suggested that an alternate transcript was initiated 3' to our mutations. Zou et al recently identified an

internal promoter in zebrafish *ttn*, which initiates transcription from a previously unrecognized transcriptional start site (TSS) located in the distal I-band portion [86]. Named Cronos, this C-terminal isoform of titin is predicted to be approximately two-thirds the size of the full-length isoforms, and to contain the distal I-band, A-band, and M-line regions, consistent with our epitope maps in the Z-disk truncation lines (Figure 2.4). Gene targeting approaches disrupting Cronos titin expression in zebrafish cause significant myofibrillar disarray[86]. Although the transcript has been detected in mammalian cardiac samples[86], until now there have not been studies identifying the Cronos titin protein or investigating its role in human cardiomyocytes. We hypothesized that the TTN-$Z^{-/-}$-CMs express Cronos titin, which allowed for some sarcomere formation in these cells.

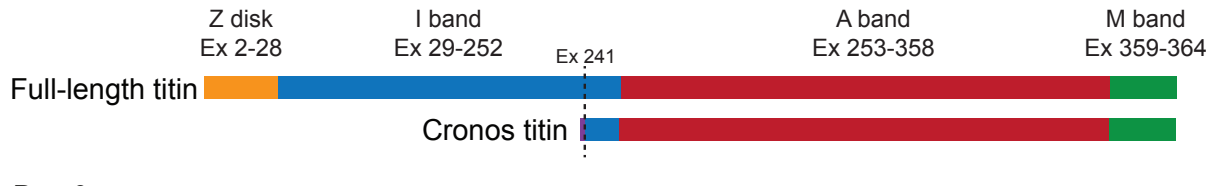

Figure 2.4. Schematic of domains expressed in full-length and Cronos titin. Purple indicates a short Cronos-specific region that is intronic to full-length titin.

To investigate this hypothesis, we revisited ChIP-Seq data from human embryonic stem cells (hESCs) undergoing cardiac differentiation[90]. We identify two peaks of H3K4me3 (a promoter specific epigenetic mark) within *TTN* in definitive cardiomyocytes 14 days after the start of differentiation that are not present during earlier stages of differentiation. One peak localizes to the 5' end of *TTN* corresponding to the TSS of full-length titin, while the second prominent peak corresponds to the locus previously

proposed for the Cronos titin TSS in the intron between Exon 240 and 241 (Figure 2.5). H3K27me3 profiles of *TTN* did not show significant peaks at any time point studied. The appearance of H3K4me3 deposition without H3K27me3 is a pattern typically observed in cardiac structural genes[90]. Together this provides genomic evidence to support the presence of an internal Cronos-specific promoter within the titin locus in human stem cell-derived cardiomyocytes.

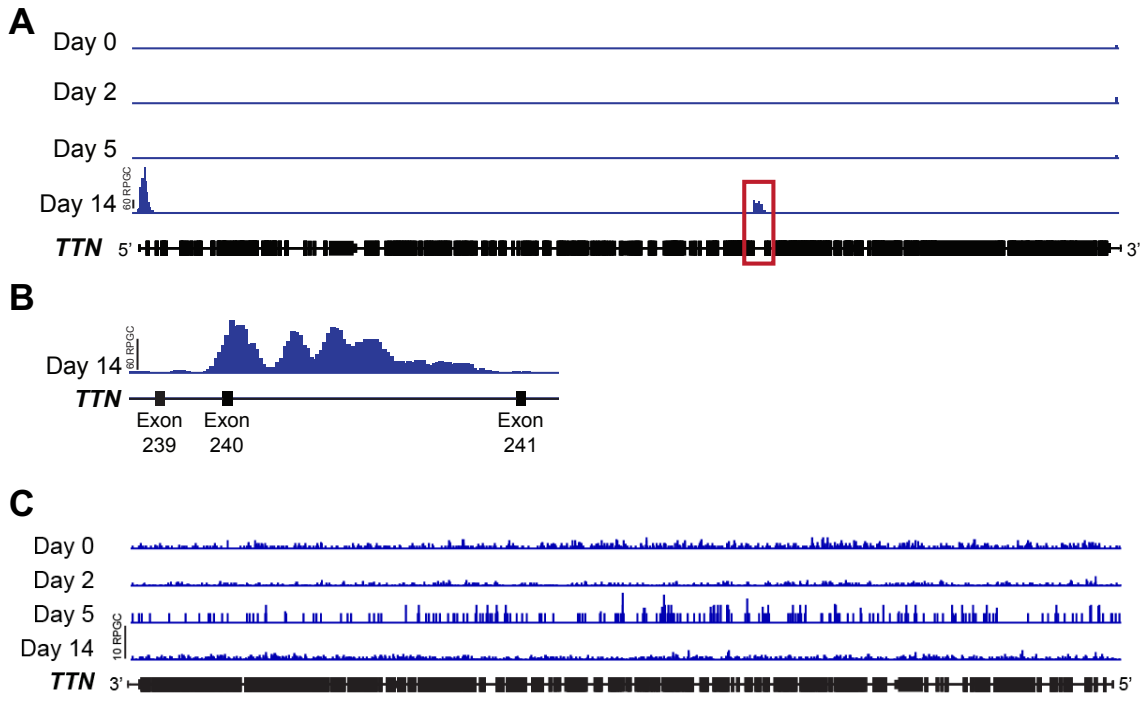

Figure 2.5. Methylation in *TTN* during hESC-CM differentiation. (A) H3K4me3 enrichment in hESC-CMs during differentiation. (B) An enlarged view of the region enclosed in a red box in panel A indicating a prominent peak near the expected Cronos titin transcription start site between exons 239 and 240. (C) H3K27me3 enrichment in hESC-CMs during differentiation.

To determine if Cronos titin protein was present in hiPSC-CMs we performed loose gel electrophoresis to distinguish titin isoforms by molecular weight. Analysis of total protein

using a Coomassie stain indicates both N2BA and T2 titin are present in WT samples, but only T2 titin in TTN-Z$^{-/-}$ cells (Figure 2.6). The T2 band has previously been described as a proteolytic degradation product of N2B and N2BA titin[15,34,91], but we and others hypothesized that this band contains the novel isoform Cronos due to its similar expected molecular weight (~2.2MDa)[86]. To test this idea we raised a custom antibody to recognize the N-terminus of Cronos, the first 13 residues of which are specific to this isoform[86] (see Methods for details). Western blots using this antibody identified the T2 band but did not detect any of the other titin isoforms present, confirming that this band includes Cronos titin. Several lower weight titin bands were detected in the TTN-A$^{-/-}$-CMs, indicating that only truncated versions of N2BA and Cronos titin are present in these cells. Taken together, these data demonstrate the T2 band includes Cronos titin, indicate that this novel isoform is expressed in hiPSC-CMs as well as human heart tissue, and reveal that TTN-Z$^{-/-}$ are solely expressing this isoform.

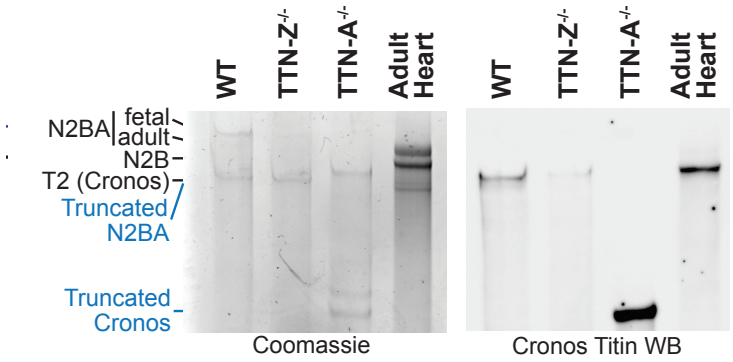

Figure 2.6. Protein gel and Western blot of titin isoforms in hiPSC-CMs. Coomassie-stained gel and Western blot of protein samples from wild type and mutant cell lines and adult human heart tissue demonstrate that the Cronos antibody is specific. Blue labels refer to the TTN-A$^{-/-}$ lane, black labels refer to all other samples.

To investigate if Cronos titin was being integrated into sarcomeres and establish its localization in the cell lines, we performed immunostaining with our custom antibody (Figure 2.7). This revealed doublet patterns surrounding the Z-disks in both wild type and TTN-$Z^{-/-}$ samples, demonstrating that Cronos titin is being expressed and integrated into sarcomeres in these cells. TTN-$A^{-/-}$ samples stained diffusely for Cronos titin, similar to the pattern observed using other titin antibodies that recognize regions upstream of the truncating mutation. This pattern is also consistent with Western blot data indicating that the TTN- $A^{-/-}$ cells are expressing a large truncation product of this isoform. Thus, we conclude that the ability of TTN-$Z^{-/-}$ mutants to form sarcomeres likely results from the ability of Cronos to substitute, at least in part, for full-length titin.

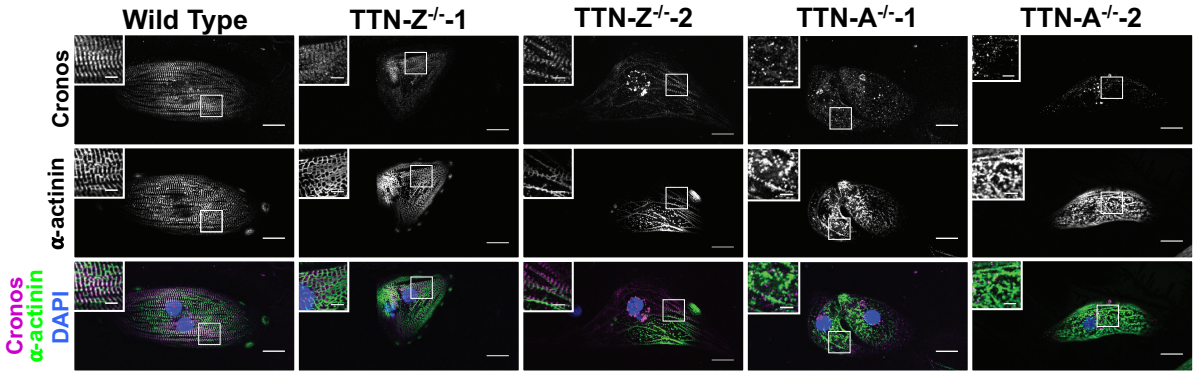

Figure 2.7. Staining for the N-terminal of Cronos titin indicates a doublet pattern around the Z-disks in WT and TTN-$Z^{-/-}$ CMs and diffuse staining in TTN-$A^{-/-}$ CMs. In each panel, large image: scale bar = 20μm, inset image: scale bar = 5μm. White boxes indicate regions magnified in inset image.

2.4.3 *Engineered heart tissue and single cell force measurements*

After observing that TTN-Z$^{-/-}$-CMs can form sarcomeres and contract using Cronos as a substitute for full-length titin, we were interested in establishing whether they had comparable contractility to WT cells. To investigate force production, we characterized the contractile function of wild type and mutant cardiomyocytes in a multicellular context using engineered heart tissues (EHTs)[84] and as single cells[85]. Consistent with observations of cardiomyocytes in monolayers, both wild type and TTN-Z$^{-/-}$ EHTs visibly contracted while TTN-A$^{-/-}$ EHTs did not visibly contract, although they did compact a similar amount (Figure 2.8D). Measurements of paced twitches 3 weeks after seeding indicate that TTN-Z$^{-/-}$ EHTs produced only ~10% of absolute force produced by wild type EHTs, and approximately 25% of active tension compared to WT (Figure 2.8A-C). The time to peak of wild type and TTN-Z$^{-/-}$ EHT twitches was slightly decreased even though the maximum rate of force development was dramatically slower (Figure 2.8F-G). Neither 50% or 90% relaxation time was significantly different in TTN-Z$^{-/-}$ EHTs, although passive force was significantly decreased (Figure 2.8D-E). Immunostaining of EHT sections revealed titin expression patterns corresponding to those observed in single cells (Figure 2.9). Taken together, these data indicate that although TTN-Z$^{-/-}$-CMs are able to form sarcomeres and contract, they produce only a small fraction of the force of wild type cells in engineered tissues.

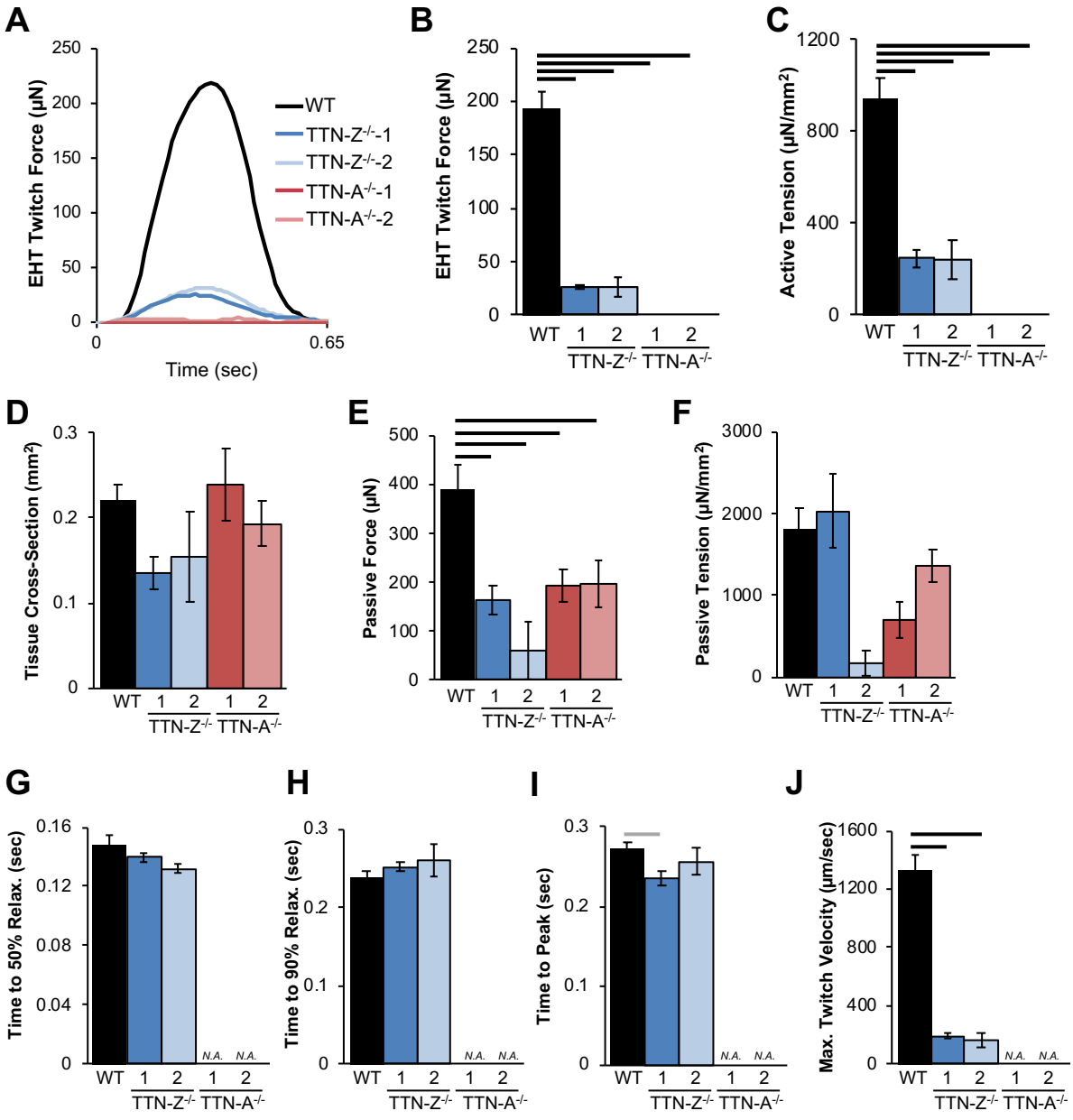

Figure 2.8. TTN-Z$^{-/-}$ and TTN-A$^{-/-}$ EHT Force Mechanics. (A) Example traces of EHT twitches from all cell lines studied. EHTs seeded with TTN-Z$^{-/-}$ CMs produce drastically lower (B) twitch force and (C) active tension compared to WT controls. EHTs seeded with TTN-A$^{-/-}$ CMs do not produce measurable twitches. (D) Tissue cross-sectional area was not significantly different between any of the groups studied. (E) Passive force was significantly lower than WT in all mutant lines studied, but (F) passive tension is not significantly different. Relaxation time to (G) 50% and (H) 90% were not significantly different between TTN-Z$^{-/-}$ EHTs and control. (I) Time to peak was slightly lower for one

TTN-$Z^{-/-}$ line, and (J) maximum twitch velocity was significantly decreased for both TTN-$Z^{-/-}$ lines compared to WT. EHTs: WT: n=23; TTN-$Z^{-/-}$-1: n=16; TTN-$Z^{-/-}$-2: n=5; TTN-$A^{-/-}$-1: n=16; TTN-$A^{-/-}$-2: n=17. Error bars indicate standard error. Gray line connecting groups: $p<0.05$; black line connecting groups: $p<0.01$.

To determine if the weak force production of TTN-$Z^{-/-}$ EHTs was caused by attenuated twitches of individual cells, we characterized single cell contractility using a micropost-based assay system[85] (Figure 2.10). TTN-$Z^{-/-}$-CMs produce significantly lower force on both a whole-cell level and when normalized for cell area. Interestingly, maximum twitch velocity, twitch power, cell size, and passive force were not different between cell types, although both upstroke and relaxation times were decreased in TTN-$Z^{-/-}$-CMs compared to controls. Notably, the force difference between single WT-CMs and TTN-$Z^{-/-}$-CMs is less dramatic than that observed in the EHT system. This may be partially due to the younger age and less mature state of cells used in the micropost system, along with the fact that multicellular forces are generated in series in the EHTs, which would be expected to increase the difference between WT and knockout cells (see Discussion).

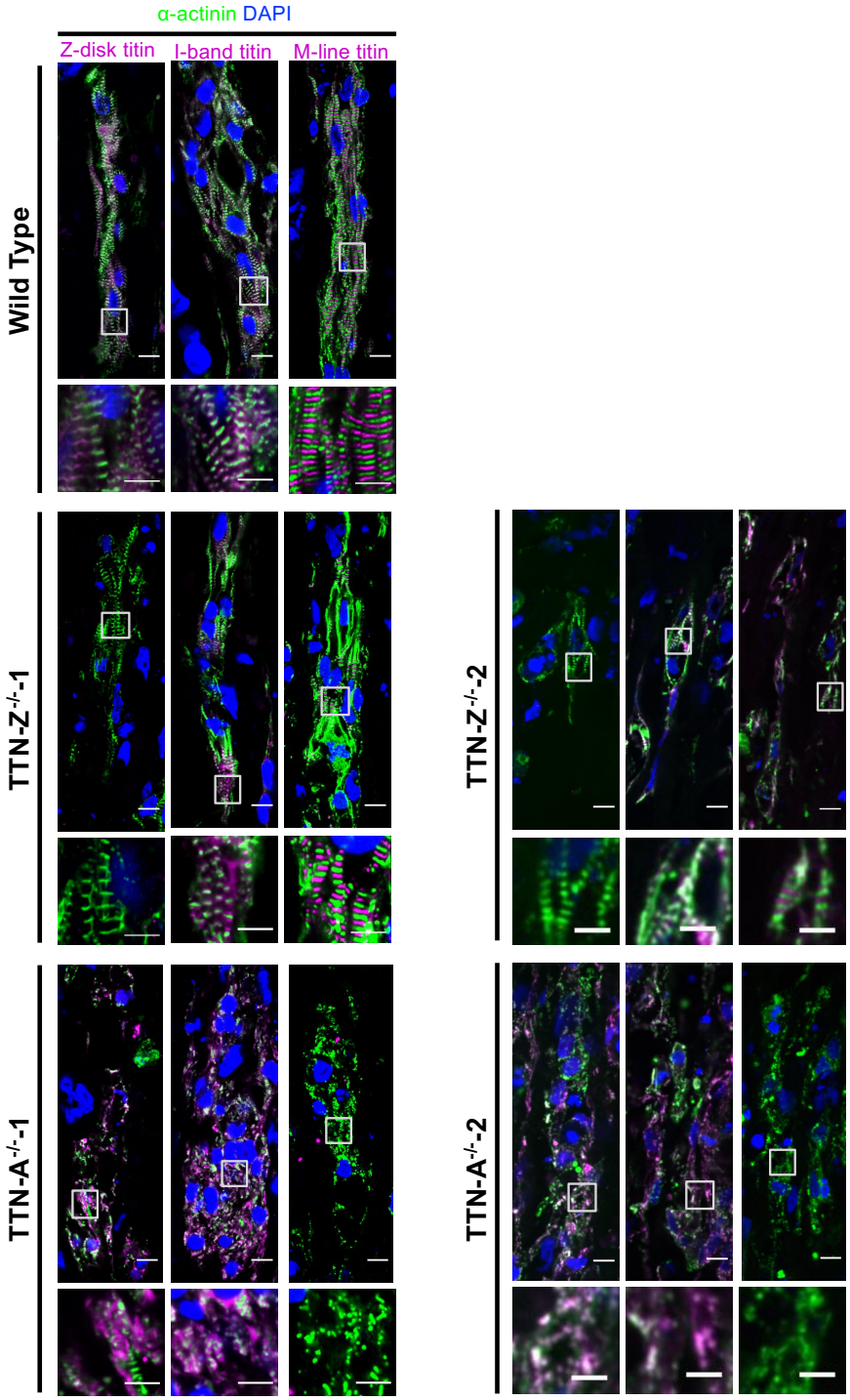

Figure 2.9. Immunostaining of EHTs for titin epitopes. Immunohistochemistry of EHTs seeded with hiPSC-CMs from each cell line using titin antibodies that recognize the Z-disk, distal I-band, and M-line regions of the protein. In each panel, large image: scale bar = 10μm, small image: scale bar = 5μm. White boxes indicate regions magnified in small image.

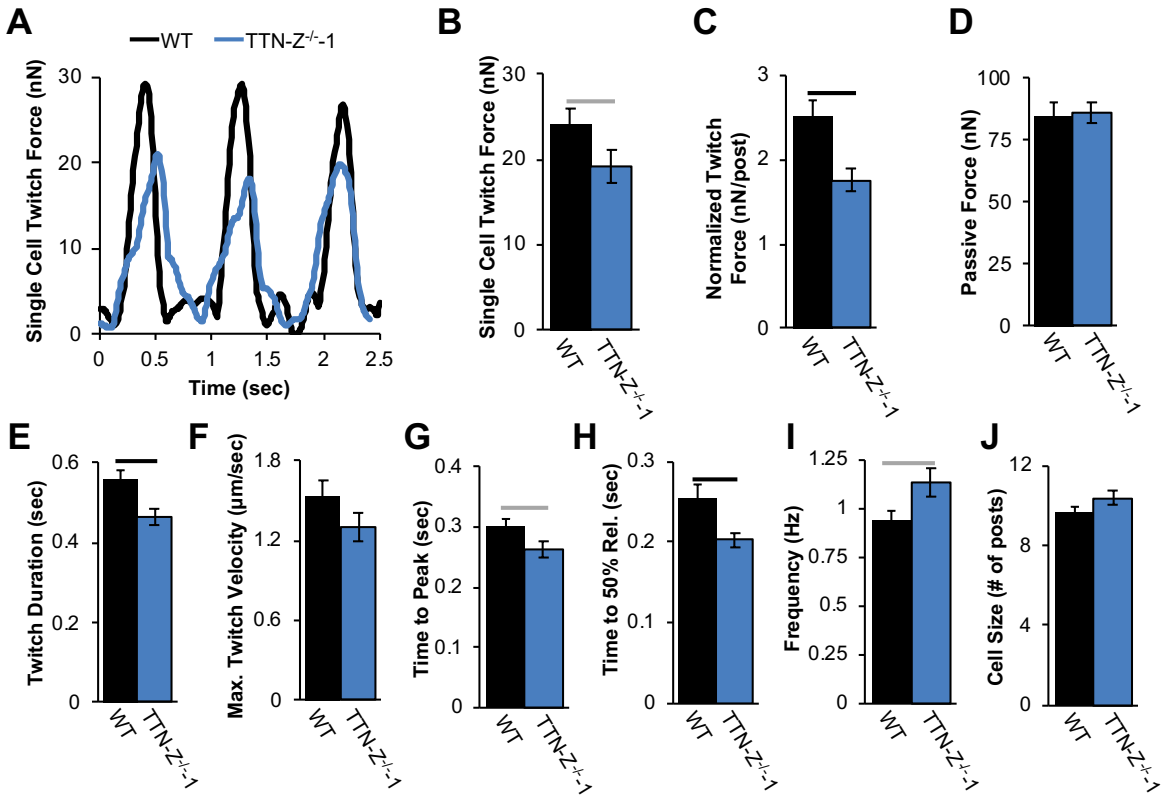

Figure 2.10. Single-cell force mechanics of WT and TTN-$Z^{-/-}$ CMs. (A) Sample twitch force traces of single cell micropost measurements. TTN-$Z^{-/-}$-CMs produce lower (B) whole-cell twitch force and (C) twitch force when normalized to cell size. (D) There was no significant difference in passive force. (E) The twitch duration for TTN-$Z^{-/-}$-CMs was significantly shorter than WT. There was no significant difference between WT and TTN-$Z^{-/-}$ cells in (F) maximum twitch velocity. In TTN-$Z^{-/-}$-CMs, (G) time to peak and (H) time to 90% relaxation were significantly shorter and (I) spontaneous beating frequency was significantly higher than wild type. As indicated by (J) number of posts each cell occupied, cell size between groups was not significantly different. WT: n=107; TTN-$Z^{-/-}$-1: n=71. Error bars indicate standard error. Gray line connecting groups: $p<0.05$; black line connecting groups: $p<0.01$.

2.4.4 *Calcium Handling of single TTN-$Z^{-/-}$ and TTN-$A^{-/-}$ CMs*

To determine if the reduced force produced by TTN-$Z^{-/-}$-CMs was caused by differences in calcium handling, we measured Ca^{2+} transients during electrical pacing of single cells plated on fibronectin-coated glass slides (Figure 2.11). Interestingly, we found that the

magnitude of calcium transients in TTN-Z$^{-/-}$ and TTN-A$^{-/-}$ CMs was not lower than wild type controls, and likely this is not responsible for the reduced contractility observed in single cells and EHTs. The time to peak and maximum rate of release trended slower for all mutant cell lines studied but was only significant in one group. Time to 50% reuptake was only significantly different in one cell line, and time to 90% reuptake trended faster in all mutated cell groups compared to WT but was only significant for two. Based on these data we conclude that differences in calcium transients do not explain attenuated force production observed in individual TTN-Z$^{-/-}$-CMs.

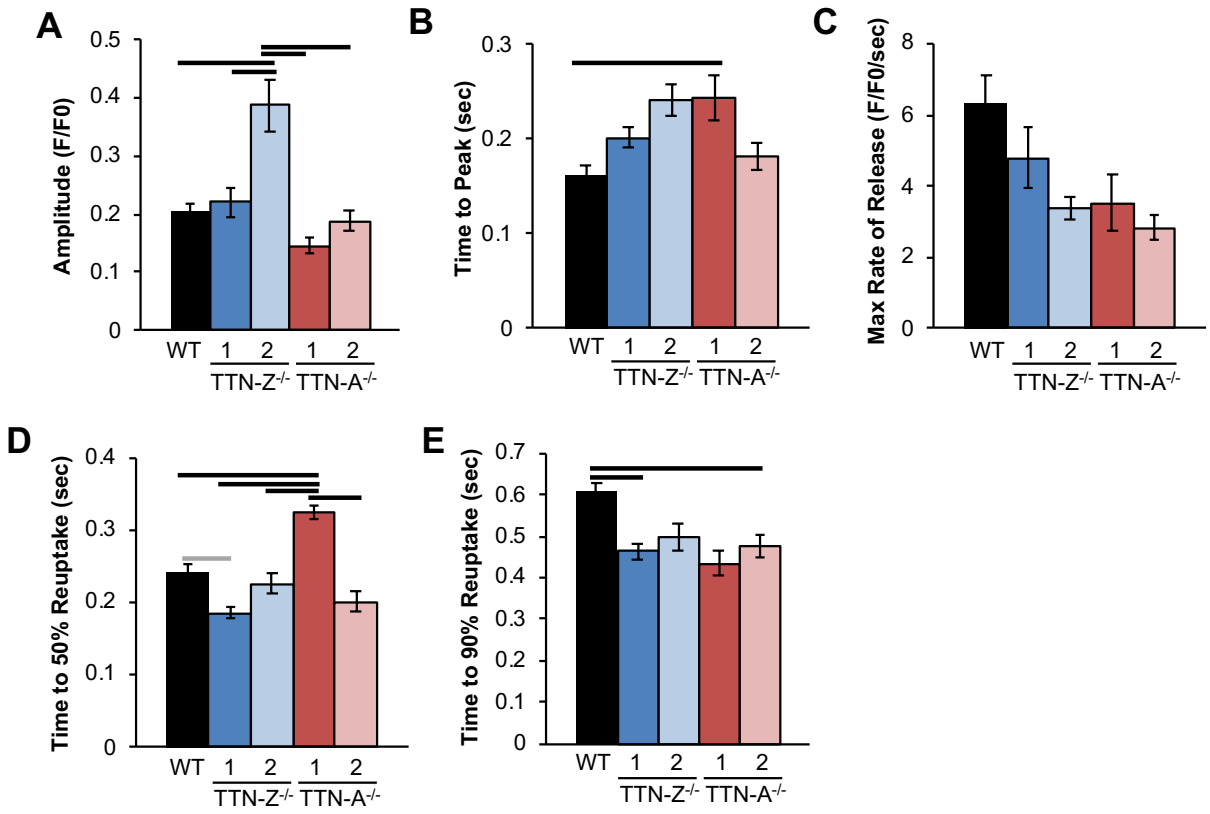

Figure 2.11. Calcium transients of WT, TTN-Z$^{-/-}$, and TTN-A$^{-/-}$ single CMs. (A) amplitude of transient is significantly larger in TTN-Z$^{-/-}$-2 CMs but no different in other groups compared to WT, (B) Time to peak is only significantly different between WT and TTN- A$^{-/-}$-1 CMs, and (C) maximum rate of release is not significantly different between any

groups studied. (D-E) Calcium reuptake kinetics are slightly perturbed with an overall trend of faster reuptake by cells carrying titin mutations. WT: n=35; TTN-$Z^{-/-}$-1: n=37; TTN-$Z^{-/-}$-2: n=12; TTN-$A^{-/-}$-1: n=24; TTN-$A^{-/-}$-2: n=28. Error bars indicate standard error. Gray line connecting groups: $p<0.05$; black line connecting groups: $p<0.01$.

2.4.5 *Morphology and Nucleation of TTN-$Z^{-/-}$ CMs*

To measure whether sarcomere morphology was distinct between WT and TTN-$Z^{-/-}$-CMs, we fixed and stained cells after culture on nanopatterned substrates for 30 and 60 days (Figure 2.12). Myofibrils in TTN-$Z^{-/-}$ cells were noticeably more disarrayed and sparser compared to WT controls, and maximum Z-disk width within each cell was found to be drastically shorter at both time points. Additionally, while WT Z-disk width significantly increased between 30 and 60 days cultured on the nanopatterns, indicative of continued hypertrophy and organization, the z-disk width of TTN-$Z^{-/-}$-CMs did not change. This could indicate that Z-disk bundling or stability is affected in these cells. Interestingly, sarcomere length was not found to be significantly different at either time point measured. Consistent with previous assays, TTN-$A^{-/-}$-CMs plated on nanopatterned surfaces did not produce sarcomeres (data not shown).

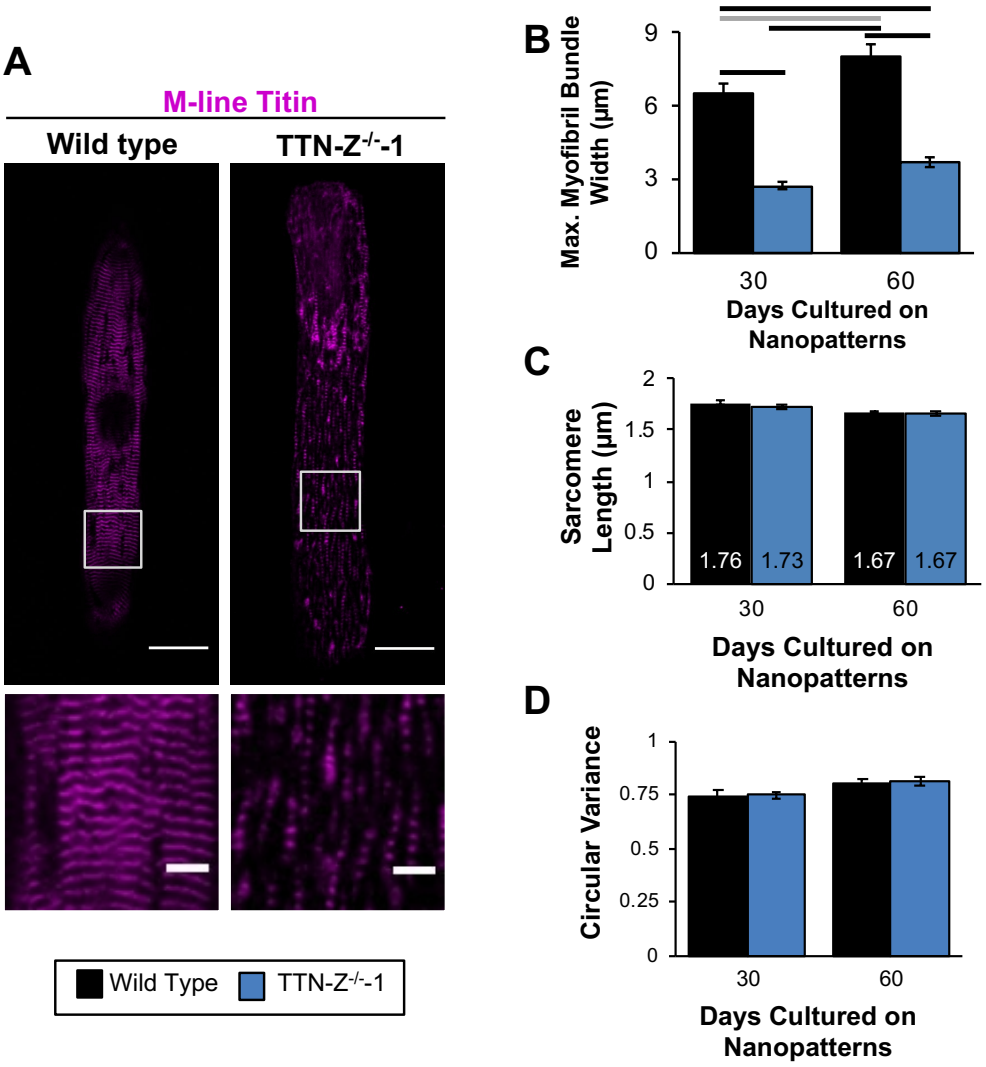

Figure 2.12. Morphology of WT and TTN-$Z^{-/-}$ CMs cultured on nanopatterned substrates. (A) Representative images of WT and TTN-$Z^{-/-}$-1 CMs cultured on nanopatterned substrates for 60 days. Top images: scale bar = 20μm; bottom images: scale bar = 5μm. White box in top image indicates region enlarged in bottom image. (B) TTN-$Z^{-/-}$ CMs have significantly smaller myofibril bundle widths at both time points studied compared to WT, but (C) sarcomere length is not different. (D) Circular variance is not significantly different between WT and TTN-$Z^{-/-}$ CMs at either time point studied. WT: n=43-57; TTN-$Z^{-/-}$: n=66-70; Error bars indicate standard error. Gray line connecting groups: $p<0.05$; black line connecting groups: $p<0.01$.

Interestingly, the TTN-$Z^{-/-}$-CMs exhibited higher multinucleation than wild type controls at the 60-day time point. Although overall rates of multinucleation were non-significantly

higher in TTN-Z$^{-/-}$ cells at this time point, there were striking incidences of cells that contained 4 or 5 nuclei (Figure 2.13). This was not observed in the wild type samples and may be explained by a nuclear role of full-length titin[32,33,92].

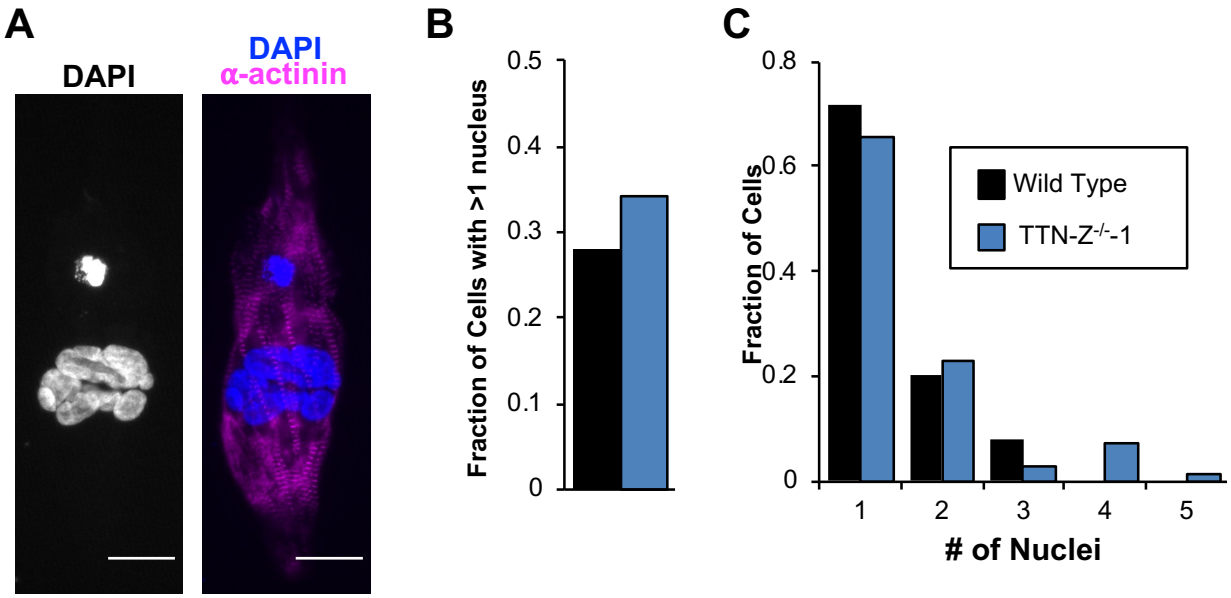

Figure 2.13. Nucleation of WT and TTN-Z$^{-/-}$ CMs cultured on nanopatterned substrates. (A) Example image of TTN-Z$^{-/-}$-1 CM cultured on nanopattern substrate for 60 days with unusual multinucleation. Scale bar = 20μm. (B) fraction of cells with more than one nucleus in WT and TTN-Z$^{-/-}$ CMs cultured on nanopatterns for 60 days and (C) histogram of how many nuclei cells in each group had.

2.4.6 *Live cell imaging to track sarcomere formation in WT and TTN-Z$^{-/-}$ CMs*

To better understand sarcomere formation in WT and TTN-Z$^{-/-}$ CMs, we transduced cardiomyocytes with a lentivirus expressing an mCherry-tagged α-actinin. The day after replating these cells, images were captured every 30 minutes for 12 hours to observe sarcomere formation dynamics in the cells. WT CMs exhibited α-actinin flow that was

circumferential near the edge of the cell and moves centripetally as the α-actinin condenses into fibers and then Z-disks at the center of the cell (Figure 2.14). This pattern of α-actinin flow was consistently observed among WT CMs, and has been previously reported by other groups[93]. During the 12 hours of imaging, the number of myofibrils and size of bundles of myofibrils grew at the center of the WT cells. In contrast, TTN-$Z^{-/-}$ CMs do not exhibit coordinated α-actinin flow, and the number of myofibrils and size of myofibril bundles decreased during the time studied. In fact, fibers of α-actinin and Z-body structures appear and disappear during the 30-minute intervals between captured images. Additionally, the myofibrils counted in the TTN-$Z^{-/-}$-1 cells were noticeably harder to distinguish from non-sarcomeric fibers of α-actinin due to their smaller size and subtle striations. This indicates that the Z-disks formed are very unstable, and normal myofibril bundling is impaired in TTN-$Z^{-/-}$ CMs.

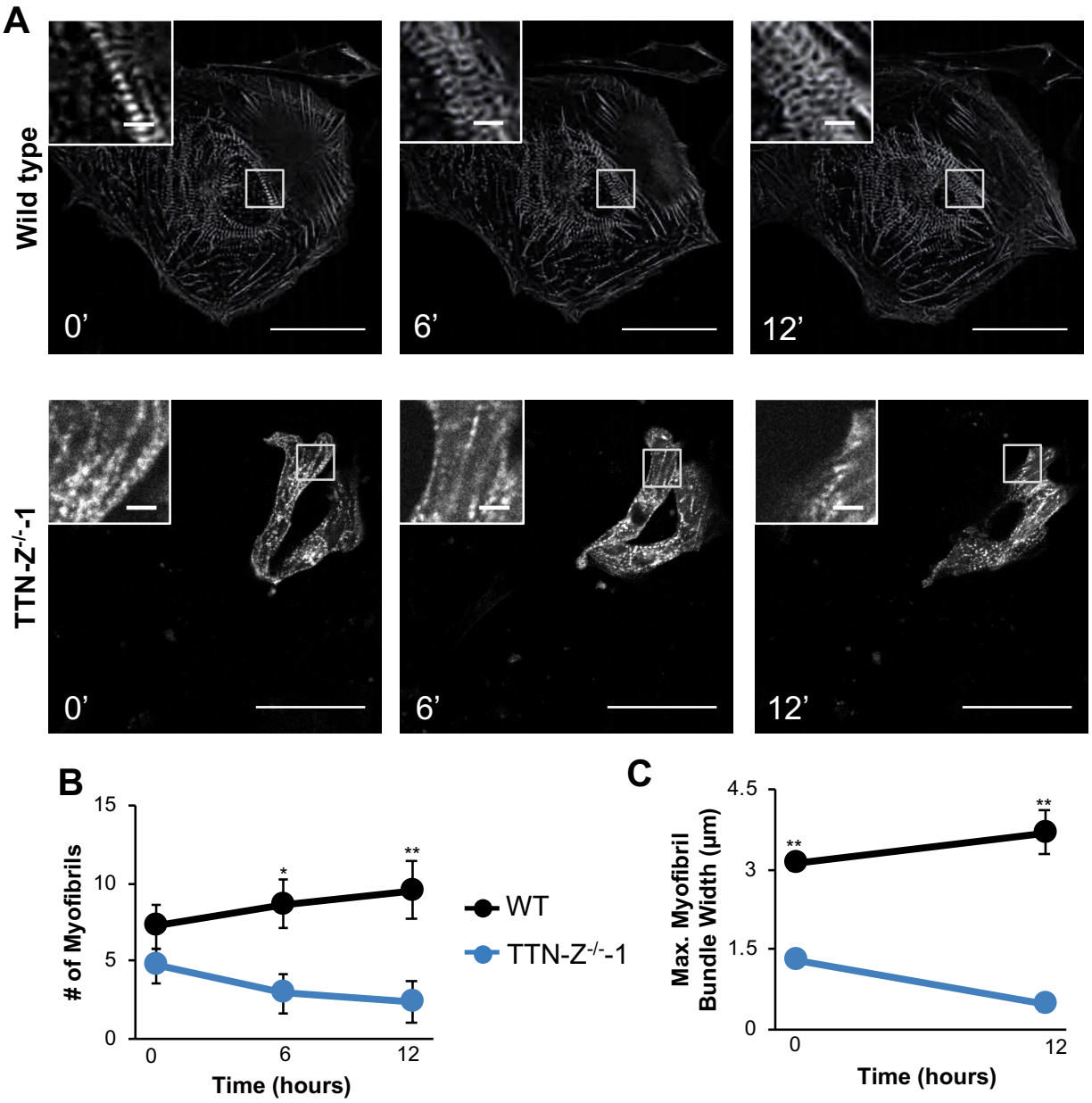

Figure 2.14. Live cell imaging of WT and TTN-$Z^{-/-}$ CMs. (A) Images taken at the beginning (0 hours), middle (6 hours) and end (12 hours) of time-lapse monitoring of sarcomere formation in WT and TTN-$Z^{-/-}$ CMs. Large images: scale bar = 50μm. Inset images: scale bar = 5μm. White box indicates region enlarged in inset image. (B) Quantification of the # of myofibrils in each type of cell at the beginning, middle, and end of videos. (C) Maximum myofibril bundle width and beginning and end of videos. WT: n=9; TTN-$Z^{-/-}$-1:

n=9. Error bars indicate standard error. *: p<0.05; **: p<0.01. Statistics were calculated for WT vs. TTN-$Z^{-/-}$-1 at that time point.

2.5 Discussion

To assess the role of titin in the formation of sarcomeres, we generated two hiPSC lines with homozygous mutations in constitutively expressed exons of *TTN*. Using immunofluorescence, we determined that TTN-$Z^{-/-}$ CMs express the Cronos titin isoform and are able to form sarcomeres. In contrast, TTN-$A^{-/-}$ CMs express what are likely N-terminal truncations of both full-length and Cronos titin and do not form myofibrils, as has been previously reported[67]. A previous study has reported that hiPSC-CMs carrying a homozygous truncation in the early I-band region of titin can also form sarcomeres. However, this mutation was in an exon that is only sometimes spliced in, and the sarcomere formation was associated with splicing out the mutated exon[67]. In the current study, the engineered Z-disk mutations are in a constitutively expressed exon, and sarcomere formation is associated with Cronos expression. Thus, we conclude that Cronos titin is sufficient for some sarcomere formation and the absence of both full-length and Cronos titin inhibits sarcomerogenesis. While a dominant-negative effect of the large N-terminal fragments in TTN-$A^{-/-}$-CMs cannot be ruled out from our data, experiments in zebrafish using a combined CRISPR/Cas9 knockout and morpholino knockdown implicate a deficiency of titin rather than a dominant-negative effect[86].

Our data are consistent with a structural role for titin, and in particular the C-terminal regions, in sarcomere formation. Signaling roles cannot be ruled out, however, given that

titin has multiple functions. For example, it is possible that the absence of the M-line region of titin disrupts signaling pathways dependent upon the titin kinase domain, which is involved in protein turnover and hypertrophy[23]. However, there are several pieces of evidence to suggest that this is not the case. Previously, a mouse embryonic stem cell line with a homozygous truncating mutation in the M-line region of titin preventing expression of both the kinase domain and C-terminal of the protein was found to lack sarcomeres when differentiated into cardiomyocytes[94]. However, a mouse model harboring a mutation that deletes the kinase domain but not the C-terminal of the protein was observed to form sarcomeres early in embryonic development[95]. This indicates that it may be the anchoring function of the carboxy terminus of titin, rather than the kinase function, that is required for sarcomere formation. This notion is consistent with our finding that cTnT and α-actinin protein are both diffusely present in TTN-A$^{-/-}$-CMs and indicates that sarcomeric proteins may still be expressed but cannot assemble into functional units. This suggests that signaling pathways relying on M-line titin may not be crucial for sarcomeric protein expression, while other functions of this domain, such as anchoring to myomesin, may be important for this stage of development.

TTN-Z$^{-/-}$-CMs produced lower force as both multicellular EHTs and single cells compared to wild type CMs, although calcium transients had similar magnitudes. Interestingly, the force deficit of individual cells was not as dramatic as in EHTs. One potential explanation for this could be the greater maturity of the cardiomyocytes in EHTs compared to monolayers[96], such that differences in the rate and extent of myofibril formation and bundling in cells become more pronounced. Another possibility is the summation of

cellular forces in series in tissue compared to single cell assays are compounding differences in force production, or that there is more compliance between coupled cells in TTN-$Z^{-/-}$ EHTs compared to WT. Additionally, if Cronos titin is expressed in different amounts depending on the maturity of the cardiomyocytes, this could affect the observed phenotype. The modulation of Cronos titin expression during human cardiac development will be addressed further in the following chapter of this dissertation.

The passive tension measured in individual TTN-$Z^{-/-}$-CMs was not significantly different compared to wild type cells (Figure 2.10). This could be explained by the immaturity of the contractile lattice in these cells, as fetal cardiac tissue has very low passive tension, especially from titin contributions[91,97,98]. Our recent studies have indicated that hiPSC-CMs matured for 80-100 days on patterned substrates have similar contractile properties to 74 day fetal tissue[70], and because the cells used in the micropost assay were significantly younger than this (35-40 days post differentiation) it is likely they were less mature. Thus, it is possible that the passive tension being measured from single-cell hiPSC-CMs on the microposts is predominantly due to other sources, such as intermediate filaments within the cells[99].

Morphological analysis of the myofibrils indicated that TTN-$Z^{-/-}$ had smaller myofibril bundle widths at the Z-disk compared to wild type (Figure 2.12), suggesting either smaller diameters of individual myofibrils or fewer myofibrils in parallel. Previously, conflicting data have been reported regarding the necessity of N-terminal titin for the formation of Z-disks[2,25], and the current study suggests that Z-disks are able to form in the absence of

the N-terminal of titin. However, the live cell images of cells expressing tagged alpha-actinin indicate the stability or bundling ability of these Z-disks is compromised, and they quickly degrade after they are formed. We found that sarcomere length was not significantly different between wild type and TTN-$Z^{-/-}$-CMs, which could indicate that full-length titin is not a major contributor to determining sarcomere length in cells at this stage of maturation. Supporting this notion, the length of I-band titin, which is missing in TTN-$Z^{-/-}$-CMs, does not influence thin filament length, even in adult mice[100].

It is striking that cardiomyocytes are able to form sarcomeres in the absence of full-length titin in TTN-$Z^{-/-}$-CMs, given that these mutations are not compatible with survival in rodent models[29,30]. We conclude that sarcomeres form in TTN-$Z^{-/-}$-CMs and not TTN-$A^{-/-}$-CMs due to the presence of Cronos titin, an isoform of titin that we demonstrate for the first time is expressed and integrated into myofibrils of human cardiomyocytes. Based on the findings of this study, it is likely that Cronos is a developmental isoform of titin. We conclude that Cronos titin is necessary for normal sarcomere development and function as full Cronos KO CMs produce lower contractile force and disarrayed sarcomeres. The discovery of this isoform in human samples motivates a closer look at how DCM is caused by truncating mutations in *TTN* and the potential role of Cronos in DCM pathogenesis. Elucidating the functions of Cronos titin in human development and DCM will be crucial for fully understanding heart development and disease.

2.6 Summary

To investigate the differences in titin truncation mutations in the Z-disk and A-band region of *TTN* we generated cell lines with homozygous mutations in each of these. We hypothesized that all of these mutations would be titin knock-out cell lines that would not form sarcomeres. Surprisingly, hiPSC-CMs carrying truncations in the Z-disk region of *TTN* produced cardiomyocytes that visibly contracted, which we determined was due to the expression of a novel isoform of titin called Cronos. Using a Cronos-specific antibody we demonstrate that a mixture of full-length and Cronos titin is expressed in wildtype cells, while cells carrying a Z-disk mutation only express Cronos. hiPSC-CMs carrying truncations in the A-band region of *TTN* did not produce sarcomeres and expressed large truncation products of full-length and Cronos titin. Cardiomyocytes that expressed only Cronos titin produced drastically reduced force in engineered heart tissues and as single cells compared to wildtype controls. Calcium transients of mutated cells were not significantly different compared to wildtype, but myofibril bundling was drastically impaired in Cronos-only cells. Live-cell imaging of cardiomyocytes transduced with an mCherry-tagged lentivirus showed that myofibrils in Cronos-only cells were incredibly dynamic, did not bundle, and were quickly degraded. In contrast, in wildtype cells consistently increased the number of myofibrils and myofibril bundle size over the observed time period. From these studies we conclude that Cronos titin can support some sarcomere formation, but that these sarcomeres are less stable compared to those containing full-length titin. We propose that Cronos titin may have important roles in human cardiomyocytes and suggest that further studies into its role are warranted.

Chapter 3. Cronos Titin is Expressed in Human Cardiac Tissue

3.1 Abstract

Cronos titin is a novel C-terminal isoform of titin that has been demonstrated to have an important role in zebrafish. Additionally, we presented data in Chapter 2 of this thesis indicating that Cronos titin is expressed in hiPSC-CMs and can support some sarcomere formation. However, it has never been definitively shown that Cronos titin is expressed in human cardiac tissue, and if the expression levels change during development. Using a combination of methylation data, transcript analysis, immunofluorescence, and western blots we demonstrate for the first time that Cronos titin is expressed in human cardiac tissue. Additionally, we show that Cronos titin is most highly expressed in fetal tissue, and that expression levels differ depending on the chamber of the heart. Cronos titin is also detected in adult left ventricular tissue, but apparently at lower levels than in fetal samples. These data indicate that Cronos titin is predominantly a developmental isoform and that its expression varies spatially within the heart. Future studies should more closely define the timeline of titin expression and investigate its expression in other chambers of the adult heart.

3.2 Rationale

The second aim of this thesis investigates the role of Cronos titin in human cardiomyocyte development and function. We hypothesize that Cronos titin is expressed most highly during development, during which time it assists in sarcomere formation, and at lower levels in adult cardiac tissue to stabilize the thick filament.

Although an internal promoter in *TTN* that would encode for Cronos titin has only been recently discovered and the presence of this protein has not been confirmed in mammals, there is some evidence of its expression pattern. Specifically, Cronos titin is hypothesized to contribute to or comprise what has previously been described as a titin degradation product, called T2. This band or set of bands on titin protein gels migrates more quickly than N2B or N2BA titin but is recognized by titin antibodies for A-band and M-line titin, the domains that would also be included in Cronos titin. Additionally, early titin extraction research found that T2 was likely to exist *in situ* within the myofibril and not solely as a proteolytic artifact of sample handling[101]. Based on the location of the proposed internal promoter within *TTN*, Cronos titin would be the same size as T2 (~2.2MDa)[86].

Interestingly, groups have previously noted that the abundance of T2 compared to N2B/N2BA in cardiac samples consistently changes during development. In rats[34,91,98], rabbits, mice, and pigs[97], T2 is most abundant during fetal and neonatal stages of development, and steadily decreases to a low but detectable level in adult cardiac tissue. Additionally, the T2 band has been observed to decrease in intensity compared to total titin in hiPSC-CMs as they are matured by extended culture[67]. Taken together, these data suggest that if Cronos titin is contributing to the T2 band observed in these assays, it is likely a developmental isoform. Given the isoform changes that occur in full-length titin and other sarcomere proteins during heart development and maturation, it is reasonable that Cronos titin would have a similarly dynamic expression profile during this process. We hypothesize that Cronos titin will be most highly expressed in fetal cardiac tissue.

3.3 Methods

3.3.1 *ChIP data*

Enriched regions were called with MACS2 broad peaks with default parameters. For fetal and adult tissue data, data was accessed and visualized on the human genome hg38 using ENCODE[102]. GEO accession numbers for samples analyzed are fetal heart: GSM772735; adult LV1: GSM910580; adult LV2: GSE101357.

3.3.2 *RNA isolation*

Fetal ventricle, atrium, and kidney samples (90-105 days old) were obtained from the Birth Defects Research Laboratory at the University of Washington and human adult heart failure samples were obtained from the laboratory of Dr. April Stempien-Otero in the Department of Cardiology at the University of Washington. Total RNA was isolated from tissue samples using RNEasy Fibrous Tissue kit (Qiagen). RNA from hiPSCs during and after cardiac differentiation following the monolayer directed differentiation protocol described previously was isolated using the RNEasy Mini kit (Qiagen). For samples collected 15 and 30 days following the start of the differentiation protocol, a small aliquot was fixed in 4% paraformaldehyde, stained for cardiac troponin T, and evaluated for cardiac purity by flow cytometry. Only samples with >70% cTnT+ cells were used.

3.3.3 *Reverse transcription and quantitative PCR*

cDNA was generated using M-MLV reverse transcriptase (Invitrogen) following the manufacturer's protocol and using 250-500ng of RNA per reaction, which was then diluted to a total volume of 200µL. Quantitative PCR was performed using 10µL SYBR Select Master Mix (Thermo Fisher), 1µL primer pairs (5µM each, sequences listed in Table A.3.), 3µL cDNA, and 6µL ddH_2O on a 7900HT Fast Real-Time PCR System (Applied BioSciences). Thermocycle programs consisted of 40 cycles each with 15 seconds at 95°C, 30 seconds at 60°C and a 30 second extension step at 72°C. Relative expression levels were determined using the $\Delta\Delta C_t$ method with HPRT as the internal housekeeping gene.

3.3.4 *Immunohistochemistry using Cronos titin antibody*

The custom Cronos titin antibody was used at a final concentration of 0.6µg/mL. Human fetal cardiac tissue samples were obtained from the Birth Defects Research Laboratory at the University of Washington, and normal human adult left ventricular samples were obtained from the National Disease Research Interchange. All samples were fixed in 4% paraformaldehyde. Before staining, paraffin-embedded samples were rehydrated and underwent antigen retrieval by boiling in citrate buffer (pH=6.0) for 20 minutes. All samples were blocked for one hour at room temperature in 1.5% normal goat serum and incubated in primary antibodies at 4°C overnight. Cronos titin was co-stained with either α-actinin (mouse monoclonal antibody, Abcam, 1:800 dilution) or β-myosin (mouse monoclonal hybridoma A4.951 supernatant, Santa Cruz Biotechnologies, 1:10 dilution).

The following day samples were incubated in AlexaFluor-conjugated goat-anti-mouse and goat-anti-rabbit secondary antibodies (Life Technologies, both diluted 1:100) for 1 hour at room temperature before coverslipping with Vectashield with DAPI (Vector Laboratories).

3.4 Results

3.4.1 *Epigenetic Marks in* TTN *of Fetal and Adult Cardiac Tissue*

As an initial inquiry into Cronos titin expression in human cardiac tissue we examined methylation marks in the *TTN* gene in whole day 91 fetal heart samples and two adult left ventricle samples (Figure 3.1). H3K3me3 marks, which are typically associated with available chromatin and active areas of the genome, were found in the fetal sample at the very 5’ end of *TTN* (at the full-length titin start site) and approximately two-thirds of the way down to the 3’ end (at the Cronos start site). In contrast, the adult samples only show a single prominent peak at the full-length titin start site. This suggests that Cronos titin is being expressed in fetal samples and is not expressed or is expressed at a lower level in adult tissue.

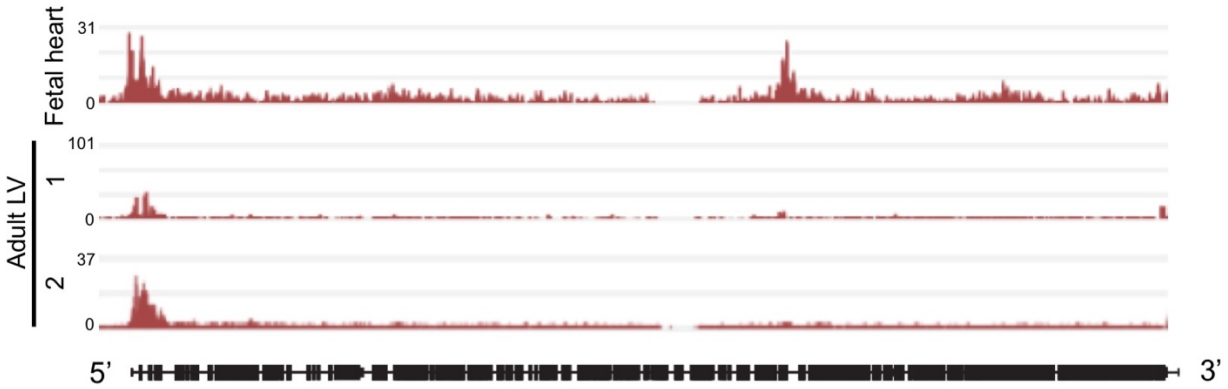

Figure 3.1. H3K4me3 enrichment of *TTN* in fetal and adult cardiac tissue samples. Enrichment is expressed as fold change over baseline and indicates the fetal heart has chromatin marks consistent with promoters at both the full-length and Cronos TSS, while the adult samples only show peaks at the full-length start site.

3.4.2 *Cronos Titin transcript is Expressed in Fetal and Adult Cardiac Tissue*

To establish expression patterns of Cronos titin in human development, we performed RT-qPCR on RNA isolated from adult and fetal human cardiac samples. The full-length titin primer pair spans the junction of exon 240-241 in *TTN*, both of which are constitutively expressed in full-length titin. The Cronos titin primer pair uses the same reverse primer in exon 241, but in conjunction with a forward primer that matches the Cronos-specific region encoded by the intron between exon 240-241. The PCR products from these reactions were visualized on a 0.8% agarose gel to confirm that only one product was amplified and sequenced to ensure that the intended sequence was being amplified (Figure 3.2).

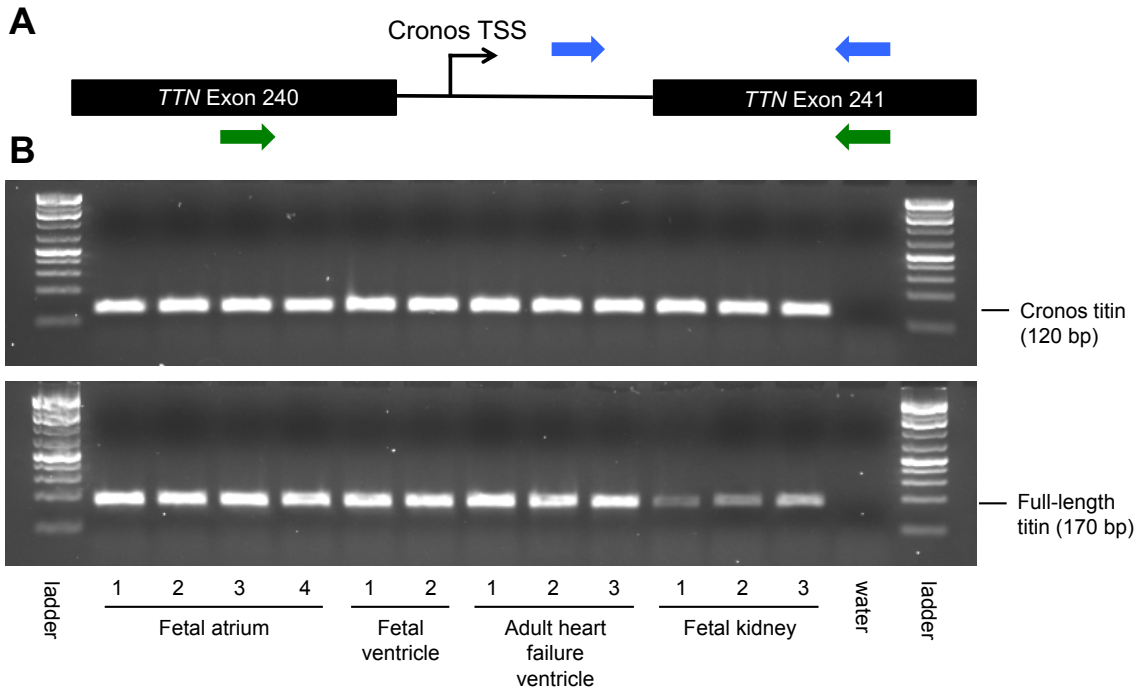

Figure 3.2. Transcript analysis strategy for Cronos and full-length titin. (A) Schematic showing primer locations to specifically amplify Cronos titin transcript (blue arrows) and full-length titin transcript (green arrows). (B) Visualization of PCR products by gel electrophoresis showing that only the intended product was amplified using each set of primers.

Cronos titin transcript was detected at low but measurable amounts in diseased adult cardiac samples and higher levels in fetal atrium and ventricle tissues (Figure 3.3). Full-length titin (N2B and N2BA) were detected at the highest levels in the adult samples and lower levels in fetal cardiac samples, similar to the cTnT expression pattern. None of the transcripts were detected in significant amounts in the fetal kidney samples, which were used as negative controls. From this we conclude that a higher proportion of total titin transcript being expressed is Cronos titin in fetal samples compared to adult.

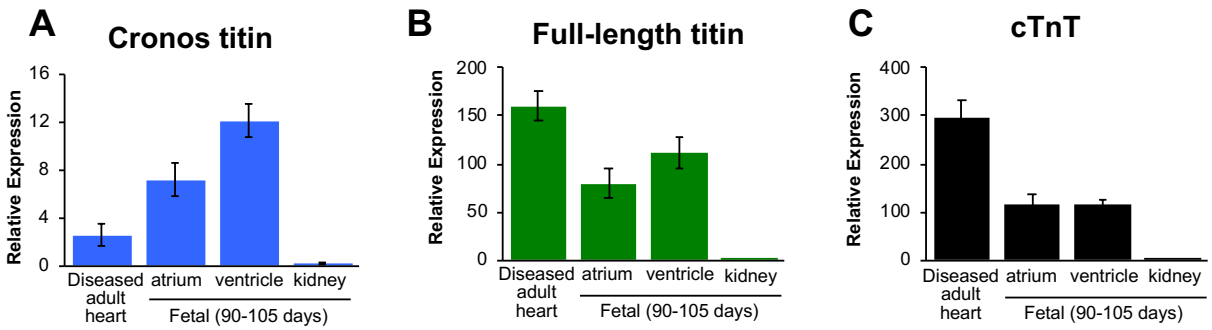

Figure 3.3. Transcript levels of titin and cardiac troponin T in adult and fetal cardiac tissue. (A) Cronos titin is most highly expressed in fetal ventricle and atrial tissue and expressed at detectable levels in diseased human adult heart tissue. (B) Full-length titin is highly expressed in diseased adult heart, and expressed at lower, similar levels in fetal atrium and ventricle samples. (C) Cardiac troponin T is expressed in a similar pattern to full-length titin. Disease human heart: N=3; fetal atrium: N=4; fetal ventricle: N=2; fetal kidney N=3. Error bars indicate standard error.

3.4.3 *Cronos Titin Protein is Expressed in Fetal Cardiac Tissue*

To further investigate expression patterns and localization of Cronos titin in human heart development, we performed immunohistochemistry on human fetal ventricle samples of four different ages (Figure 3.4). Staining for β-myosin heavy chain revealed clear striations in all samples studied, with increasing density and alignment of myofibrils in older fetal samples. Cronos titin staining was clearly visible throughout the tissue of day 54, 81, and 105 samples, but appears to drop off dramatically in Day 105 sample.

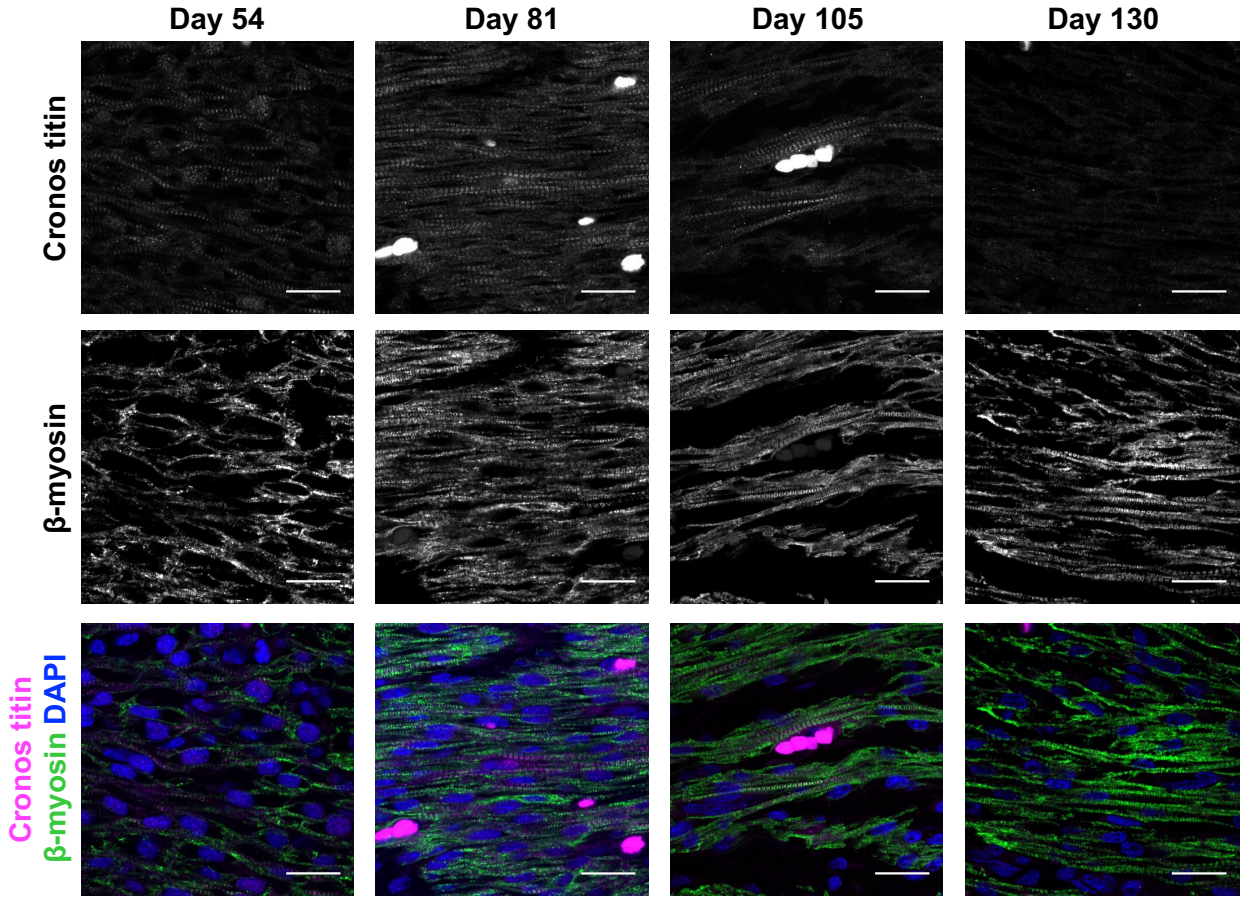

Figure 3.4. Low-magnification images of fetal ventricle samples stained for Cronos titin and β-myosin heavy chain. Scale bars = 20μm.

Magnified images show that Cronos titin is found within the sarcomere forming doublets corresponding to the edge of the β-myosin staining closest to the Z-disk, indicating the end of the thick filament (Figure 3.5). The observed staining is consistent with Cronos titin extending from just outside the thick filament to the M-band of the sarcomere, which is the expected position given the domains of titin it is expected to contain (i.e. short distal I-band, full A-band, and M-line regions). Myofibril density and Cronos titin staining was noticeably higher in the day 81 than the day 54 sample, and although myofibril density continues to increase in the day 105 and 130 samples as indicated by β-myosin staining,

Cronos titin expression drops off dramatically. Interestingly, Cronos titin staining was drastically reduced in the day 130 fetal sample, where it was only observed in isolated portions of the tissue. In sections that Cronos titin was observed, it remained in a striated pattern with the doublet pattern observed in earlier fetal samples. In the Day 81 sample, which stained for the highest level of sarcomeric Cronos titin, the antibody also picked up a less organized signal near the nucleus. This nuclear signal was not observed in any other fetal samples examined and did not appear in the hiPSC-CM samples stained for Cronos titin. This signal in the Day 81 samples could result from Cronos that has been translated in the endoplasmic reticulum and not yet integrated into sarcomeres. Alternatively, it could represent a nuclear role for Cronos titin, as has been reported for full-length titin[31,32,92,103].

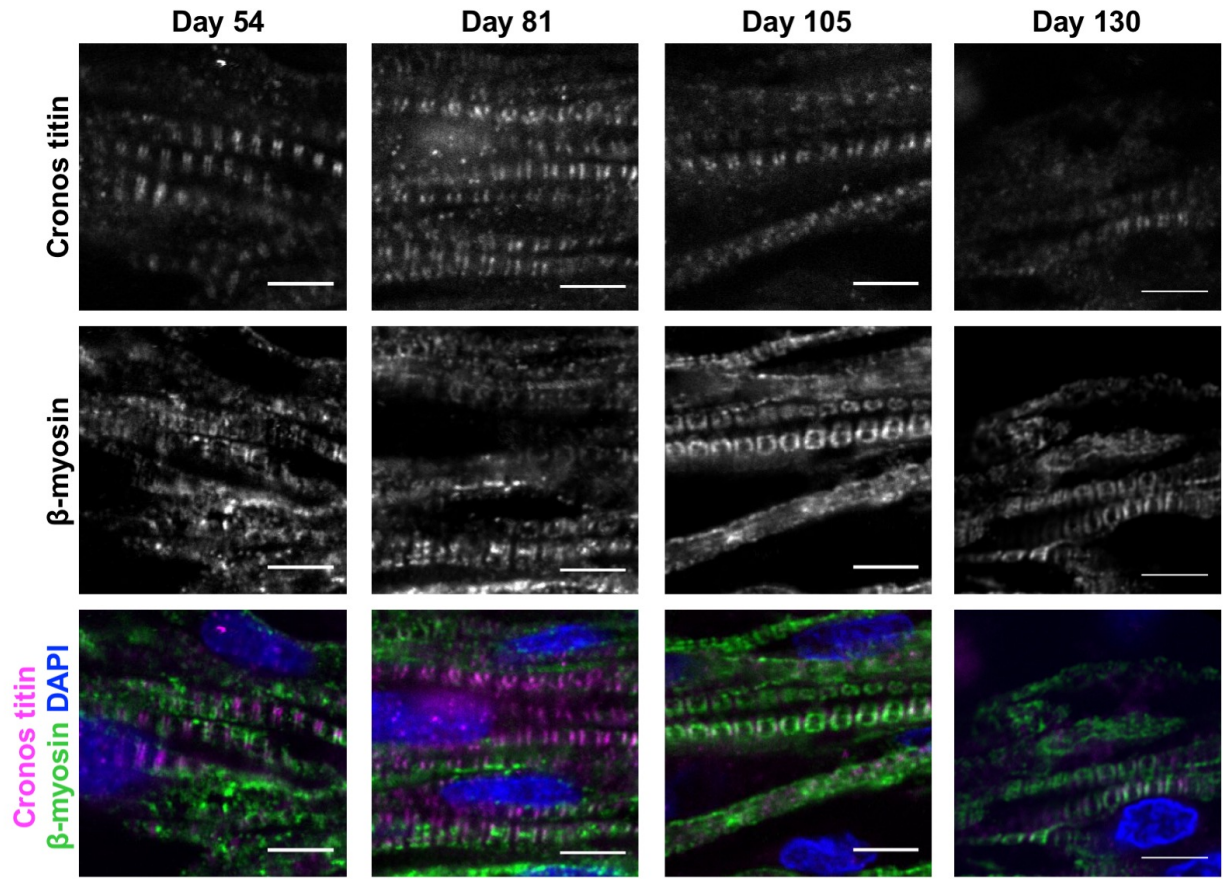

Figure 3.5. High-magnification images of fetal ventricle samples stained for Cronos titin and β-myosin heavy chain. Scale bars = 5μm.

To investigate spatial expression of Cronos titin in the developing heart the four chambers of a day 117 fetal heart were stained for Cronos titin and β-myosin heavy chain (Figure 3.6). The left ventricle showed staining patterns similar to the day 107 and 115 samples discussed above with relatively high myofibril density and alignment indicated by β-myosin heavy chain but only patches of Cronos titin staining. Staining in the right ventricle shows a similar density and organization of β-myosin heavy chain, but with a barely detectible level of Cronos titin. In contrast, both atria stain strongly for Cronos titin, the left atrium more so than the right. As expected, β-myosin heavy chain does not stain the left

atrium, and only sporadically stained the right atrium. These data indicate that Cronos titin expression varies between chambers of the heart.

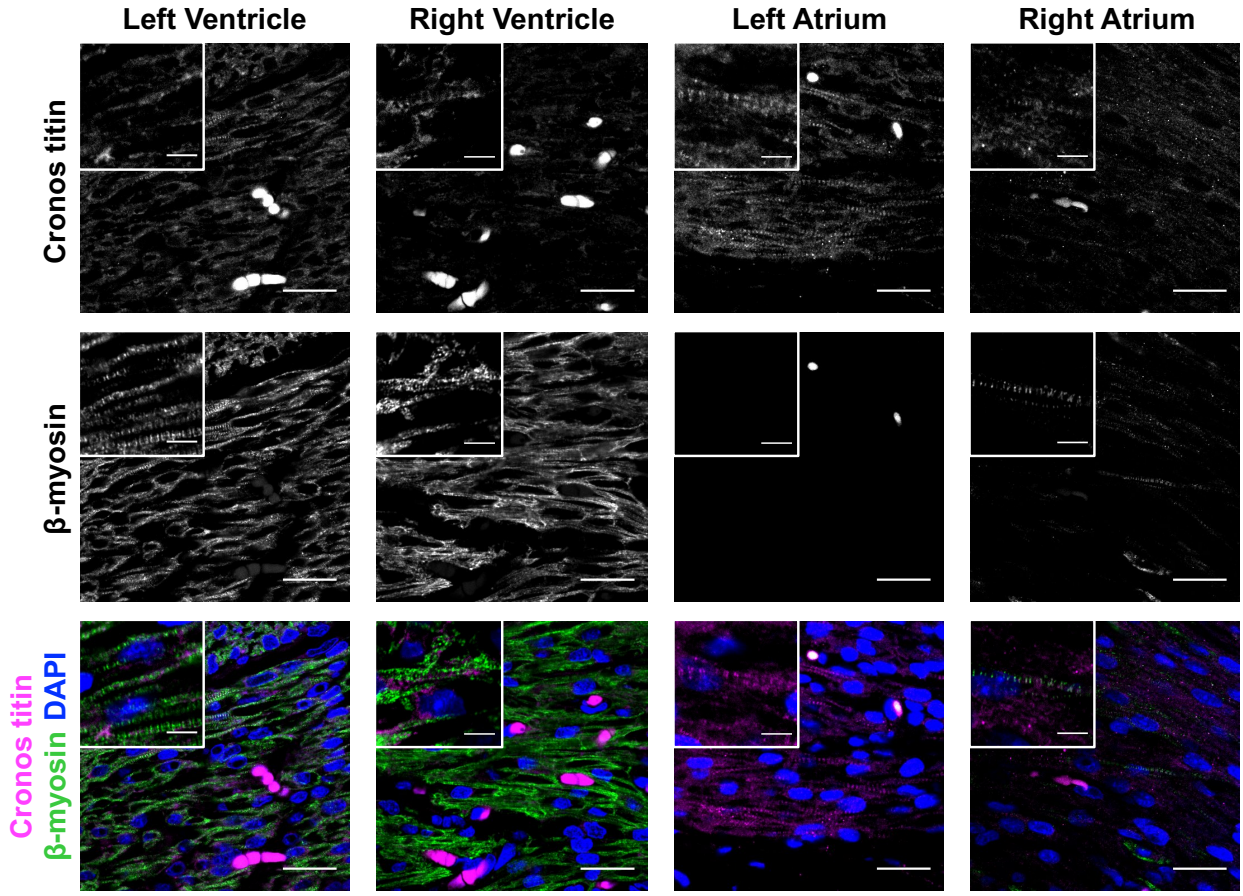

Figure 3.6. Four chambers of day 117 fetal heart stained for Cronos titin and β-myosin heavy chain. Larger images: scale bars = 20μm; smaller images: scale bars = 5μm.

3.4.4 *Evidence of Cronos Titin Expression in Adult Cardiac Tissue*

To investigate the expression of Cronos titin in adult cardiac tissue we stained left ventricular samples for Cronos titin and β-myosin heavy chain (Figure 3.7). As expected, β-myosin heavy chain staining showed dense and well-organized sarcomeres in the sample. Cronos titin staining was very faint in these samples and did not localize to the

edge of the thick filament as was observed in fetal samples. It is difficult to determine if the fluorescent signal observed in these samples is in fact from a positive Cronos titin stain, or autofluorescence of the myofibrils, although it does appear to be brighter than a secondary-only control sample.

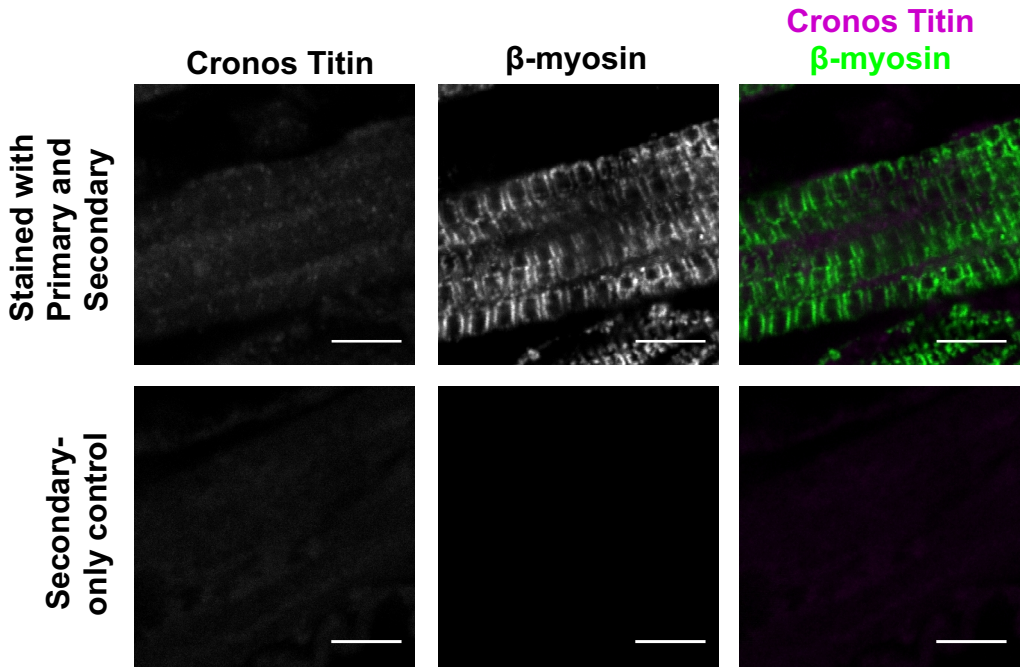

Figure 3.7. Human adult left ventricle samples stained for Cronos titin and β-myosin heavy chain. Scale bars = 5μm.

However, western blot analysis indicates that Cronos titin is present in human heart samples (Figure 3.8). The Coomassie-stained gel shows the expected expression of more N2B than N2BA as well as distinct T2 bands. When this sample was used in a western blot to probe for Cronos titin, the T2 band stained strongly. This indicates that although there is not a clear Cronos titin signal in the immunohistochemistry of adult left

ventricle sample there is still strong evidence Cronos titin is being expressed in the human adult heart.

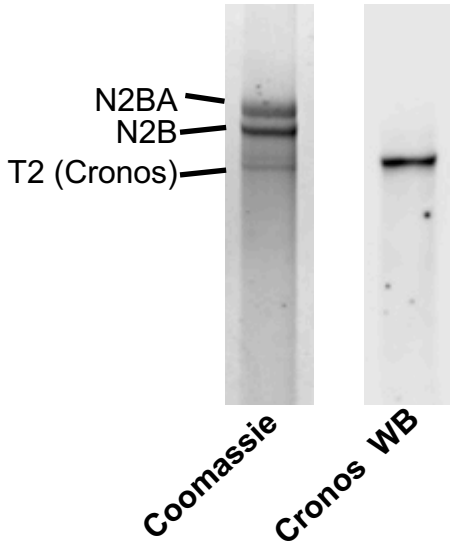

Figure 3.8. Human adult heart sample run on vertical agarose gel to characterize titin expression. Left is a Coomassie-stained gel, and right is the western blot (WB) using the Cronos titin-specific antibody.

3.4.5 *RT-qPCR during hiPSC-CM directed differentiation*

To determine if the Cronos titin transcript is detectable in hiPSC-CMs and establish its expression pattern during directed differentiation, we performed RT-qPCR to determine Cronos and full-length titin levels during the first week of differentiation and in samples 30 days after differentiation (Figure 3.9). We found that the Cronos titin transcript is not present in undifferentiated hiPSCs and is first detectable starting 5 days after the start of differentiation. Similar to the pattern for full-length titin and cTnT, Cronos titin is then upregulated on day 7 and 30 following the start of differentiation. This suggests that

Cronos titin transcript is present in very early stage human cardiomyocytes, although not in pluripotent stem cells or early mesoderm, similar to other sarcomere proteins.

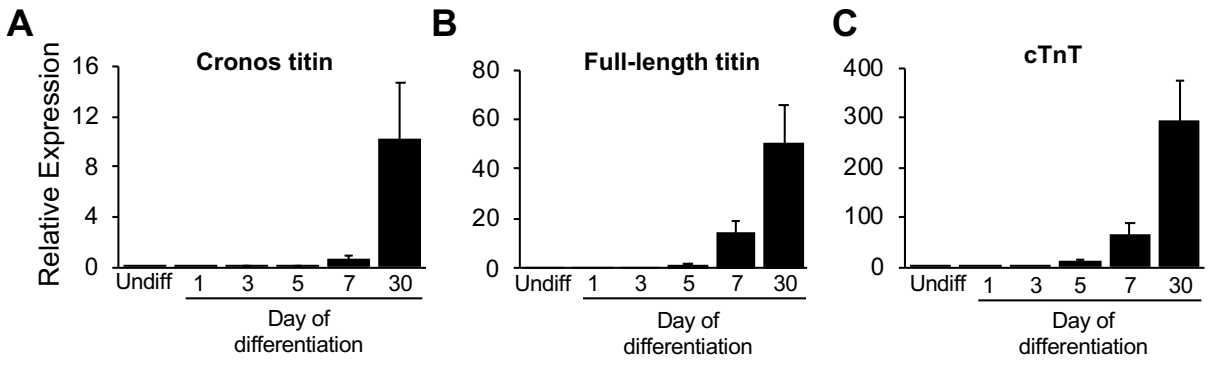

Figure 3.9. Transcript levels of titin and cardiac troponin T in hiPSC during cardiac differentiation. (A) Cronos titin transcript increases in a similar fashion to both (B) full-length titin and (C) cardiac troponin T (cTnT). For all: N = 3; error bars indicate standard error. All values are expressed as relative expression normalized to HPRT.

3.5 Discussion

To investigate the expression levels of Cronos titin during human development we studied a number of fetal and adult samples on the genome, transcript, and protein level. Fetal samples showed a similar H3K4me3 profile to hESC-CMs with distinctive peaks at the full-length and Cronos titin start sites, indicating open chromatin at both sites. This genome-level indication of the Cronos titin TSS being more active in fetal cardiac tissue than adult has been reported previously by ChiP-Seq data[29], but interestingly DNAse-Seq has also indicated that there is a prominent promoter peak at the Cronos titin TSS in *TTN* in adult tissue[86], which has not been observed in chromatin methylation. This mixed message of expression in fetal compared to adult heart samples was observed in other

assays used to compare Cronos titin. Fetal samples showed the highest expression of Cronos transcript and protein, while adult samples showed lower but still detectable levels in both assays. The fetal ventricular levels of Cronos titin transcript were nearly double that observed in diseased adult human heart, and atrial samples were lower than ventricular but still higher than in adult samples. The age of the samples used for transcript analysis (day 90-105) corresponds with the samples that stained strongly for Cronos titin protein (day 105). Interestingly, the fetal ventricle samples that were 81 days old stained the most strongly for Cronos titin, with day 54 and 105 samples also showing distinct, but lower, Cronos titin signals. It would be informative to perform RT-qPCR analysis on a wider range of ages of fetal tissue to determine if a similar trend occurs in the transcript as is observed in immunofluorescence and perform protein gel electrophoresis and western blots on fetal samples of a range of ages to quantify the differences in Cronos titin protein.

Additional differences were observed in Cronos expression based on chamber of the fetal heart studied. Both ventricles of a day 117 heart stained spottily for Cronos titin, which is consistent with the pattern observed in day 105 and day 117 fetal ventricular samples. Interestingly, both atria stained strongly for Cronos titin. Although this observation contradicts RT-qPCR data from fetal samples, this may be explained by a difference in age between the samples (day 90-105 for RNA, day 117 for immunohistochemistry). Overall, this data indicates that Cronos titin expression varies based on chamber of the heart, similar to other sarcomeric proteins[104,105], including full-length titin[106]. It would be informative to compare changes in Cronos titin expression with these other isoforms that

are differentially expressed in areas of the heart, particularly those proteins found in the thick filament (myosin heavy and light chains). Because Cronos titin contains mostly domains of titin that are known to interact with the thick filament, it could be that Cronos titin expression associates other specific thick filament isoforms. In fetal and adult tissue, the differences in titin isoform expression between N2BA and N2B explain changes in passive tension between atrial and ventricular tissue[34,91,97,106]. It would be interesting to quantify the differences in Cronos expression between chambers and age of tissue and correlate this with differences in mechanical properties as well. Further studies are necessary to quantify these differences and understand if this difference changes during different stages of development and if it remains in adult tissue.

Studies of adult tissue samples present conflicting evidence regarding Cronos titin expression. H3K4me3 enrichment does not indicate that this marker is present on the Cronos titin TSS in adult LV tissue, and immunostaining does not show a clear Cronos signal. However, a western blot of adult tissue shows a clear Cronos titin band. This may indicate that Cronos titin is expressed in low amounts in adult left ventricular tissue that is not detectable by immunostaining, particularly because of the high autofluorescence of myofibrils. Alternatively, it could indicate that Cronos titin is expressed in chambers of the adult heart that are not the left ventricle, as in the day 115 fetal heart studied.

Overall, staining of human tissue indicated that Cronos titin is most highly expressed in early fetal cardiac tissue, suggesting that it is predominantly a developmental isoform. The T2 band, which we demonstrate includes Cronos titin, has been shown to

consistently decrease in intensity in cardiac samples as animals mature[91] and as hiPSC-CMs are aged in culture[67], supporting the notion that Cronos titin is predominantly a developmental isoform. However, because of variability in expression based on chamber within the fetal heart, further analysis is necessary. This putative role of Cronos titin as a developmental isoform also may help explain functional differences observed in Chapter 2 where the functional deficit observed in TTN-Z$^{-/-}$ EHTs compared to WT was greater than in single cells. Because hiPSC-CMs mature more rapidly in three-dimensional culture compared to two-dimensional[107], cells in the EHTs may be more mature and thus expressing more full-length titin, while single cells on microposts are younger and thus may be expressing mostly Cronos titin.

It would additionally be informative to investigate Cronos titin expression in diseased hearts. It has been previously demonstrated that an array of embryonic sarcomeric genes are upregulated in the adult heart during disease[108]. Given our current understanding of Cronos as a developmental isoform, it may be upregulated during disease along with these other genes. This could be particularly interesting in the context of truncated-titin DCM. If Cronos titin is upregulated during diseased states, this could explain why truncations downstream of the Cronos titin start site are more pathogenic than those upstream of the start site. This hypothesis requires further investigation to understand Cronos expression during diseased states and its role in DCM.

3.6 Summary

In this chapter we investigate the expression of Cronos titin in developing and adult human cardiac tissue. This is, to our knowledge, the first time that Cronos titin has been detected in human cardiac tissue. We demonstrate that histone methylation marks associated with promoters are present at the Cronos titin TSS in fetal cardiac tissue but not adult. Additionally, using RT-qPCR we show that the Cronos titin transcript is present at higher levels in fetal atrial and ventricular tissue compared to adult. Similar results were obtained by immunofluorescence of a range of ages of fetal ventricular tissue, which all stained for Cronos titin to varying degrees. Staining of all four chambers of a day 117 fetal heart indicate that Cronos is most highly expressed in the atria at this time point, although Cronos was still detectable in the ventricles. This indicates that Cronos titin varies both spatially and temporally within the heart. Finally, although Cronos immunofluorescence of an adult left ventricle did not show a clear staining pattern, a western blot for Cronos revealed that some protein is expressed in adult tissue. Taken together, these data indicate Cronos titin is predominantly a developmental isoform. Future studies should more closely map the spatiotemporal pattern of Cronos expression and investigate if it is re-upregulated as part of the fetal gene profile expressed during heart failure.

Chapter 4. Cronos Titin is Necessary for Proper Sarcomere Formation

4.1 Abstract

In the previous two chapters of this thesis we have demonstrated that Cronos titin supports some sarcomere formation in stem cell-derived cardiomyocytes and is expressed in both fetal and adult cardiac tissue. Additionally, it appears to be regulated to change expression levels depending on developmental stage and location within the heart. This suggests that Cronos titin plays a specific role in the sarcomere, an idea which we test by generating two Cronos knock-out (KO) hiPSC lines. Both cell lines differentiated into high-purity populations of cardiomyocytes that did not express Cronos titin but did express full-length titin at similar levels to wild type cells. Engineered heart tissues constructed with Cronos KO cells produced approximately half the force of wildtype samples, although calcium transients of single cells were not significantly different than wildtype. The myofibrils of Cronos KO EHTs were significantly more disarrayed than wildtype controls. This indicates that in human cardiomyocytes Cronos titin is necessary for proper sarcomere formation and function.

4.2 Background & Motivation

We have previously demonstrated that Cronos titin is expressed in human stem-cell derived cardiomyocytes, and human fetal and adult cardiac tissue. Analysis of expression levels by RT-qPCR and immunohistochemistry show that Cronos titin levels differ depending on developmental stage and chamber of the heart, indicating that Cronos may play important roles in heart development. Additionally, the promoter-associated

chromatin mark H3K4me3 appears on the Cronos start site during cardiac differentiation of human stem cells and in fetal cardiac samples studied but is not observed in adult tissue samples. This provides further indication that Cronos titin is expressed in a controlled manner so as to play a specific role in cardiogenesis and cardiac development. However, the potential function of Cronos titin in the sarcomere remains unknown.

Cronos titin is composed of distal I-band, A-band, and M-line regions of full-length titin, as indicated by the location of the start site within *TTN*, western blots, and immunohistochemistry. The presence of these domains gives us some indication of possible functions of Cronos titin within the sarcomere based on the function of full-length titin. The I-band of full-length titin acts as a tunable spring to provide passive tension to the sarcomere and cardiomyocyte as a whole. It can be adjusted based on alternative splicing (i.e. shifting between the more compliant isoform N2BA and the stiffer isoform N2B) and post-translational modifications. However, the regions of titin that are differentially spliced and modified to adjust passive tension are proximal to the Cronos titin start site. Additionally, the ability of full-length titin to act as a spring in the sarcomere relies upon anchoring at either end of the spring, in the Z-disk and the thick filament/M-line. Cronos titin does not contain the Z-disk domains of full-length titin, and our immunohistochemistry has indicated that the N-terminal of the protein rests on the edge of the thick filament. This suggests that although Cronos titin does contain some I-band regions it is likely not contributing to the passive tension of the sarcomere.

The A-band region of titin is known to interact with the thick filament, although its role is still unclear. It is proposed to have a role in thick filament patterning[17–19,109,110], although this has been discounted by some groups[20,21]. Additionally, it has been proposed that titin domains in the A-band are responsible for patterning of myosin binding protein-C (MYBPC) in the C-zone of the thick filament[109]. Although the role of titin in establishing patterning within the A-band is controversial, it is well-known that this region interacts with myosin heavy chain[111] and MYBPC[112], and it is likely that Cronos titin also has these interactions given its presence in the A-band.

Cronos titin also includes the M-band region of full-length titin, which anchors to myomesin and plays important roles in cell signaling and protein turnover[22,23]. When the M-band is deleted in mouse cardiomyocytes, they are initially able to form small myofibrils but these are not able to bundle properly and degrade[113]. Of particular importance in the M-band is the tyrosine kinase domain, which acts a mechanical sensor to induce protein turnover in response to stretch in the sarcomere[23,114]. When this region is specifically deleted in mice, their hearts develop hypertrophy and reduced contractility, indicating it is of central importance to maintaining correct cardiac homeostasis[115]. Additionally, a reduction in titin tyrosine kinase signaling has recently been proposed to account for some functional abnormalities of cardiomyocytes carrying DCM-associated titin truncations, specifically through blunting of the β-adrenergic response[77]. Because Cronos titin also includes the M-band and tyrosine kinase domains, it is likely to also contribute to these important roles in the sarcomere.

Interestingly, nearly every domain present in Cronos titin is also present in full-length titin. This redundancy suggests that Cronos titin may not have an important, distinct role in sarcomere formation and function. In fact, it has been suggested that the existence of Cronos titin is merely a leftover from when two distinct C- and N-terminal giant sarcomeric proteins fused to form titin along the evolutionary timeline, acting essentially as a vestigial protein[86]. However, the evidence we have shown indicating that Cronos is expressed in a distinct pattern from full-length titin, including both during development and spatially within the heart, indicate that it may have a distinct role. We hypothesize that knocking out Cronos titin in human cardiomyocytes will caused a reduction in force production and perturb the sarcomeric structure. To test this hypothesis, we have generated two hiPSC lines in which Cronos titin is specifically knocked out, but full-length titin is unaffected. These Cronos KO hiPSC differentiate into visibly contract cardiomyocytes, and form sarcomeres as detected by immunostaining. When engineered heart tissues were made with these cells, the recorded active force was significantly decreased compared to wild type, which we determine is due to markedly increased sarcomeric disarray in the absence of Cronos titin. We conclude that Cronos titin is necessary for proper sarcomere formation and function in cardiomyocytes.

4.3 Methods

4.3.1 *Gene Editing to Knock Out Cronos Titin in hiPSC*

The gene editing to generate the Cronos knock out hiPSC lines was done in collaboration with the Institute for Stem Cells and Regenerative Medicine Gene Editing Core at the

University of Washington. To target Cronos, an sgRNA was designed using the online CRISPR design tool (crispr.mit.edu) to target the Cronos-specific region preceding Exon 241 of *TTN*. This gRNA was ligated into PX458 (Cas9-2A-GFP)[62] and 1 million WTC cells were transfected with 5µg of plasmid using Amaxa nucleofector (Human Stem Cell kit 2) in presence of ROCK inhibitor. The next day, cells were FACS sorted for the GFP positive population. Individual colonies were hand-picked several days later and plated into 96 well plates. DNA was extracted using Quick Extract DNA extraction solution (Epicentre) and nested PCR was performed. The PCR product was purified using EXO-SAP enzyme (ThermoFisher) and sent for Sanger sequencing analysis (Genewiz). For all cell lines generated, colonies with homozygous or compound heterozygous mutations causing premature stop codons were also screened for mutations in the top 5 genes predicted to be most susceptible to off-target effects. Primers were designed using Primer-BLAST[81] and used to amplify the area surrounding the predicted off-target cut site using GoTaq Flexi DNA polymerase (Promega) and sequenced using the forward primer (see Table S3 for accession numbers and primers). Mutant cell lines were cryopreserved and karyotyped (Diagnostic Cytogenetics Inc, Seattle, WA).

4.3.2 *Cronos titin immunostaining*

Cronos KO hiPSC-CMs were replated at day 30 post-differentiation onto fibronectin-coated (5µg/mL, Life Technologies) flat glass coverslips at 100,000 cells/coverslip. Seven days after replating cells were fixed in 4% paraformaldehyde for 10 minutes at room temperature. Cells were then rinsed in PBS three times for five minutes each and then blocked in 1.5% normal goat serum for one hour at room temperature. Cells were

incubated in primary antibodies diluted in blocking buffer at 4°C overnight. The Cronos titin primary antibody (Life Technologies) was diluted to a final concentration of 0.65µg/mL in 1.5% normal goat serum, and the α-actinin primary antibody (Abcam) was diluted 1:800 in 1.5% normal goat serum. Secondary-only controls were only incubated in the α-actinin primary antibody. The following day, cells were washed three times in PBS for five minutes each and then incubated with AlexaFluor-conjugated goat anti-mouse and anti-rabbit antibodies (Life Technologies) diluted 1:100 in 1.5% normal goat serum for 1 hour at room temperature. Cells were washed three times in PBS for five minutes each and then mounted onto glass slides using Vectashield with DAPI (Vector Laboratories). Images were captured using a Yogokawa spinning-disk confocal (Institute for Stem Cells and Regenerative Medicine Garvey Imaging Core, University of Washington) with stained WT cells used as a control.

4.3.3 *Engineered heart tissue immunohistochemistry and image processing*

After imaging for force production calculations, engineered heart tissues (EHTs) we relaxed in 150mM KCl and fixed on their posts in 4% paraformaldehyde for 15 minutes at room temperature. Tissues were then washed in PBS and stored in 30% sucrose overnight. The following day EHTs were cryoembedded in OCT using an ethanol-dry ice bath and sectioned. Slides were immediately washed in PBS for 5 minutes each and then blocked in 1.5% normal goat serum for one hour at room temperature. Slides were incubated overnight at 4°C in α-actinin primary antibody (Abcam) was diluted 1:800 in 1.5% normal goat serum. The following day, slides were washed in PBS three times for

five minutes each and then incubated at room temperature for an hour in AlexaFluor488-conjugated goat-anti-mouse (Life Technologies) diluted 1:100. After washing three more times in PBS for five minutes each, slides were coverslipped with Vectashield with DAPI (Vector Laboratories). Slides were imaged using a Yogokawa spinning-disk confocal (Institute for Stem Cells and Regenerative Medicine Garvey Imaging Core, University of Washington) and a 60x oil objective. For each tissue, 2-3 images were taken, each of a 3x3 grid of fields of view. Cytospectre was used to evaluate sarcomere length (wavelength mode) and circular variance of the mixed component[116].

4.3.4 *Statistical analysis*

For assays with two groups, student's t-tests were performed in Excel. For assays with more than two groups, one-way ANOVAs were performed in MATLAB using the "anova1" function, and if the returned p-value was less than 0.01 Tukey's post-hoc analysis was performed using the "multcompare" function. Adjusted p-values were computed using the Benjamini & Hochberg method[89].

4.4 Results

4.4.1 *Generation of Cronos Knock Out hiPSC Lines*

To knock out Cronos titin without affecting the full-length titin protein the premature stop codon must be within the Cronos-only region of *TTN* upstream of exon 241, a stretch of only 35 base pairs. This small region limited the possibilities for sgRNA design for CRISRP/Cas9 use, which requires an "NGG" PAM site in the targeted area downstream

of the sgRNA match site[62]. To increase the number of sgRNA we could test for cutting efficiency, we investigated CRISPR systems other than the WT Cas9, which have different requirements for PAM sites. A summary of Cas variants tried are summarized in Table 4.4. In the end, the wildtype Cas9 sgRNA tested was the only that showed any cutting efficiency at the intended locus, and thus the two knock-out cell lines were both generated using this sgRNA.

Table 4.4. Cas variants and sgRNA tested for Cronos titin knock out

Cas name	**PAM site**	**gRNA Sequence (5' to 3')**	**Demonstrated cutting efficiency?**
SaCas9[62]	ACGAGT	tttcttccctctcgaaaag	No
SpCas9 VQR variant[65]	CGA	ttcttccctctcgaaaag	No
SpCas9 WT	NGG	GATCCGCCCAAAAACCCTGA	Yes

Both Cronos KO cell lines generated were compound heterozygotes that are predicted to produce short Cronos titin truncation products (

Figure **4.1**, 15 and 58 residues respectively). Additionally, because all generated mutations are at least 5 base pairs upstream of the intron-exon border, these mutations should not affect the full-length titin transcript.

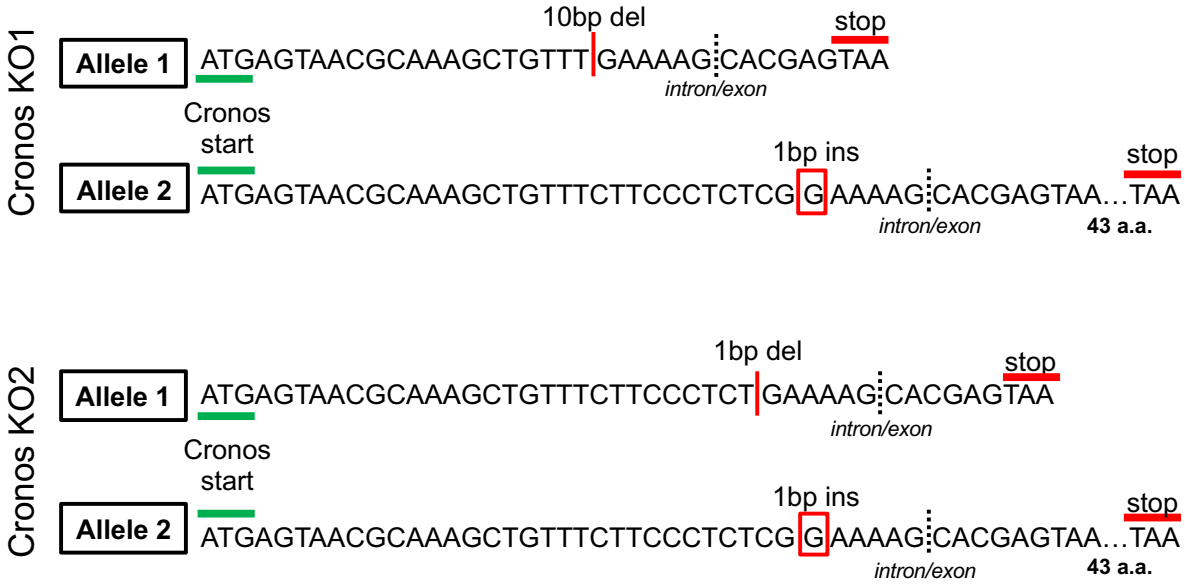

Figure 4.1. Overview of Cronos titin knock-out genotypes.

4.4.2 *Titin Protein Expression of Cronos Knock Out hiPSC-CMs*

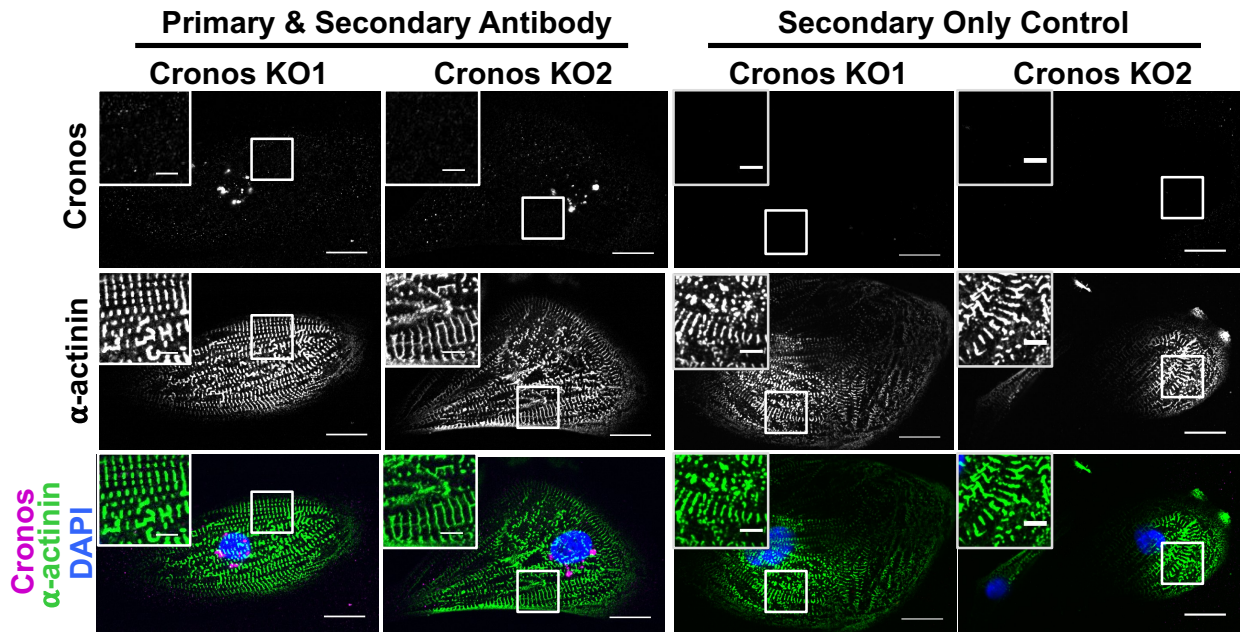

Figure 4.2. Cronos titin staining of Cronos KO CMs. Staining for Cronos titin indicates that none is integrated into sarcomeres in Cronos KO CMs. A perinuclear signal is present

in Cronos KO CMs that is not observed in secondary-only controls. Large images: scale bars = 20μm; inset images: scale bars=5μm. White box indicates region enlarged in inset image.

Both Cronos KO hiPSC lines differentiated into visibly beating CMs, and immunostaining for Cronos titin indicated that none was integrated into sarcomeres (Figure 4.2). Interestingly, there was some staining for Cronos around the nuclei of the Cronos KO CMs, which was not present in the secondary-only controls. This may indicate that a small Cronos truncation product is still being produced in these cells but is remaining in the endoplasmic reticulum or could be non-specific binding (although these same patterns do not appear in WT CMs stained for Cronos titin), and likely does not function as normal Cronos titin does. Staining for domains present in full-length titin were still present and correctly localized relative to alpha-actinin, indicating that as expected full-length titin is not affected by the Cronos KO mutations (Figure 4.3).

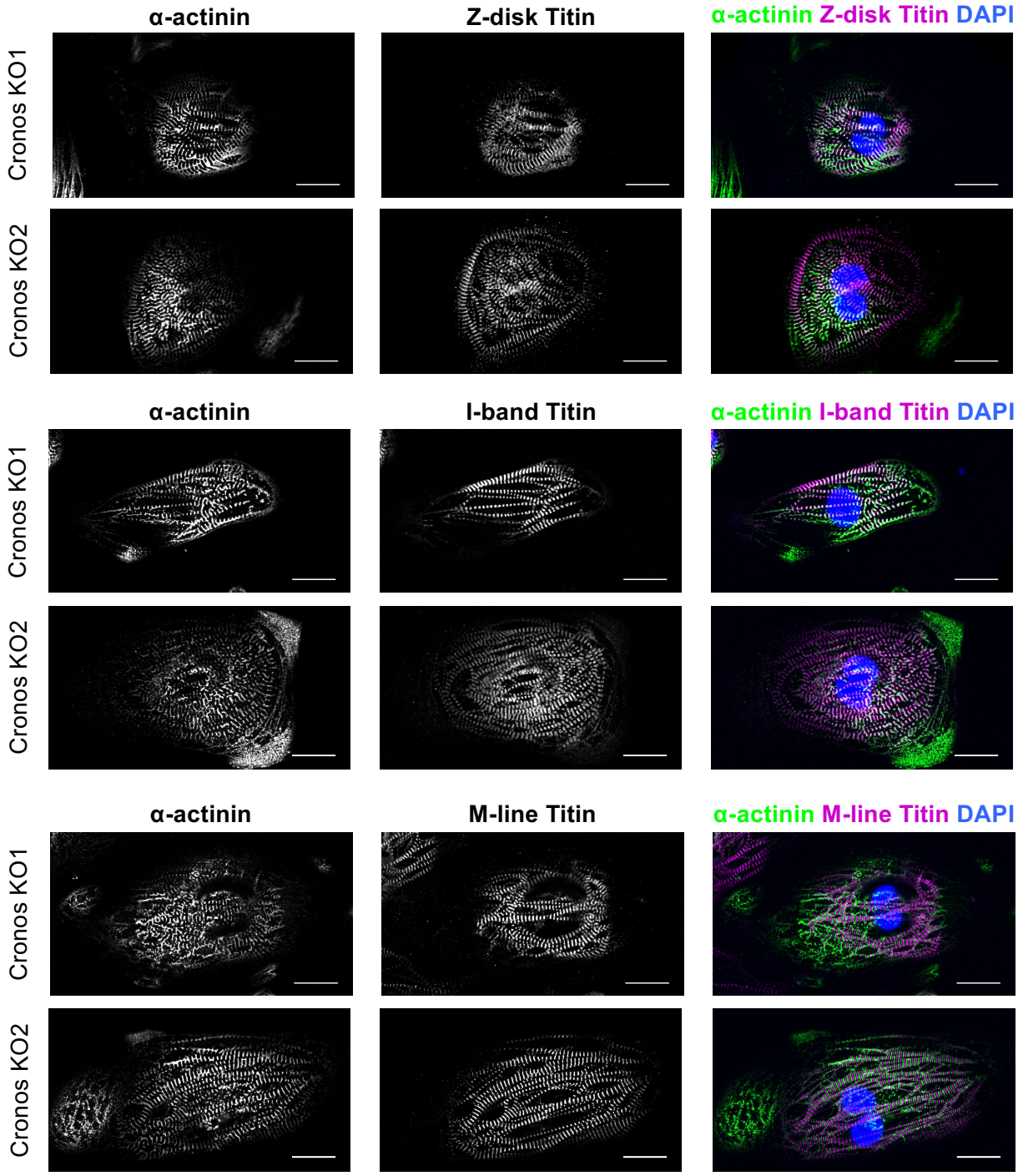

Figure 4.3. Titin epitope staining of Cronos KO CMs. Staining for Z-disk, I-band, and M-line titin indicates that these domains are still expressed and correctly integrated into sarcomeres in Cronos KO CMs. Scale bars = 20μm.

4.4.3 *Titin Transcript Expression of Cronos KO CMs*

To investigate if there was any compensatory upregulation of full-length titin in the Cronos KO cells we performed RT-qPCR for full-length and Cronos titin on day 30 hiPSC-CMs (Figure 4.4). Interestingly, full-length titin transcript levels were no different in Cronos KO cells compared to WT. This could be accounted for by the fact that there is also no difference in Cronos titin transcript between the knock-out lines and WT. This indicates that although there is a premature stop codon on the Cronos KO lines, there is no measurable non-sense mediated decay of the transcript.

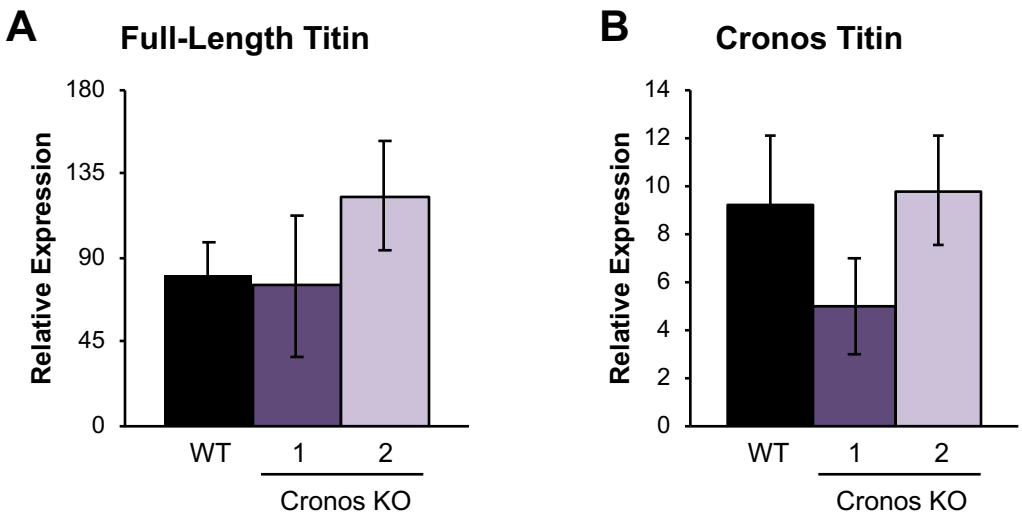

Figure 4.4. Cronos KO titin transcript measurements. There is no significant difference in levels of (A) full-length titin or (B) Cronos titin transcript levels. WT: n=5; Cronos KO1: n=4; Cronos KO2: n=5. Errors bar indicate standard error.

4.4.4 *Force Production of Cronos KO EHTs*

To investigate if knocking out Cronos titin affected contractility of hiPSC-CMs we took force measurements using engineered heart tissues (EHTs). Twitch force and active

tension were significantly decreased in both Cronos KO lines, producing less than half the force and tension of WT EHTs (Figure 4.5). Passive force and tension were not significantly different in the Cronos KO lines compared to WT, but maximum twitch velocity was significantly decreased in both Cronos KO lines. Time to peak, 50% and 90% relaxation were not consistently different in Cronos KO lines compared to WT, although there were some individual differences. Cross-sectional area was only significantly decreased in Cronos KO2 EHTs compared to both WT and Cronos KO1 EHTs. Overall, these data indicate that EHTs without Cronos produce significantly reduced active force compared to WT, suggesting Cronos titin is necessary for proper cardiomyocyte function.

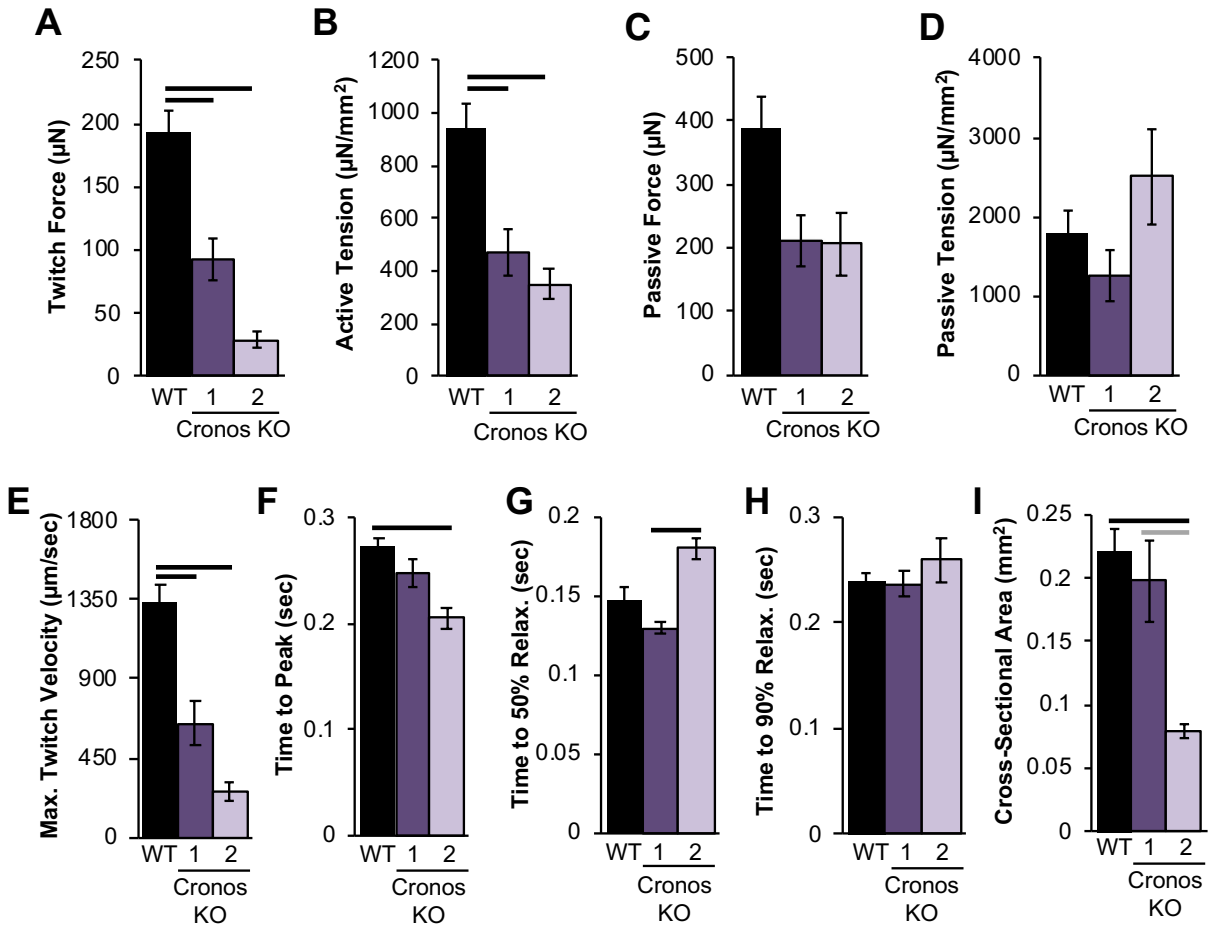

Figure 4.5. Cronos KO EHT force measurements. Force measurements of EHTs seeded with Cronos KO CMs have significantly reduced (A) twitch force and (B) active

tension compared to WT. (C) Passive force and (D) passive tension are not significantly different. (E) Maximum twitch velocity is significantly decreased on Cronos KO EHTs compared to WT but (F) time to peak is significantly decreased in only one Cronos KO line. Time to (G) 50% and (H) 90% relaxation were not significantly different between WT and Cronos KO EHTs. (I) Cross-sectional area of EHTs from Cronos KO2 was significantly smaller than the other Cronos KO line and WT samples. WT: n=23; Cronos KO-1: n=12; Cronos KO-2: n=6. Error bars indicate standard error. Black line connecting groups: $p<0.01$; gray lines connecting groups: $p<0.05$.

4.4.5 *Sarcomere Morphology of Cronos KO EHTs*

Given the strong Cronos staining observed in hiPSC-CMs, we hypothesized that removing Cronos may disrupt sarcomere morphology. To investigate this hypothesis, we stained sections of WT and Cronos KO EHTs for α-actinin and analyzed the sarcomere morphology (Figure 4.6). Circular variance, a measure of the alignment of the myofibrils in which a lower number indicates a higher degree of alignment, was significantly higher in both Cronos KO line EHTs than in WT. Interestingly, sarcomere length was not significantly changed in the Cronos KO EHTs compared to WT. These data indicate that removing Cronos titin disrupts myofibril morphology, which could explain the reduced force production of EHTs.

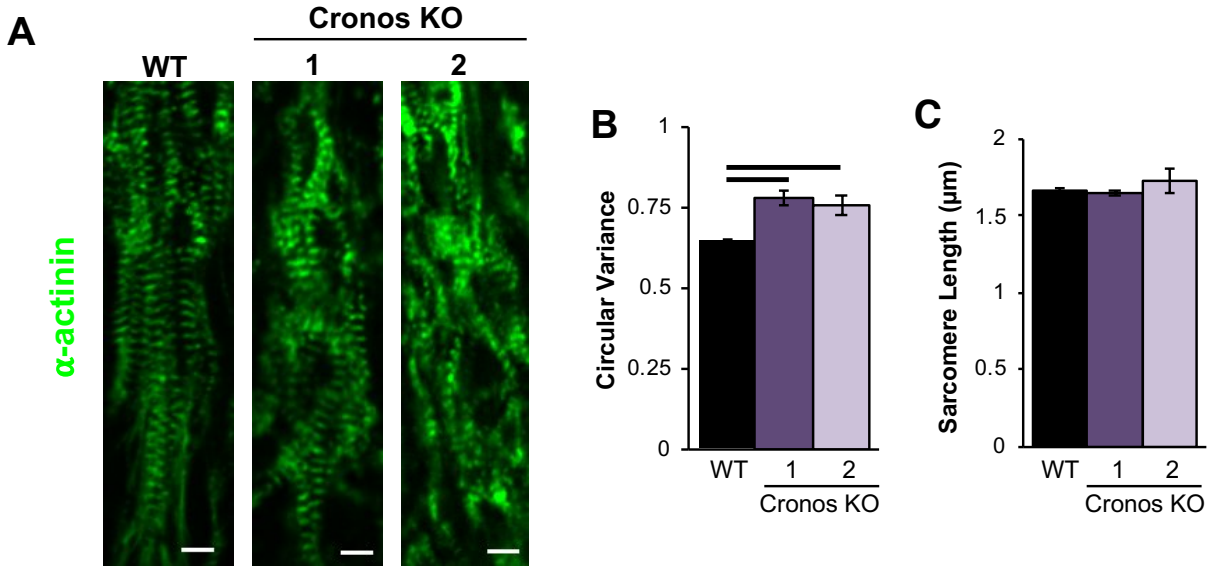

Figure 4.6. Sarcomere morphology of WT and Cronos KO EHTs. (A) representative images of WT and Cronos KO EHTs stained for α-actinin. Scale bars = 5μm. (B) Circular variance, a measure of myofibrillar disarray, is significantly higher in both Cronos KO lines compared to WT but (C) sarcomere length is not significantly different between any groups. WT: n=6; Cronos KO-1: n=5; Cronos KO-2: n=5. Error bars represent standard error. Black bars connecting groups: $p<0.01$.

4.4.6 *Calcium Transient of Cronos KO CMs*

To investigate whether the reduced force production of Cronos KO EHTs was due to differences in calcium handling single-cell calcium measurements were taken (Figure 4.7). The amplitude of calcium transient was not different between Cronos KO and WT cells. Time to peak was slightly higher in one Cronos KO cell line, and the maximum rate of release was drastically reduced in both Cronos KO lines compared to WT. Time to 50% calcium reuptake was not significantly changed in Cronos KO cells, and time to 90% reuptake was slightly faster in the Cronos KO cells. Overall, the calcium data do not account for the reduced contractility of Cronos KO EHTs.

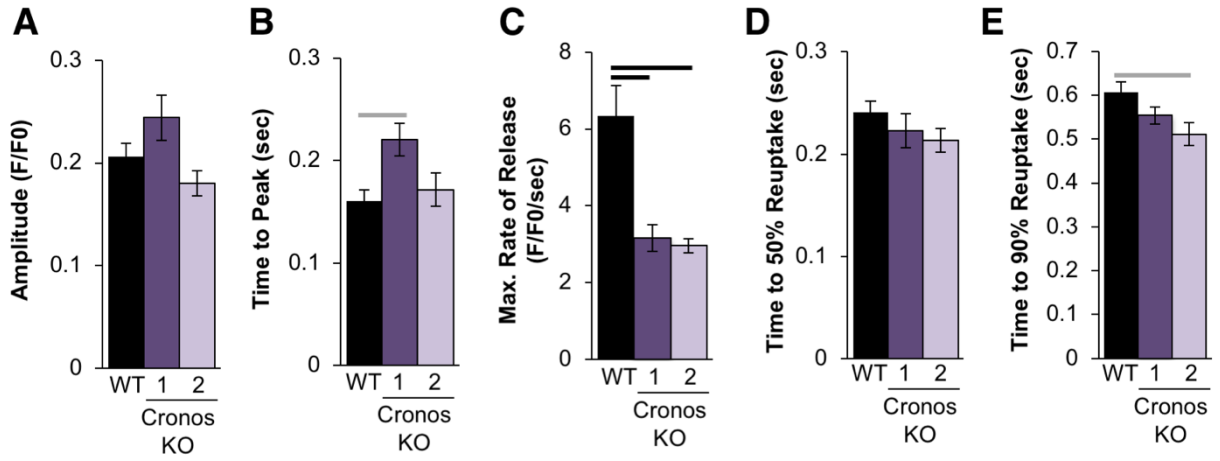

Figure 4.7. Cronos KO single cell calcium transients. (A) The amplitude of calcium transients not significantly different between WT and Cronos KO cells but (B) the time to peak of one Cronos KO cell line is slower. (C) Both Cronos KO cell lines have a significantly slower maximum rate of release compared to WT but time to (D) 50% and (E) 90% reuptake is only marginally slower compared to WT. WT: n=35; Cronos KO-1: n=32; Cronos KO-2: n=22. Error bars indicate standard error. Black line connecting groups: $p<0.01$. Gray lines connecting groups: $p<0.05$.

4.5 Discussion

To investigate the role of Cronos titin in human cardiomyocytes, we generated two Cronos KO hiPSC lines. The Cronos KO hiPSC differentiated into visibly beating cardiomyocytes, and immunostaining revealed these cells did not express any Cronos titin protein but did produce full-length titin. Interestingly, there was no evidence of non-sense mediated decay of the Cronos titin transcript, or any significant upregulation of the full-length titin transcript. Additionally, there was some positive perinuclear staining for Cronos titin in the KO cardiomyocytes. Together with the transcript data, this suggests that a small Cronos titin product is being translated but is not being integrated into the sarcomere and may be remaining the endoplasmic reticulum. We do not anticipate that this will have an impact

on the characterization of the Cronos KO CMs because the sarcomeres did not stain for any Cronos titin.

To characterize these cardiomyocytes, we produced EHTs seeded with the WT and Cronos KO cells. The Cronos KO EHTs produced less than half the force of the WT EHTs, both in absolute terms and when normalized for cross-sectional area. While maximum rate of force production was also affected, passive force, tension, and relaxation kinetics were largely unchanged. It is intriguing that active force production is reduced so drastically considering that the full-length titin that is still present in these cells contains nearly all of the domains of the Cronos titin that is absent. The only domain that is not present in full-length titin that is present in Cronos titin is a 13-residue region at the N-terminal of the Cronos protein. However, this region is only 60% homologous between humans and mice, indicating it likely does not play an important role (i.e. has not been preserved through evolution)[86].

This indicates that Cronos titin may be playing a structural role that is somewhat distinct from full-length titin. Supporting this idea, Cronos KO EHTs demonstrate significant myofibrillar disarray compared to WT. This indicates that either myofibril formation or stability is affected. Due to the fact that Cronos titin is mostly composed of the A-band, we hypothesize that this mainly affects the structure of the thick filament. It would be informative to track thick filament formation by creating a Cronos KO in a cell line with a fluorescently tagged β-myosin heavy chain and performing live cell imaging. By comparing thick filament formation and degradation in WT and Cronos KO cells, any

effects on stability of the thick filament caused by the absence of Cronos would be uncovered. This characterization will be crucial for fully understanding the role of Cronos in human cardiomyocytes.

Importantly, the reduced force production and perturbed sarcomere morphology of Cronos KO CMs indicate that Cronos titin is crucial for normal cardiomyocyte function. This is particularly important when considering the possible role of Cronos in titin truncation DCM. This indicates that titin truncations downstream of the Cronos titin start site will affect two forms of titin that we have demonstrated to be functionally important in hiPSC-CMs, and that neither of these forms can completely compensate for the absence of the other. This is particularly important when evaluating hiPSC models of titin truncations, as mutations in different regions will affect the cells differently. Although further studies are necessary to determine how Cronos titin impacts DCM pathology in the human heart, the hiPSC-CM models presented here indicate that it may be an important factor.

4.6 Summary

We have demonstrated in the previous chapters that Cronos titin is expressed in hiPSC-CMs and fetal and adult human cardiac tissue but did not understand the function of this novel isoform of Cronos titin. In this chapter we have described the generation of two genetically engineered hiPSC lines that carry premature stop codons in the Cronos-specific region of *TTN* such that they are Cronos knock-out cells that still express full-length titin normally. When engineered heart tissues are created with these cells, they

produce approximately half the force produced by wildtype controls. This is likely due to the significant myofibrillar disarray observed in the Cronos KO EHTs, which indicates that Cronos titin is necessary for correct sarcomere formation and function. These findings have implications for our understanding of titin biology, titin-based dilated cardiomyopathy, and disease modeling in hiPSC-CMs. We have demonstrated that disrupting this isoform in hiPSC-CMs affects the myofibril structure and contractility of these cells. This indicates that any mutation studied in hiPSC-CMs that is downstream of the Cronos start site in *TTN* must be considered as affecting two functional isoforms of titin. These results should be further explored in the context of truncated titin DCM to determine if Cronos titin is contributing to the pathogenicity observed in A-band mutations but largely absent in mutations found in the Z-disk.

Chapter 5. Thesis Summary & Conclusion

Studies on the giant sarcomeric protein titin have been published since the 1970s, and yet much remains unknown about this complex and important component of striated muscle. Of particular interest recently is the role of titin truncations in familial dilated cardiomyopathy. These mutations are the most common cause of dilated cardiomyopathy, and yet the mechanism by which they cause disease is largely unknown. Additionally, these mutations are unevenly distributed within the *TTN* gene such that most occur in the final two-thirds of the gene. This uneven distribution of pathogenic mutations, which cannot be entirely explained by considering the frequency with which exons are expressed, is the motivation for this thesis.

In the first aim of this thesis in Chapter 2, we investigate this concentration of DCM mutations by genetically engineering hiPSC lines to carry homozygous mutations in the Z-disk or A-band. We expected both of these types of mutations to block sarcomere formation but were surprised to find Z-disk mutants still formed sarcomeres. We attribute this to the expression of a novel isoform of titin called Cronos, which had not been previously observed in human cardiomyocytes. Cells expressing only Cronos titin are able to form sarcomeres but produce reduced contractile force and are not able to properly bundle myofibrils. From this we conclude that Cronos titin is able to support some sarcomere formation in hiPSC-CMs.

To determine if Cronos titin is expressed in human cardiac tissue and if so at what developmental stage we evaluated fetal and cardiac tissue on the genomic, transcript,

and protein level in Chapter 3. Data in all cases support Cronos titin being expressed most highly in fetal tissue, although there is also evidence it is expressed in adult left ventricular tissue. Additionally, in the fetal heart Cronos titin expression differed depending on which chamber was studied. These data provide important evidence that Cronos titin is expressed in human cardiac tissue and is not just an artifact of stem cell-derived cardiomyocytes.

In Chapter 4 we investigate the role of Cronos titin in human cardiomyocytes by generating two Cronos knock-out hiPSC lines. These cells differentiate into cardiomyocytes, do not express Cronos titin, but do express full-length titin at normal levels. When EHTs are created with these cells, they produce drastically reduced twitch force, and exhibit significant myofibrillar disarray. From this we conclude that Cronos titin is necessary for sarcomere formation and function, despite the fact that nearly all domains present in Cronos titin are also in full-length titin.

The results presented in this thesis provide important new insight into the role of titin in human cardiac biology. We have shown here that a previously unstudied isoform of titin is expressed in human cardiomyocytes and is important for proper myofibril formation and function. This opens up many more avenues of investigation to fully understand the role of this isoform in health and disease. In particular, its role in titin truncation dilated cardiomyopathy must be further studied to understand if it contributes to the difference in phenotype observed between mutations within and outside the A-band region of *TTN*.

Significant work remains to fully elucidate the role of Cronos titin, and the research presented in this thesis provides the foundation on which it can be built.

BIBLIOGRAPHY

1. Fürst, D. O., Osborn, M., Nave, R. & Weber, K. The organization of titin filaments in the half-sarcomere revealed by monoclonal antibodies in immunoelectron microscopy: a map of ten nonrepetitive epitopes starting at the Z line extends close to the M line. *J. Cell Biol.* **106,** 1563–72 (1988).
2. Gregorio, C. C. *et al.* The NH2 terminus of titin spans the Z-disc: Its interaction with a novel 19-kD ligand (T-cap) is required for sarcomeric integrity. *J. Cell Biol.* **143,** 1013–1027 (1998).
3. Young, P., Ferguson, C., Bañuelos, S. & Gautel, M. Molecular structure of the sarcomeric Z-disk: Two types of titin interactions lead to an asymmetrical sorting of α-actinin. *EMBO J.* **17,** 1614–1624 (1998).
4. Witt, C. C. *et al.* Nebulin regulates thin filament length, contractility, and Z-disk structure in vivo. **25,** 3843–3855 (2006).
5. Labeit, S. *et al.* Expression of Distinct Classes of Titin Isoforms in Striated and Smooth Muscles by Alternative Splicing, and Their Conserved Interaction with Filamins. *J. Mol. Biol.* **362,** 664–681 (2006).
6. Freiburg, A. *et al.* Series of exon-skipping events in the elastic spring region of titin as the structural basis for myofibrillar elastic diversity. *Circ. Res.* **86,** 1114–1121 (2000).
7. Granzier, H. L. & Irving, T. C. Passive tension in cardiac muscle: contribution of collagen, titin, microtubules, and intermediate filaments. *Biophys. J.* **68,** 1027–

1044 (1995).

8. Krüger, M. *et al.* Protein kinase G modulates human myocardial passive stiffness by phosphorylation of the titin springs. *Circ. Res.* **104,** 87–94 (2009).
9. Fukuda, N., Wu, Y., Nair, P. & Granzier, H. L. Phosphorylation of titin modulates passive stiffness of cardiac muscle in a titin isoform-dependent manner. *J. Gen. Physiol.* **125,** 257–271 (2005).
10. Hidalgo, C. *et al.* PKC phosphorylation of titin's PEVK element: A novel and conserved pathway for modulating myocardial stiffness. *Circ. Res.* **105,** 631–638 (2009).
11. Grützner, A. *et al.* Modulation of titin-based stiffness by disulfide bonding in the cardiac titin N2-B unique sequence. *Biophys. J.* **97,** 825–834 (2009).
12. Alegre-Cebollada, J. *et al.* S-glutathionylation of cryptic cysteines enhances titin elasticity by blocking protein folding. *Cell* **156,** 1235–1246 (2014).
13. Linke, W. a. & Hamdani, N. Gigantic business: Titin properties and function through thick and thin. *Circ. Res.* **114,** 1052–1068 (2014).
14. Nagueh, S. F. *et al.* Altered titin expression, myocardial stiffness, and left ventricular function in patients with dilated cardiomyopathy. *Circulation* **110,** 155–162 (2004).
15. Makarenko, I. *et al.* Passive stiffness changes caused by upregulation of compliant titin isoforms in human dilated cardiomyopathy hearts. *Circ. Res.* **95,** 708–716 (2004).
16. Cazorla, O. *et al.* Differential expression of cardiac titin isoforms and modulation of cellular stiffness. *Circ. Res.* **86,** 59–67 (2000).

17. Whiting, A., Wardale, J. & Trinick, J. Does titin regulate the length of muscle thick filaments? *J. Mol. Biol.* **205,** 263–268 (1989).

18. Müller, S., Lange, S., Gautel, M. & Wilmanns, M. Rigid Conformation of an Immunoglobulin Domain Tandem Repeat in the A-band of the Elastic Muscle Protein Titin. *J. Mol. Biol.* **371,** 469–480 (2007).

19. Bennett, P. M. & Gautel, M. Titin domain patterns correlate with the axial disposition of myosin at the end of the thick filament. *J. Mol. Biol.* **259,** 896–903 (1996).

20. Tskhovrebova, L., Bennett, P., Gautel, M. & Trinick, J. Titin ruler hypothesis not refuted. *Proc. Natl. Acad. Sci. U. S. A.* **112,** E1172 (2015).

21. Granzier, H. L. *et al.* Deleting titin's I-band/A-band junction reveals critical roles for titin in biomechanical sensing and cardiac function. *Proc. Natl. Acad. Sci.* **111,** 14589–14594 (2014).

22. Obermann, W. M., Gautel, M., Weber, K. & Fürst, D. O. Molecular structure of the sarcomeric M band: mapping of titin and myosin binding domains in myomesin and the identification of a potential regulatory phosphorylation site in myomesin. *EMBO J.* **16,** 211–20 (1997).

23. Lange, S. *et al.* The kinase domain of titin controls muscle gene expression and protein turnover. *Science* **308,** 1599–603 (2005).

24. Kontrogianni-Konstantopoulos, A., Ackermann, M. A., Bowman, A. L., Yap, S. V & Bloch, R. J. Muscle giants: Molecular Scaffolds in Sarcomerogenesis. *Physiol. Rev.* **89,** 1217–67 (2009).

25. Bowman, A. L. *et al.* The rho-guanine nucleotide exchange factor domain of

obscurin regulates assembly of titin at the Z-disk through interactions with Ran binding protein 9. *Mol. Biol. Cell* **19,** 3782–92 (2008).

26. Seeley, M. *et al.* Depletion of zebrafish titin reduces cardiac contractility by disrupting the assembly of Z-discs and A-bands. *Circ. Res.* **100,** 238–245 (2007).
27. Xu, X. *et al.* Cardiomyopathy in zebrafish due to mutation in an alternatively spliced exon of titin. *Nat. Genet.* **30,** 205–9 (2002).
28. Myhre, J. L., Hills, J. A., Prill, K., Wohlgemuth, S. L. & Pilgrim, D. B. The titin A-band rod domain is dispensable for initial thick filament assembly in zebrafish. *Dev. Biol.* **387,** 93–108 (2014).
29. Schafer, S. *et al.* Titin-truncating variants affect heart function in disease cohorts and the general population. *Nat. Genet.* **49,** 46–53 (2017).
30. Gramlich, M. *et al.* Stress-induced dilated cardiomyopathy in a knock-in mouse model mimicking human titin-based disease. *J. Mol. Cell. Cardiol.* **47,** 352–358 (2009).
31. Machado, C. & Andrew, D. J. D-Titin: A giant protein with dual roles in chromosomes and muscles. *J. Cell Biol.* **151,** 639–651 (2000).
32. Zastrow, M. S., Flaherty, D. B., Benian, G. M. & Wilson, K. L. Nuclear titin interacts with A- and B-type lamins in vitro and in vivo. *J. Cell Sci.* **119,** 239–249 (2006).
33. Qi, J., Chi, L., Labeit, S. & Banes, A. J. Nuclear localization of the titin Z1Z2Zr domain and role in regulating cell proliferation. *Am. J. Physiol. Cell Physiol.* **295,** C975–C985 (2008).
34. Opitz, C. a., Leake, M. C., Makarenko, I., Benes, V. & Linke, W. A.

Developmentally regulated switching of titin size alters myofibrillar stiffness in the perinatal heart. *Circ. Res.* **94,** 967–75 (2004).

35. Trombitás, K., Wu, Y., Labeit, D., Labeit, S. & Granzier, H. Cardiac titin isoforms are coexpressed in the half-sarcomere and extend independently. *Am. J. Physiol. Heart Circ. Physiol.* **281,** H1793-9 (2001).
36. Hershberger, R. E., Hedges, D. J. & Morales, A. Dilated cardiomyopathy: the complexity of a diverse genetic architecture. *Nat. Rev. Cardiol.* **10,** 531–547 (2013).
37. Maron, B. J. *et al.* Contemporary definitions and classification of the cardiomyopathies: An American Heart Association Scientific Statement from the Council on Clinical Cardiology, Heart Failure and Transplantation Committee; Quality of Care and Outcomes Research and Functio. *Circulation* **113,** 1807–1816 (2006).
38. Roura, S. & Bayes-Genis, A. Vascular dysfunction in idiopathic dilated cardiomyopathy. *Nat. Rev. Cardiol.* **6,** 590–598 (2009).
39. Herman, D. S. *et al.* Truncations of titin causing dilated cardiomyopathy. *N. Engl. J. Med.* **366,** 619–28 (2012).
40. McNally, E. M., Golbus, J. R. & Puckelwartz, M. J. Genetic mutations and mechanisms in dilated cardiomyopathy. *J. Clin. Invest.* **123,** 19–26 (2013).
41. Akinrinade, O., Alastalo, T.-P. & Koskenvuo, J. W. Relevance of truncating titin mutations in dilated cardiomyopathy. *Clin. Genet.* **90,** 49–54 (2016).
42. Norton, N. *et al.* Exome sequencing and genome-wide linkage analysis in 17 families illustrate the complex contribution of TTN truncating variants to dilated

cardiomyopathy. *Circ. Cardiovasc. Genet.* **6,** 144–153 (2013).

43. Pugh, T. J. *et al.* The landscape of genetic variation in dilated cardiomyopathy as surveyed by clinical DNA sequencing. *Genet. Med.* **16,** 601–8 (2014).
44. van Spaendonck-Zwarts, K. Y. *et al.* Titin gene mutations are common in families with both peripartum cardiomyopathy and dilated cardiomyopathy. *Eur. Heart J.* **35,** 2165–73 (2014).
45. Haas, J. *et al.* Atlas of the clinical genetics of human dilated cardiomyopathy. *Eur. Heart J.* **36,** 1123–1135 (2015).
46. Ware, J. S. *et al.* Shared Genetic Predisposition in Peripartum and Dilated Cardiomyopathies. *N. Engl. J. Med.* **374,** 233–241 (2016).
47. Roberts, A. M. *et al.* Integrated allelic, transcriptional, and phenomic dissection of the cardiac effects of titin truncations in health and disease. *Sci. Transl. Med.* **7,** 270ra6-270ra6 (2015).
48. Deo, R. C. *Alternative Splicing, an Internal Promoter, Nonsense-Mediated Decay, or All Three: Explaining the Distribution of Truncation Variants in* Titin. *Circulation: Cardiovascular Genetics* (2016). doi:10.1161/CIRCGENETICS.116.001513
49. Gerull, B. *et al.* Mutations of TTN, encoding the giant muscle filament titin, cause familial dilated cardiomyopathy. *Nat. Genet.* **30,** 201–204 (2002).
50. Zaunbrecher, R. & Regnier, M. Connecting sarcomere protein mutations to pathogenesis in cardiomyopathies: The development of ‘disease in a dish’ models. *Front. Physiol.* **7,** 2014–2017 (2016).
51. Geisterfer-Lowrance, A. a. T. *et al.* A molecular basis for familial hypertrophic cardiomyopathy: A β cardiac myosin heavy chain gene missense mutation. *Cell*

62, 999–1006 (1990).

52. Seidman, C. E. & Seidman, J. G. Identifying sarcomere gene mutations in hypertrophic cardiomyopathy: A personal history. *Circ. Res.* **108,** 743–750 (2011).

53. Thomson, J. A. *et al.* Embryonic stem cell lines derived from human blastocysts. *Science* **282,** 1145–7 (1998).

54. Takahashi, K. & Yamanaka, S. Induction of Pluripotent Stem Cells from Mouse Embryonic and Adult Fibroblast Cultures by Defined Factors. *Cell* **126,** 663–676 (2006).

55. Kehat, I. *et al.* Human embryonic stem cells can differentiate into myocytes with structural and functional properties of cardiomyocytes. *J. Clin. Invest.* **108,** 407–414 (2001).

56. Spater, D., Hansson, E. M., Zangi, L. & Chien, K. R. How to make a cardiomyocyte. *Development* **141,** 4418–4431 (2014).

57. Lin, B. *et al.* Modeling and study of the mechanism of dilated cardiomyopathy using induced pluripotent stem cells derived from individuals with Duchenne muscular dystrophy. *Dis. Model. Mech.* **8,** 457–66 (2015).

58. Siu, C.-W. *et al.* Modeling of lamin A/C mutation premature cardiac aging using patient-specific induced pluripotent stem cells. *Aging (Albany. NY).* **4,** 803–822 (2012).

59. Lan, F. *et al.* Abnormal Calcium Handling Properties Underlie Familial Hypertrophic Cardiomyopathy Pathology in Patient-Specific Induced Pluripotent Stem Cells. *Cell Stem Cell* **12,** 101–113 (2013).

60. Sun, N. *et al.* Patient-Specific Induced Pluripotent Stem Cells as a Model for

Familial Dilated Cardiomyopathy. *Sci. Transl. Med.* **4,** 130ra47-130ra47 (2012).

61. Wu, H. *et al.* Epigenetic Regulation of Phosphodiesterases 2A and 3A Underlies Compromised β-Adrenergic Signaling in an iPSC Model of Dilated Cardiomyopathy. *Cell Stem Cell* **17,** 89–100 (2015).
62. Ran, F., Hsu, P., Wright, J. & Agarwala, V. Genome engineering using the CRISPR-Cas9 system. *Nat. Protoc.* **8,** 2281–308 (2013).
63. Cells, P. S. *et al.* Small Molecules Enhance CRISPR Genome Editing in Small Molecules Enhance CRISPR Genome Editing in Pluripotent Stem Cells. *Stem Cell* **16,** 142–147 (2015).
64. Chu, V. T. *et al.* Increasing the efficiency of homology-directed repair for CRISPR-Cas9-induced precise gene editing in mammalian cells. *Nat. Biotechnol.* **33,** 543–548 (2015).
65. Kleinstiver, B. P. *et al.* Engineered CRISPR-Cas9 nucleases with altered PAM specificities. *Nature* **523,** 481–485 (2015).
66. Kleinstiver, B. P. *et al.* Broadening the targeting range of Staphylococcus aureus CRISPR-Cas9 by modifying PAM recognition. *Nat. Biotechnol.* **33,** 1293–1298 (2015).
67. Hinson, J. T. *et al.* Titin mutations in iPS cells define sarcomere insufficiency as a cause of dilated cardiomyopathy. *Science (80-.).* **349,** 982–986 (2015).
68. Polacheck, W. J. & Chen, C. S. Measuring cell-generated forces: a guide to the available tools. *Nat. Methods* **13,** 415–423 (2016).
69. Tzatzalos, E., Abilez, O. J., Shukla, P. & Wu, J. C. Engineered heart tissues and

induced pluripotent stem cells: Macro- and microstructures for disease modeling, drug screening, and translational studies. *Adv. Drug Deliv. Rev.* **96,** 234–244 (2016).

70. Pioner, J. M. *et al.* Isolation and Mechanical Measurements of Myofibrils from Human Induced Pluripotent Stem Cell-Derived Cardiomyocytes. *Stem Cell Reports* **6,** 885–896 (2016).
71. Yang, X., Pabon, L. & Murry, C. E. Engineering adolescence: Maturation of human pluripotent stem cell-derived cardiomyocytes. *Circ. Res.* **114,** 511–523 (2014).
72. Bedada, F. B. *et al.* Acquisition of a quantitative, stoichiometrically conserved ratiometric marker of maturation status in stem cell-derived cardiac myocytes. *Stem Cell Reports* **3,** 594–605 (2014).
73. Ding, Q. *et al.* Enhanced Efficiency of Human Pluripotent Stem Cell Genome Editing through Replacing TALENs with CRISPRs. *Cell Stem Cell* **12,** 393–394 (2013).
74. Roberts, B. *et al.* Systematic gene tagging using CRISPR/Cas9 in human stem cells to illuminate cell organization. *Mol. Biol. Cell* **28,** 2854–2874 (2017).
75. Steinbeck, J. a *et al.* Optogenetics enables functional analysis of human embryonic stem cell–derived grafts in a Parkinson's disease model. *Nat. Biotechnol.* **33,** 204–209 (2015).
76. Gramlich, M. *et al.* Antisense-mediated exon skipping: a therapeutic strategy for titin-based dilated cardiomyopathy. *EMBO Mol. Med.* (2015).
77. Schick, R. *et al.* Functional abnormalities in induced Pluripotent Stem Cell-derived

cardiomyocytes generated from titin-mutated patients with dilated cardiomyopathy. *PLoS One* **13,** e0205719 (2018).

78. Person, V., Kostin, S., Suzuki, K., Labeit, S. & Schaper, J. Antisense oligonucleotide experiments elucidate the essential role of titin in sarcomerogenesis in adult rat cardiomyocytes in long-term culture. *J. Cell Sci.* **113 Pt 21,** 3851–9 (2000).
79. Kreitzer, F. R. *et al.* A robust method to derive functional neural crest cells from human pluripotent stem cells. *Am. J. Stem Cells* **2,** 119–31 (2013).
80. Kent, W. J. *et al.* The human genome browser at UCSC. *Genome Res.* **12,** 996–1006 (2002).
81. Ye, J. *et al.* Primer-BLAST: A tool to design target-specific primers for polymerase chain reaction. *BMC Bioinformatics* **13,** 134 (2012).
82. Palpant, N. J. *et al.* Generating high-purity cardiac and endothelial derivatives from patterned mesoderm using human pluripotent stem cells. *Nat. Protoc.* **12,** 15–31 (2016).
83. Tohyama, S. *et al.* Distinct metabolic flow enables large-scale purification of mouse and human pluripotent stem cell-derived cardiomyocytes. *Cell Stem Cell* **12,** 127–137 (2013).
84. Bielawski, K. S., Leonard, A., Bhandari, S., Murry, C. E. & Sniadecki, N. J. Real-Time Force and Frequency Analysis of Engineered Human Heart Tissue Derived from Induced Pluripotent Stem Cells Using Magnetic Sensing. *Tissue Eng. Part C Methods* **22,** 932–940 (2016).
85. Rodriguez, M. L. *et al.* Measuring the Contractile Forces of Human Induced

Pluripotent Stem Cell-Derived Cardiomyocytes With Arrays of Microposts. *J. Biomech. Eng.* **136,** 051005 (2014).

86. Zou, J. *et al.* An internal promoter underlies the difference in disease severity between N- and C-terminal truncation mutations of Titin in zebrafish. *Elife* **4,** 1–22 (2015).
87. Macadangdang, J. *et al.* Capillary Force Lithography for Cardiac Tissue Engineering. *J. Vis. Exp.* 1–8 (2014). doi:10.3791/50039
88. Schindelin, J. *et al.* Fiji: An open-source platform for biological-image analysis. *Nat. Methods* **9,** 676–682 (2012).
89. Benjamini, Y. & Hochberg, Y. Controlling the False Discovery Rate : A Practical and Powerful Approach to Multiple Testing Author (s): Yoav Benjamini and Yosef Hochberg Source : Journal of the Royal Statistical Society . Series B (Methodological), Vol . 57 , No . 1 Published by : *R. Stat. Soc.* **57,** 289–300 (1995).
90. Paige, S. L. *et al.* A temporal chromatin signature in human embryonic stem cells identifies regulators of cardiac development. *Cell* **151,** 221–232 (2012).
91. Opitz, C. A. & Linke, W. A. Plasticity of cardiac titin/connectin in heart development. *J. Muscle Res. Cell Motil.* **26,** 333–342 (2005).
92. Machado, C., Sunkel, C. E. & Andrew, D. J. Human autoantibodies reveal titin as a chromosomal protein. *J. Cell Biol.* **141,** 321–333 (1998).
93. Chopra, A. *et al.* Force Generation via β-Cardiac Myosin, Titin, and α-Actinin Drives Cardiac Sarcomere Assembly from Cell-Matrix Adhesions. *Dev. Cell* **44,** 87–96.e5 (2018).

94. Musa, H. *et al.* Targeted homozygous deletion of M-band titin in cardiomyocytes prevents sarcomere formation. *J. Cell Sci.* **119,** 4322–31 (2006).

95. Weinert, S., Bergmann, N., Luo, X., Erdmann, B. & Gotthardt, M. M line-deficient titin causes cardiac lethality through impaired maturation of the sarcomere. *J. Cell Biol.* **173,** 559–570 (2006).

96. Tulloch, N. L. *et al.* Growth of engineered human myocardium with mechanical loading and vascular coculture. *Circ. Res.* **109,** 47–59 (2011).

97. Lahmers, S., Wu, Y., Call, D. R., Labeit, S. & Granzier, H. Developmental Control of Titin Isoform Expression and Passive Stiffness in Fetal and Neonatal Myocardium. *Circ. Res.* **94,** 505–513 (2004).

98. Warren, C. M., Krzesinski, P. R., Campbell, K. S., Moss, R. L. & Greaser, M. L. Titin isoform changes in rat myocardium during development. *Mech. Dev.* **121,** 1301–1312 (2004).

99. Granzier, H. L. & Irving, T. C. Passive tension in cardiac muscle: contribution of collagen, titin, microtubules, and intermediate filaments. *Biophys. J.* **68,** 1027–1044 (1995).

100. Kolb, J. *et al.* Thin filament length in the cardiac sarcomere varies with sarcomere length but is independent of titin and nebulin. *J. Mol. Cell. Cardiol.* **97,** 286–294 (2016).

101. Maruyama, K., Kimura, S., Yoshidomi, H., Sawada, H. & Kikuchi, M. Molecular size and shape of beta-connectin, an elastic protein of striated muscle. *J. Biochem.* **95,** 1423–1433 (1984).

102. Dunham, I. *et al.* An integrated encyclopedia of DNA elements in the human

genome. *Nature* **489,** 57–74 (2012).

103. Fabian, L. *et al.* Titin in insect spermatocyte spindle fibers associates with microtubules, actin, myosin and the matrix proteins skeletor, megator and chromator. *J. Cell Sci.* **120,** 2190–2204 (2007).
104. Reiser, P. J., Portman, M. a, Ning, X. H. & Schomisch Moravec, C. Human cardiac myosin heavy chain isoforms in fetal and failing adult atria and ventricles. *Am. J. Physiol. Heart Circ. Physiol.* **280,** H1814–H1820 (2001).
105. Morano, I. Tuning the human heart molecular motors by myosin light chairs. *J. Mol. Med.* **77,** 544–555 (1999).
106. Wu, Y., Cazorla, O., Labeit, D., Labeit, S. & Granzier, H. Changes in titin and collagen underlie diastolic stiffness diversity of cardiac muscle. *J. Mol. Cell. Cardiol.* **32,** 2151–2161 (2000).
107. Schwan, J. & Campbell, S. G. Prospects for In Vitro Myofilament Maturation in Stem Cell-Derived Cardiac Myocytes. *Biomark. Insights* **10,** 91–103 (2015).
108. Rajabi, M., Kassiotis, C., Razeghi, P. & Taegtmeyer, H. Return to the fetal gene program protects the stressed heart: A strong hypothesis. *Heart Fail. Rev.* **12,** 331–343 (2007).
109. Kellermayer, M. *et al.* Topology of interaction between titin and myosin thick filaments. *J. Struct. Biol.* **203,** 46–53 (2018).
110. Tonino, P. *et al.* The giant protein titin regulates the length of the striated muscle thick filament. *Nat. Commun.* **8,** 1041 (2017).
111. Myhre, J. L. & Pilgrim, D. A Titan but not Necessarily a Ruler: Assessing the Role of Titin During Thick Filament Patterning and Assembly. *Anat. Rec.* **297,** 1604–

1614 (2014).

112. Freiburg, a & Gautel, M. A molecular map of the interactions between titin and myosin-binding protein C. Implications for sarcomeric assembly in familial hypertrophic cardiomyopathy. *Eur. J. Biochem.* **235,** 317–323 (1996).

113. Weinert, S., Bergmann, N., Luo, X., Erdmann, B. & Gotthardt, M. M line-deficient titin causes cardiac lethality through impaired maturation of the sarcomere. *J. Cell Biol.* **173,** 559–570 (2006).

114. Puchner, E. M. *et al.* Mechanoenzymatics of titin kinase. *Proc. Natl. Acad. Sci. U. S. A.* **105,** 13385–13390 (2008).

115. Peng, J. *et al.* Cardiac hypertrophy and reduced contractility in hearts deficient in the titin kinase region. *Circulation* **115,** 743–751 (2007).

116. Kartasalo, K. *et al.* CytoSpectre: A tool for spectral analysis of oriented structures on cellular and subcellular levels. *BMC Bioinformatics* **16,** 1–23 (2015).

117. Spandidos, A., Wang, X., Wang, H. & Seed, B. PrimerBank: A resource of human and mouse PCR primer pairs for gene expression detection and quantification. *Nucleic Acids Res.* **38,** 792–799 (2009).

APPENDIX A

Table A.1. Primer sequences used for genotyping

Name	Sequence (5' to 3')	Reference
TTN_Ex2genotyping_F	CCCTTAGCTGGGACACCCT	Designed on Primer-BLAST[81]
TTN_Ex2genotyping_R	GCAGGGCTTAAACTTGGCGTC	Designed on Primer-BLAST[81]
TTN_Ex326genotyping_F	CCTGAAGGACCTTTGGCTGT	Designed on Primer-BLAST[81]
TTN_Ex326genotyping_R	CCCAGTGATTTCTGAACCACC	Designed on Primer-BLAST[81]

Table A.2. Genes screened for off-target mutations

sgRNA	Gene accession number	Forward primer (5' to 3')	Reverse primer (5' to 3')
TTN_Ex2_gRNA1	NM_152335	CCCTCCGCAGTTTGAGATCC	ACACACCTGAAAGGAACCCC
TTN_Ex2_gRNA1	NM_176819	CTCTTGACTGCTACGGGCAT	TCTCCTGGTCTCTGGTCAGG
TTN_Ex2_gRNA1	NM_001024628	GGACACCCGATGGAATGAGG	AGTCTTCCCCGTTGGAGCTA
TTN_Ex2_gRNA1	NM_080872	TGACCACCGTTTCCGTAGTT	TGGTAGACACTGGCTCTCCT
TTN_Ex2_gRNA1	NM_015123	TCAGACCATATGTGCTCCCG	TTCGGGTAAGAACTGGCGTG
TTN_Ex2_gRNA2	NM_002019	AACTCCAGAGGTAGTCAGGCT	AAATATCTCAGCGCGTAGGAC
TTN_Ex2_gRNA2	NM_198827	CAGCAGACACTCTCCAGCTC	ACCTGCATGAGGATGGCAAA
TTN_Ex326_gRNA1	NM_001040113	TGACCAGTCTGTCTGGGAGA	TTCTACCACCAGCTACGGGA
TTN_Ex326_gRNA1	NM_001206966	CTGCAGGTGAGGGGTTTGAT	GGGTCTGGCTTTCTCCACTC
TTN_Ex326_gRNA1	NM_001146336	GTAGGGGCAGTGACAGTGTG	CTGGGCTGGAAACCACTCAT
TTN_Ex326_gRNA1	NM_015668	GGCTATAGTTGGGCTCCACAAA	GTTCCCTGAATGCTCGCAGAA
TTN_Ex326_gRNA1	NM_001278371	ATCACCTGTGACGACGTGTG	CAACCCGTGTACCCAAAGGT
TTN_Ex326_gRNA2	NM_021044	AAACACTTCCATTCAGAGGGTGA	TTTCCCACCTGGGACAACC
TTN_Ex326_gRNA2	NM_022474	TCTTGCTATTTGCTCGGCCA	ATCCCAGGCTGCACATAAGG
TTN_Ex326_gRNA2	NR_102336	AGCCTTGATTCTTTGACTTGCTG	TGTTTGATACCTGGGGCTACTTT
TTN_Ex326_gRNA2	NM_005242	TCTGAGTTTCGAATCGGCGG	ATTCGTAGAGATGGGTGCCG
TTN_Ex326_gRNA2	NM_003887	CAAGATCCTGCCTCTACGGAAT	TGATAGCTGCAACCTCACAAAT

Table A.3. Quantitative PCR primers

Name	Sequence (5' to 3')	Source
HPRT_qPCR_F	TGACACTGGCAAAACAATGCA	Harvard Primer Bank[117]
HPRT_qPCR_R	GGTCCTTTTCACCAGCAAGCT	Harvard Primer Bank[117]
cTnT_qPCR_F	GGAGGAGTCCAAACCAAAGCC	Harvard Primer Bank[117]

cTnT_qPCR_R	TCAAAGTCCACTCTCTCTCCATC	Harvard Primer Bank[117]
FullTTN_qPCR_F	TTTTGCACAACTGTCGCCTG	Designed on Primer-BLAST[81]
CronosandFullTTN_qPCR_R	CTTCGTAGGAGAGCTCGCAG	Designed on Primer-BLAST[81]
CronosTTN_qPCR_F	ACGCAAAGCTGTTTCTTCCC	Designed on Primer-BLAST[81]